SAPIENZA
UNIVERSITÀ DI ROMA

Mass logarithms effects in deep-inelastic scattering and their resummation to all orders

Faculty of mathematical, physical and natural sciences

Corso di Laurea Magistrale in Theoretical Physics

Candidate

Andrea Barontini

ID number 1769895

Thesis Advisor

Dr. Marco Bonvini

Academic Year 2021/2022

Thesis defended on 18 October 2021
in front of a Board of Examiners composed by:

Prof. P.Bagnaia (chairman)
Prof. E.Majorana
Prof. F.Bellini
Prof. R.Bonciani
Prof. F.Trequattrini
Prof. L.Baldassarre
Prof. F.Ferrarotto

Mass logarithms effects in deep-inelastic scattering and their resummation to all orders
Master's thesis. Sapienza – University of Rome

This thesis has been typeset by LaTeX and the Sapthesis class.

Author's email: andreabarontini97@gmail.com

Abstract

Precision physics is nowadays considered to be the key to understand many unknown aspects of the phenomenology beyond the Standard Model (SM) and, in the next future, with the coming, for instance, of the LHC (Large Hadron Collider) phase III, the experimental precision will considerably increase. This requires the theoretical precision to improve as well, at least at the same level, in order to make the distinction between Standard Model and new physic signals possible. This thesis arises in this framework and, in particular, in the context of precision predictions on hadron collider processes. The most relevant contribution to such processes is given by QCD but, in some kinematical regimes, it can not be treated in a standard perturbative way because of the appearance of non-perturbative mass logarithmic terms. In these cases, in order to obtain accurate phenomenological predictions, it is necessary to resum such terms to all orders. The main goal of this thesis is then the construction of a method to include mass-power corrections to the results obtained trough the resummation, in such a way to obtain a prediction that is reliable in a wide kinematic region. This method is completely general but, for clarity sake, it is applied to deep-inelastic scattering and, in particular, to the proton electromagnetic structure functions. The final predictions for such observables are obtained with different prescriptions, some of which constitute the original proposal of this thesis, and their consequences are analyzed in detail. Moreover, the proposal of this thesis will soon make possible to treat the N^3LO deep-inelastic scattering and so it will give access to the next generation of the parton distribution functions (PDFs).

Contents

Introduction

High energy physics will soon enter in a new high precision era. With the coming LHC (Large Hadron Collider) phase III, scheduled at the end of 2024 [1], the experimental precision will increase considerably. This new run of the hadron-hadron collider will have a centre-of-mass energy of 14 TeV and a luminosity, which is proportional to the number of collisions that occur in a given amount of time, of $300\,\text{fb}^{-1}$ and, therefore, will have a strong discovery power [2]. In particular it will allow to explore energy scales which are far from the ones explored so far and hence to answer some of the unsolved questions of fundamental physics which are at the frontier of the Standard Model (SM). These BSM (Beyond the Standard Model) questions are related for instance to the so-called hierarchy problem and to Higgs physics and their answers will be essential to better understand many interesting aspects of high energy physics.

However, in order to be able to extract informations from the collected data, it is fundamental for the theoretical precision to reach at least the same level of the experimental precision. This is true for both background and new physics signal predictions. Therefore, it is necessary to reduce the theoretical uncertainties using the currently available tools and to think of new ones.

The main model adopted to compute predictions for hadron collider processes is Quantum Chromodynamics (QCD). This is not surprising since it describes strong interactions which are the most important ones between hadrons like those colliding, for instance, at the large hadron collider. There are, of course, other relevant interactions, such as Electroweak (EW) ones, which happen in a typical hadron collider event but they have a less important impact on the predictions, since it can be stated roughly that $\alpha_{\text{EM}} \sim \alpha_s^2$, and in this thesis they will never be considered.

Quantum Chromodynamics is the quantum field theory of hadron constituents, quarks and gluons, and it is very similar to Quantum Electrodynamics (QED), that is the model which describes electromagnetic interactions, even if they differ from each other in two main aspects. The first one is that QCD is a non-abelian gauge theory and this implies several important features which are completely new with respect to QED. The second one is asymptotic freedom: the strong coupling, α_s, tends to zero when the energy scale of the process grows. This last property, which is actually a consequence of the non-abelianity, ensures the possibility to safely use perturbation theory to get reliable predictions for hadron collider processes, thanks to the high value of the energy reached by the colliders. In Chapter 1 QCD is analyzed in more details.

However, there are two main complications. The first one is that the internal dynamics of the hadrons which collide with each other is intrinsically at low-energy. In fact, its typical energy scale is of the order of the hadron mass, which is, usually, several order of magnitude smaller than the centre-of-mass energy of the collider. This means that it is not possible to apply perturbation theory to describe their internal structure and so an important theoretical ingredient is not computable.

A solution to this problem was found in the late 1960s by Richard Feynman who proposed the so-called parton model, on which the currently used improved parton model is based [3]. In Chapter 1, also this aspect of how modern predictions are computed is analyzed in detail. For the sake of completeness it is necessary to mention that there is another technique, called lattice QCD, which is based on space-time discretization and that is able, in principle, to describe low-energy objects. However, this approach is not suitable in every context and, in particular, to apply it to an LHC process, there would be required about 4×10^8 lattice units for each direction, too much for the currently available computing resources [4].

The second complication is that, in certain conditions, usually when the process in computation involves more than one energy scale, in the perturbative series powers of logarithms of energy scale ratios appear. These log terms, in certain kinematic regions, can be large and are responsible for making terms belonging to different perturbative orders of same size. Clearly, in this condition, the truncated perturbative series is no more predictive because the retained terms and the neglected terms are of comparable size. A possible solution is to resum these logarithms to all orders and this is done with different techniques depending on the nature of the considered log terms. In this thesis, only the so-called collinear logarithms (or mass logarithms), coming from gluon splittings in two quarks in the limit in which they are collinear, will be analyzed, but there are also other interesting cases. For instance, when looking to transverse momentum q_T differential cross-sections, logarithms of q_T appear in the perturbative series and they become large in the soft limit, i.e. when q_T tends to zero, causing the same problem of the collinear logarithms. In Chapter 3, the method by which collinear logarithms can be resummed to all orders and a reliable prediction can be obtained in a wide range of the phase space is presented.

For definiteness, such a method is applied to a real process: deep-inelastic scattering (DIS). This process has been chosen because experimentally it is clean, in the sense that it is relatively easy to reconstruct one of its event, and theoretically it is very well known. It consists in a hadron to lepton scattering with high momentum transfer, which implies that the internal structure of the initial state hadron can break down and form new hadrons in the final state. Moreover, in order to underline the impact of the proposed procedure to predictions, only a specific set of the possible DIS events will be considered: the set in which heavy quarks are produced. In fact, looking to heavy quark production, the impact of resumming log of heavy quark masses will be more evident. Clearly, for a quark to be heavy or light is a matter of convention and it depends on the energy scale to which its mass is being compared. In the context of DIS, the up, down, strange and charm (u,d,s,c) quarks are usually considered as light, even if the charm case is actually borderline, while the bottom (b) is usually considered as heavy because the typical energy scale of a DIS process is of the order of some GeV, higher than the first four quark masses ($m_u \approx 2\,\text{MeV}$, $m_d \approx 5\,\text{MeV}$, $m_s \approx 100\,\text{MeV}$ and $m_c \approx 1\,\text{GeV}$) but lower than the b mass ($m_b \approx 5\,\text{GeV}$). Regarding the top quark (t), it is very heavier than the others ($m_t \approx 170\,\text{GeV}$) and so it can be usually completely neglected, as explained in more detail in Chapter 1. In Chapter 2, some important notions about deep-inelastic scattering will be provided, including the observables that are usually computed, and the adopted notation will be clarified.

The main goal of this thesis is to construct a scheme which provides a reliable prediction in the two relevant kinematic regions, the one in which the energy scale is similar to the heavy quark mass and the one in which it is higher. In order to achieve this result, it is not enough to use the resummation technique mentioned above, but it is necessary to include the bottom mass effects, essential for the first kinematic region. In literature there are already examples of this kind of schemes, such as

FONLL [5], ACOT [6, 7] and TR [8], which are equivalent to all orders [9], but differ from each other in how the perturbative series is truncated. In Chapter 4 the general method will be explicitly applied to some DIS observables and the proposed perturbative counting will be shown and justified. In Chapter 5 the numerical results will be presented, including several side results which are part of an in-depth study of the proposed scheme consequences.

The complete road map of the thesis is then the following:

- In Chapter 1 the fundamental aspects of Quantum Chromodynamics (QCD) will be recalled, emphasizing the ones which will be used in the rest of the thesis. In particular, after having introduced the lagrangian of the model and its group structure, the attention will be devoted to the renormalization group equation (RGE) and to one of its main consequences: the running coupling. Then, the fundamental aspects of perturbative QCD will be recalled and the improved parton model, which is the extension of the Feynman parton model including QCD corrections, will be presented. Finally, for the sake of the comprehension of the next chapters, an overview of different renormalization schemes will be provided, including some details on how some quark flavours can be considered inactive.

- In Chapter 2 the deep-inelastic scattering process will be analyzed in detail. After some generalities on the process, the focus will be directed on the heavy quark production channel and on its perturbative counting. At the end of the chapter, an explicit calculation of the leading perturbative order will be carried out, in such a way to explicitly show how the logarithm terms arise, whose resummation will be addressed in the following chapter.

- In Chapter 3 the proposed methodology to solve the large logarithms problem will be presented. The procedure will be as general as possible, despite the fact that, for the sake of clarity, it will be applied to DIS. However, the obtained expressions will always be at all orders, in such a way to show that they are equivalent to the ones obtained by the other schemes available in literature. This feature is mandatory since observables have to be scheme independent and so they can differ from each other only if the perturbative series is truncated at a certain finite order. The details on which pertubative counting is applied in this thesis and on how it differs from the one adopted by the other schemes, will be provided in Chapter 4. The latter will also contain the explicit final expressions that are implemented in the following chapter.

- In Chapter 5 the obtained numerical results will be presented and they will be compared with the results obtained following the FONLL prescription. It will be shown that following the proposed methodology, the numerical results improve both in smoothness (there are less pronounced discontinuity) and from an uncertainty point of view.

Chapter 1

Elements of Quantum Chromodynamics

In this chapter, Quantum ChromoDynamics (QCD), the model that is currently used to describe the strong interactions happening inside the hadrons, is described in some details. QCD was first introduced in the 1960s and, since then, its predictive power was confirmed by many experiments, making it the main tool for the computation of theoretical predictions at the hadron colliders.

It is the theory of quarks, gluons and their interactions and it is a gauge theory, like Quantum Electrodynamics (QED). It bears also other similarities to QED, for instance, as electrons carry the electric charge, the quarks carry the QCD charge, called color. However, while there is only one kind of electric charge, color comes in three versions, sometimes called red, green and blue. Also, the gluon is not color neutral, unlike the photon which does not carry an electric charge. Actually, the gluon can be though of as carrying both color and anti-color charges, for a total of eight different combinations. All these differences and many others are linked to the fact that, although QCD and QED are both gauge theories, QCD is non-abelian. This is a fundamental difference which is responsible for many important feature in QCD that are not present in QED, as it is shown in the next sections.

Another major difference between QCD and QED is the coupling. The strong coupling α_s tends to zero quite fast at high energy scales (this property is often called asymptotic freedom), while the electromagnetic coupling α_{EM} grows as the energy scale increases. At LHC energy, its value ranges between $\alpha_s = 0.08$ at a scale of 5 TeV, which is thus an energy scale suitable for the application of perturbation theory, to $\alpha_s \approx 1$ at 0.5 GeV. Its high value at low-energy is responsible for the possibility of quarks to aggregate and form color neutral physical states, the hadrons, (this property is often called confinement) but clearly deprives perturbation theory of the capability of making predictions at such low energies. In order to solve this problem, the modern predictions for scattering at high energy are computed using the improved parton model, which is based on the original parton model designed by Feynman but improved with the addition of QCD corrections.

In the following sections, every point that was mentioned in this introduction will be analyzed in detail. In particular, in Section 1.1 the QCD lagrangian and its symmetries will be recalled, in Section 1.2 the fundamental aspects of perturbative QCD will be derived focusing on divergences treatment and in Section 1.3 the parton model and its extension to QCD corrections will be analyzed in some details. However, this chapter will clearly not be a complete treatment of every topic of QCD, which can be found for instance in [3, 4], but rather an introduction on every

QCD aspect which will be relevant for the rest of the thesis.

1.1 Lagrangian and group structure

The fields entering the QCD Lagrangian are the quark fields, ψ_a, which are spinors (since quarks are fermions) that carry the color index a ranging from 1 to 3, and the gluon fields, $\mathcal{A}^C_\mu$, which are vector fields that carry the color index C ranging from 1 to 8. The theory is constructed to be gauge invariant under local $SU(3)$ symmetry group, i.e. invariant under the field transformations

$$\begin{aligned} \psi_a &\to e^{i\theta^C(x)t^C_{ab}}\psi_b \\ \mathcal{A}^C_\mu t^C &\to e^{i\theta^D(x)t^D}\left(\mathcal{A}^C_\mu t^C - \frac{1}{g_s}\partial_\mu\theta^C(x)t^C\right)e^{-i\theta^E(x)t^E}, \end{aligned} \tag{1.1}$$

where $\theta^C(x)$ are eight arbitrary real functions of the space-time position x, t^C are the eight $SU(3)$ group generators, the index μ is a Lorentz index and, as in the rest of this thesis, the repeated indices have to be understood as if it were summed over them, following the Einstein notation.

In equation 1.1, the flavour index has been kept implicit, as it will be done in the rest of this chapter. The quark flavours are six and they can be grouped in three families depending on their physical masses and electric charges. The up (u) and the down (d) quarks belong to the first family. They are the lighter of the six ($m_u \approx 2\,\text{MeV}$ and $m_d \approx 5\,\text{MeV}$) and their electric charges are respectively $e_u = 2/3$ and $e_d = -1/3$. The other two families follow the same electric charge structure but the quark masses grow a lot: the charm (c) and the strange (s), belonging to the second family, have masses $m_c \approx 1\,\text{GeV}$ and $m_s \approx 100\,\text{MeV}$, while the top ($t$) and the bottom ($b$) reach the masses $m_t \approx 170\,\text{GeV}$ and $m_b \approx 5\,\text{GeV}$. The physical reason why there are more than one essentially equivalent quark families is currently not known and it is also not known if others families exist. Although this may seem a fundamental lack of the theory, it does not affect the predictions which nowadays can be validated by experiments. This is a very relevant aspect from the point of view of this thesis and it will be analyzed in detail in 1.2.1.

From equation 1.1, it is also possible to notice that quark fields transform with the fundamental representation of $SU(3)$, while the gluon fields with the adjoint representation, except for the fact that the parameters $\theta^C(x)$ are not constants but are function of the space-time coordinate x. Requiring the invariance of the theory under a local group transformation is the standard procedure to construct a gauge theory like QCD and QED.

The $SU(3)$ group generators t^C are hermitian matrices which have to follow the so-called Lie algebra of the group

$$[t^A, t^B] = if^{ABC}t^C, \tag{1.2}$$

where on the left hand side there is the commutator between the generators and, on the right hand side, f^{ABC} is a completely antisymmetric tensor whose entries are called structure constants of $SU(3)$. The fact that f^{ABC} is not identically zero is due to the fact that color $SU(3)$ is a non abelian group, i.e. the generators do not necessarily commute with each other. Equation 1.2 holds all the informations of the group. Adopting the Gell-man convention

$$\text{Tr}(\text{t}^\text{A}\text{t}^\text{B}) = \text{T}_\text{R}\delta_\text{AB} \quad \text{T}_\text{R} = \frac{1}{2}, \tag{1.3}$$

where Tr is the trace operator, it is possible to find the explicit form of the generators in the fundamental representation

$$t^1 = \frac{1}{2}\begin{pmatrix}0&1&0\\1&0&0\\0&0&0\end{pmatrix}\ t^2 = \frac{1}{2}\begin{pmatrix}0&-i&0\\i&0&0\\0&0&0\end{pmatrix}\ t^3 = \frac{1}{2}\begin{pmatrix}1&0&0\\0&-1&0\\0&0&0\end{pmatrix}\ t^4 = \frac{1}{2}\begin{pmatrix}0&0&1\\0&0&0\\1&0&0\end{pmatrix}$$
$$t^5 = \frac{1}{2}\begin{pmatrix}0&0&-i\\0&0&0\\i&0&0\end{pmatrix}\ t^6 = \frac{1}{2}\begin{pmatrix}0&0&0\\0&0&1\\0&1&0\end{pmatrix}\ t^7 = \frac{1}{2}\begin{pmatrix}0&0&0\\0&0&-i\\0&i&0\end{pmatrix}\ t^8 = \frac{1}{2\sqrt{3}}\begin{pmatrix}1&0&0\\0&1&0\\0&0&-2\end{pmatrix}. \tag{1.4}$$

From this explicit representation of the generators, it is possible to notice that there are two diagonal matrices, t^3 and t^8. Being diagonal, one of them commutes with the other, hence the rank of $SU(3)$ is 2 (in general for $SU(N)$ the rank is $N-1$). This is relevant because the rank is equal to the number of the Casimir of the group, which in turn are linked to important properties of the particles. In particular in $SU(3)$, t^3 is related to strong isospin and t^8 to strong hypercharge. Thanks to this properties, it is possible to classify the particles belonging to the different representations of the group.

The generators of the adjoint representation, which is the one implementing the gluon field transformation, are instead defined as

$$(T^A)^{BC} = -if^{ABC}, \tag{1.5}$$

which correctly are matrices of dimension 8.

In QCD computations there are some color related quantities which usually appear in the cross-sections. In particular, when quarks are involved one recurring combination is

$$\sum_A t^A_{ab} t^A_{bc} = C_F \delta_{ac}, \quad C_F = \frac{N^2-1}{2N} = \frac{4}{3}, \tag{1.6}$$

while, when only gluons are involved,

$$\mathrm{Tr}(\mathrm{T^A T^B}) = \mathrm{C_A}\delta^{\mathrm{AB}}, \quad \mathrm{C_A = N} = 3 \tag{1.7}$$

often recurs, where $N = 3$ for $SU(3)$.

From what has been discussed so far, it should be clear that the group structure of QCD is very rich but, in the context of this thesis, the provided details are more than enough to ensure the understanding of the next chapters. For this reason, the focus of the discussion will be now devoted to the lagrangian of the theory, from which it is possible to extract Feynman rules that will be important for the next chapter.

The QCD Lagrangian can be written as

$$\mathcal{L}_{QCD} = \mathcal{L}_q + \mathcal{L}_G + \mathcal{L}_{\text{quantum}}, \tag{1.8}$$

where $\mathcal{L}_q$ is the quark part, $\mathcal{L}_G$ the purely gluonic part and $\mathcal{L}_{\text{quantum}}$ has to be added to correctly quantize the theory. The quark part can be written as

$$\mathcal{L}_q = \overline{\psi}_a (i \not{D}_{ab} - m\delta_{ab})\psi_b, \tag{1.9}$$

where

$$\not{D}_{ab} = \gamma^\mu \partial_\mu \delta_{ab} + i g_s \gamma^\mu t^C_{ab} \mathcal{A}^C_\mu \tag{1.10}$$

is called covariant derivative and it is used in place of the standard derivative to promote the global $SU(3)$ symmetry to the local one of eq. (1.1). The covariant derivative has an extra piece with respect to the standard derivative which is responsible for the interactions between quarks and gluons. As it is possible to see from eq. (1.10), these interactions are not diagonal in the color and this means that when a gluon interacts with a quark, it, in general, changes its color.

The second part contains the dynamics and the interactions of the gluons with themselves. Defining the field-strength tensor as

$$F^A_{\mu\nu} = \partial_\mu \mathcal{A}^A_\nu - \partial_\nu \mathcal{A}^A_\mu - g_s f^{ABC} A^B_\mu A^C_\nu, \tag{1.11}$$

the gluonic lagrangian is

$$\mathcal{L}_G = -\frac{1}{4}\mathrm{Tr}(\mathrm{F}_{\mu\nu}\mathrm{F}^{\mu\nu}), \tag{1.12}$$

where the trace operator is applied on the color index. It is important to notice that the term $g_s f^{ABC} A^B_\mu A^C_\nu$ in eq. (1.11) is one of the major differences with QED. It is caused by the non-abelianity of QCD and it is responsible, as it will be discussed in the next section, for the three and four gluons vertices, which have no counterparts in QED.

The combination of the field-strength tensor in eq. (1.12) is the simplest gauge-invariant object that respects also the requirement to be at most of energy dimension 4. This last property is fundamental because it ensures the renormalizability of the theory. However, there is another object that is in principle allowed, namely

$$\mathcal{L}_{CP} = \theta \frac{\alpha_s}{4\pi}\mathrm{Tr}(\mathrm{F}_{\mu\nu}\tilde{\mathrm{F}}^{\mu\nu}), \tag{1.13}$$

where θ is a dimensionless parameter, $\alpha_s = g_s^2/4\pi$ and $\tilde{F}_{\mu\nu} = \frac{1}{2}\epsilon_{\mu\nu\rho\sigma}F^{\rho\sigma}$ with $\epsilon_{\mu\nu\rho\sigma}$ being a pseudo-tensor. The reason why this term is often not considered is that it explicitly violates CP (parity and charge-conjugation) symmetry which experimentally appears to be respected by strong-interactions. This means that either this term has not to be included in the lagrangian or θ is small enough to make CP violation so unlikely to happen that it has not been observed yet. Since this aspect of QCD lagrangian has not a central role in this thesis, that piece will be simply neglected from now on.

The last piece of the lagrangian is not gauge-invariant and has to be added to correctly quantize the theory. In fact, because of the gauge symmetry of the theory, there are redundant degrees of freedom which make canonical quantization not applicable in QCD case. In order to solve this problem, the Faddev-Popov method consists in removing these redundant degrees of freedom adding to the lagrangian the gauge-fixing term

$$\mathcal{L}_{g.f.} = -\frac{1}{2\xi}\sum_A |\partial_\mu \mathcal{A}^\mu_A|^2, \tag{1.14}$$

which forces the theory to be in the so-called ξ-gauge. From this gauge, one can obtain, for instance, the Feynman gauge choosing $\xi = 1$ and the Landau gauge for $\xi = 0$.

However, this method implies the addition of another term to the lagrangian, the ghost term

$$\mathcal{L}_{\text{ghost}} = \overline{\eta}_A \partial_\mu D^\mu_{AB} \eta_B, \tag{1.15}$$

which, together with the gauge-fixing term, completes the quantization part. This term introduces another kind of fields, the ghost fields η, which are complex scalar

fields but obey Fermi statistics. This property make them unphysical and therefore not linked to physical particles but, in order to compute observable quantities, they have, in general, to be considered.

This last paragraph completes the discussion about the main aspects of QCD lagrangian. In the next section the fundamental notions of perturbative QCD will be recalled focusing on divergences treatment, which is a central matter of this thesis, and on the running coupling.

1.2 Perturbative QCD

Perturbation theory, in every field it is applied, consists in writing a certain observable as an order-by-order expansion in a small parameter. In QCD, the standard small parameter is the strong coupling α_s, as in QED is α_{EM}, and so an observable quantity computed in perturbation theory takes the form

$$F = f^{(0)} + f^{(1)}\alpha_s + f^{(2)}\alpha_s^2 + f^{(3)}\alpha_s^3 + \cdots + f^{(n)}\alpha_s^n + \mathcal{O}(\alpha_s^{n+1}), \tag{1.16}$$

where the perturbative series is truncated at order α_s^n. Notice the round parenthesis notation that will be adopted in the rest of the thesis.

Clearly, for perturbation theory to be predictive, it is not only necessary that the parameter in which the expansion is performed is actually small, but also that the factors $f^{(i)}$ do not contain terms growing too fast with i. In other words, the necessary requirement to make perturbation theory reliable is that $f^{(i)}\alpha_s^i$ is a parametrically descending function in i, and this clearly imposes conditions on both the coupling and the factors.

Regarding the coupling, as mentioned at the beginning of this chapter, in QCD it is a decreasing function of the energy scale of the process. This behaviour is the opposite with respect to the one of the QED coupling and it is caused, as in QED case, by the renormalization of UltraViolet (UV) divergences (some details on the running coupling and on renormalization can be found in sec. 1.2.1). Its value, in the usually observed kinematic regions, can vary up to an order of magnitude, and so it is not always suitable for the application of perturbation theory. Hence, in QCD, there are two separate kinematic regions: the perturbative region, which is roughly above 1 GeV, and the non-perturbative region. This means that it is not possible to make predictions, with the standard techniques, on the low-energy internal dynamics of objects like hadrons and, therefore, on processes involving them. However, thanks to the Feynman parton model it is possible to overcome this problem to make predictions on hadron initiated processes, at LHC for instance, even if many aspects of their structure remain unknown. Parton model is a rather central aspect of this thesis and it will be the main argument of section 1.3.

Regarding the coefficients $f^{(i)}$, the main way of calculating them is through the use of Feynman diagrammatic techniques. From the QCD lagrangian of the previous section, it is possible to obtain the so-called QCD Feynman rules (fig. 1.1) from which the Feynman diagrams linked to the coefficients $f^{(i)}$ can be computed. Notice that, the second and the third rule in fig. 1.1 are exactly given by the last term of eq. (1.11) and so they are, as mentioned in the previous section, one of the main differences between QCD and QED.

Once computed the coefficients $f^{(i)}$, it may happen that, when their calculation involves more than one energy scale, some logarithms of the ratio of those energy scales appear. Therefore, in some kinematic regions, these log terms can be large and, depending on the power to which they are raised, can make the factors $f^{(i)}$ too

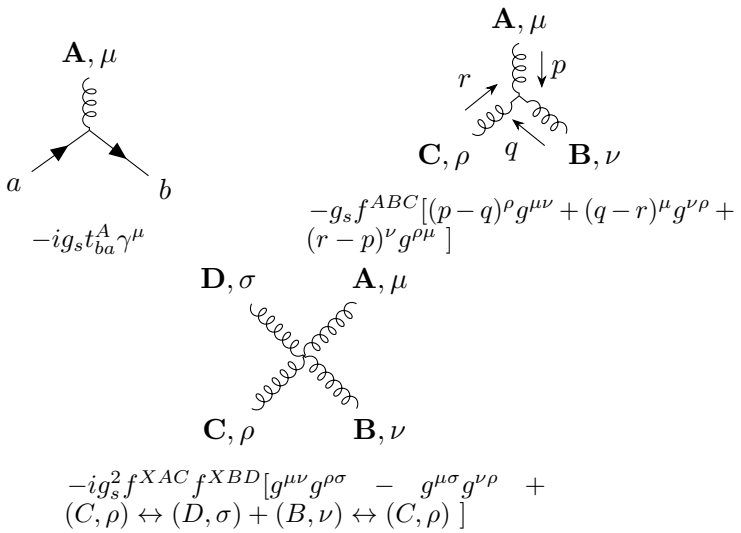

Figure 1.1. Interactions vertices of the Feynman rules of QCD

large for the application of perturbation theory. Clearly, perturbation theory is not simply either applicable or not applicable. In some cases, and the one faced in this thesis is one of them, the perturbative series is quite predictive despite the presence of the log terms but, resumming them to all orders, is a correction which increases the precision.

In this thesis, only the collinear logarithms will be considered. They come from the phase-space integration of $g \to q\overline{q}$ splitting in the limit in which the final quarks become collinear. If the final quarks are heavy, so their masses are considered different from zero, the logarithms take the form $\log^k m_q^2/Q^2$, where m_q is the mass of the quarks (and that is why they are also called mass logarithms), Q is the hard energy scale of the process and the power k is less or equal to the perturbative order i of the coefficient $f^{(i)}$ in computation. If, instead, the quarks are light, the collinear logarithms become InfraRed (IR) collinear divergences which have to be regularized, for instance, with dimensional regularization. In Chapter 2 an example of both the massless and the massive case in a DIS calculation is provided in order to explicitly show the origin of the collinear logarithms and divergences. In 1.2.2 their origin and the way in which they are regularized are presented, including a more general discussion on other kinds of IR divergences.

1.2.1 UV divergences: renormalization group equation and running coupling

Computing a quantity in perturbation theory at an order higher than leading order, the phase-space integrals, in some cases, start to be divergent in both the UV, i.e. high energy, and the IR, i.e. low-energy, regions. There are different ways to deal with these divergences depending on their nature. In this and in the next sections the main aspects of their regularization will be analyzed, focusing on the most relevant ones for this thesis. However, for a detailed description of these techniques one may refer to [10, 11].

The standard procedure to regularize UV divergences is renormalization. It basically consists in redefining both the fields and the constant terms, like the coupling, in the lagrangian in such a way to make them absorb the infinities. In the

QCD case this means to rescale the quark and the gluon fields, the quark masses and the coupling in this way

$$\psi^b = \sqrt{Z_2}\psi, \quad \mathcal{A}^b = \sqrt{Z_3}\mathcal{A}, \quad m^b = \frac{Z_m}{Z_2}m, \quad g_s^b = \frac{Z_1}{Z_2\sqrt{Z_3}}g_s, \tag{1.17}$$

where the apex b denotes a bare, i.e. not renormalized yet, quantity and, for the sake of simplicity, the color indices are omitted.

Since in dimensional regularization, which is the standard method used to regularize also IR divergences, the lagrangian is constructed to be of dimension $d = 4 - 2\epsilon$, the energy dimensions of fields and constants change. In particular

$$\begin{aligned} [\psi] &= \frac{d-1}{2} = \frac{3}{2} - \epsilon \\ [\mathcal{A}] &= \frac{d-2}{2} = 1 - \epsilon \\ [g_s] &= d - 2[\psi] - [\mathcal{A}] = \frac{4-d}{2} = \epsilon, \end{aligned} \tag{1.18}$$

which means that, in order to keep working with a dimensionless coupling, one may write

$$\alpha_s^b = \frac{Z_1^2}{Z_2^2 Z_3}\alpha_s \tilde{\mu}^{2\epsilon}, \quad \tilde{\mu}^{2\epsilon} \equiv \frac{\mu^2 e^\gamma}{4\pi} \tag{1.19}$$

where γ is the Euler's gamma and μ is called renormalization scale and it is a fictitious scale in which the energy dimension is retained. The second part of the last equation defines a particular scheme of renormalization called modified minimal subtraction scheme ($\overline{MS}$), which is the most used in modern computations and that will be used in this thesis as well.

Adopting this convention, the Z terms are fixed, order by order in perturbation theory, so that the observables are UV finite. At $\mathcal{O}(\alpha_s)$ they take the form

$$\begin{aligned} Z_2 &= 1 - C_F \frac{\alpha_s}{4\pi}\frac{1}{\epsilon} \\ Z_3 &= 1 + \left[\frac{5}{3}C_A - \frac{4}{3}n_f T_F\right]\frac{\alpha_s}{4\pi}\frac{1}{\epsilon} \\ Z_1 &= 1 - [C_F + C_A]\frac{\alpha_s}{4\pi}\frac{1}{\epsilon} \end{aligned} \tag{1.20}$$

where n_f is the number of flavours and C_F, C_A and $T_F = T_R$ are the color factors that were mentioned in the previous section.

Using these last expressions, it is possible to write the log of the bare coupling as

$$\begin{aligned} \log \alpha_s^b &= \log \frac{Z_1^2}{Z_2^2 Z_3} + \log \alpha_s + \epsilon \log \tilde{\mu}^2 \\ &= \log \alpha_s + \epsilon \log \tilde{\mu}^2 - \frac{1}{\epsilon}\frac{11C_A - 4n_f T_F}{12\pi}\alpha_s + \mathcal{O}(\alpha_s^2) \\ &= \log \alpha_s + \epsilon \log \tilde{\mu}^2 + \frac{G_1(\alpha_s)}{\epsilon} + \frac{G_2(\alpha_s)}{\epsilon^2} + \frac{G_3(\alpha_s)}{\epsilon^3} + \cdots \end{aligned} \tag{1.21}$$

where in the last line the G_i functions are implicitly defined. Since the bare coupling has to be scale independent, it follows that

$$\begin{aligned} 0 &= \mu^2 \frac{d}{d\mu^2} \log \alpha_s^b \\ &= \mu^2 \frac{d}{d\mu^2} \log \alpha_s + \epsilon + \mu^2 \frac{d}{d\mu^2} \alpha_s \left(\frac{G_1'(\alpha_s)}{\epsilon} + \frac{G_2'(\alpha_s)}{\epsilon^2} + \frac{G_3'(\alpha_s)}{\epsilon^3} + \cdots \right) \\ &= \frac{1}{\alpha_s} \left[\epsilon \alpha_s + \mu^2 \frac{d}{d\mu^2} \alpha_s \left(1 + \frac{\alpha_s G_1'(\alpha_s)}{\epsilon} + \frac{\alpha_s G_2'(\alpha_s)}{\epsilon^2} + \frac{\alpha_s G_3'(\alpha_s)}{\epsilon^3} + \cdots \right) \right]. \end{aligned} \tag{1.22}$$

Therefore, requiring the $G_n'(\alpha_s)$ with $n \geqslant 2$ to cancel all the ϵ poles in the $d \to 4$ limit, in such a way to make the renormalized coupling finite in this limit, leads to the renormalization group equation (RGE) of QCD

$$\mu^2 \frac{d}{d\mu^2} \alpha_s(\mu^2) = \beta(\alpha_s(\mu^2)) \tag{1.23}$$

with

$$\beta(\alpha_s(\mu^2)) = -\epsilon \alpha_s - (\beta_0 \alpha_s^2 + \beta_1 \alpha_s^3 + \mathcal{O}(\alpha_s^4)), \tag{1.24}$$

where the coefficients β_i are computed in perturbation theory (they are currently known up to β_4). In particular,

$$\beta_0 = \frac{11 C_A - 4 n_f T_F}{12\pi} = \frac{33 - 2 n_f}{12\pi} \tag{1.25}$$

which is positive for $n_f < 17$. Since, as far as it is currently known, $n_f = 6$, β_0 is negative and this is the reason why the QCD coupling value decreases as the energy scale increases. In fact, the solution of eq. (1.23) at leading order with $d = 4$ reads

$$\alpha_s(\mu^2) = \frac{\alpha_s(\mu_0^2)}{1 + \alpha_s(\mu_0^2) \beta_0 \log \mu^2/\mu_0^2} = \frac{1}{\beta_0 \log \mu^2/\Lambda_{QCD}^2}, \tag{1.26}$$

where $\Lambda_{QCD} \approx 200\,\text{MeV}$ is the Landau pole which is already in the non-perturbative region. For comparison, the RGE for QED is

$$\mu^2 \frac{d}{d\mu^2} \alpha_{EM} = \frac{1}{3\pi} \alpha_{EM}^2 + \mathcal{O}(\alpha_{EM}^3), \tag{1.27}$$

which gives a similar equation to (1.26) but, since in QED case β_0 is positive, α_{EM} grows with the energy scale.

The strong coupling trend as a function of the energy scale is presented in fig. 1.2, where it has been extracted using different degrees of QCD perturbation theory.

To conclude this subject, there is another rather important matter which has to be analyzed: whether to consider the renormalization scale μ to be exactly equal to the energy scale of the considered process Q or not. A similar, but much more relevant, matter will then be addressed regarding the so-called matching scale of the quarks, μ_q, and their masses (chapter 3). In both cases there is not a physical reason to keep them equal but, if they are chosen to be different, log terms of their ratio, $\log \mu^2/Q^2$ or $\log \mu_q^2/m_q^2$, appear in the perturbative series. These log terms become large if the ratio is large and can spoil the accuracy of the perturbative series. Therefore, it is important to keep them of the same order of magnitude or even equal, which is the most common approach. In this thesis project, although we usually take $\mu^2 = Q^2$, the threshold scales will be kept different from the quark masses. The variation of the computed quantities caused by this choice will be used to estimate the theoretical uncertainties, for reasons that will be explained in the following chapters.

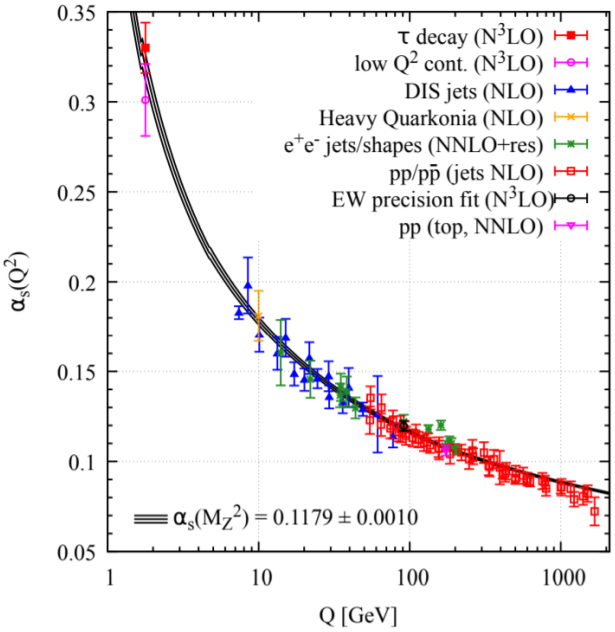

Figure 1.2. Summary of measurements of α_s as a function of the energy scale Q obtained using different degrees of QCD perturbation theory (NLO: $\mathcal{O}(\alpha_s)$; NNLO: $\mathcal{O}(\alpha_s^2)$; NNLO+res.: $\mathcal{O}(\alpha_s^2)$ matched with a resummed calculation; N^{3}LO: $\mathcal{O}(\alpha_s^3)$) [12].

Decoupling theorem and variable flavour number scheme

In the previous section, it has been underlined that the factors Z_i, and thus also the coefficients β_i, contain a dependence on the number of flavours n_f. From the point of view of the $\overline{MS}$ scheme, this number have to include all the existing quark flavours, also the not yet known ones. In fact, the contribution proportional to n_f comes from a quark-bubble correction $\Pi^{\mu\nu}$ to the gluon propagator which can be written as

$$\Pi^{\mu\nu} = (k^2 g^{\mu\nu} - k^\mu k^\nu)\Pi(k^2) \tag{1.28}$$
$$\Pi(k^2) \propto \int_0^1 x(1-x)\left(\frac{1}{\epsilon} - \frac{1}{2}\log\frac{x(1-x)k^2 + m^2 - i0}{\mu^2}\right)dx,$$

where k is the gluon four-momentum and m is the mass of the quark running in the loop. Therefore, the $\overline{MS}$ subtraction of the ϵ pole is independent on the quark mass and so every quark flavour, independently of its mass, has to be considered in n_f. However, this does not make sense because, physically, if a particle is much heavier than the energy scale of the process, its contribution to observables must be negligible (Applequist-Carazzone decoupling theorem [13]). This observation also clarifies the reason why not knowing if other quark families actually exist is not a lack of the theory.

This feature is correctly obtained adopting a different scheme, the so-called decoupling scheme (DS). In this scheme the previous quantity is UV regularized as

$$\Pi(k^2) - \Pi(0) \propto \int_0^1 x(1-x)\left(\frac{1}{2}\log\frac{x(1-x)k^2 + m^2 - i0}{m^2 - i0} + \mathcal{O}(\epsilon)\right)dx, \tag{1.29}$$

where the result correctly vanishes for $m^2 \gg k^2$, i.e. the heavy-quark decouples.

In practice, in order to make n_f be the number of active flavours also in the running coupling, one introduces effective field theories (EFT) where the heavy-quarks, which are heavy or not depending on the considered energy scale, are integrated out of the theory, i.e. they are no more a dynamical degree of freedom of the theory. As a result, the coupling changes its running depending on the renormalization scale. In the following the adopted notation will be that $\alpha_s^{[n]}$ is the coupling renormalized with $n_f = n$.

In the construction of the main result of this thesis (Chapter 4), this matter will play a rather important role. In fact, the EFT approach allows the construction of a variable flavour-number scheme (VFNS) in which, depending on the energy scale of the process, the number of *active* flavours changes. A flavour is considered *active* if participates to the evolutions, i.e. the running coupling and DGLAP (which is presented in sec. 1.3). Adopting a VFNS makes possible to construct reliable predictions on a wide kinematic range, as it will be explained in the next chapters. In this context, it will be necessary to switch from $\alpha_s^{[n_f]}$ to $\alpha_s^{[n_f+1]}$ and this is made possible by the matching equation

$$\frac{\alpha_s^{[n_f+1]}(\mu^2)}{\alpha_s^{[n_f]}(\mu^2)} = 1 + \frac{\alpha_s^{[n_f]}}{6\pi} \log \frac{\mu^2}{m_{n_f+1}^2} + \mathcal{O}(\alpha_s^2). \tag{1.30}$$

This equation provides the relation between the couplings in the two schemes so, using it, one is free to choose whether to expand an observable in $\alpha_s^{[n_f]}$ or in $\alpha_s^{[n_f+1]}$.

1.2.2 IR divergences: soft and collinear

The other kind of divergences one may encounter computing a QCD observable is the IR one. They come from the low-energy region of phase-space integrals and can be of two kinds: soft, which is linked to the low-energy of the particle, and collinear, which is linked to the collinearity between emitted and emitting particles. Either of them can come from initial or final state particles and the way in which they are regularized is very different in these two cases.

The reason of this difference in the regularization process relies in the following two theorems [14]:

1. Bloch-Nordsieck theorem: IR singularities cancel between real and virtual diagrams when summing up all resolution-indistinguishable final states at a certain perturbative order.

2. Kinoshita-Lee-Nauenberg theorem: mass singularities ($m \to 0$) of external particles (i.e. both initial and final) are cancelled if all mass-degenerate states are summed up.

The first theorem ensures the cancellation of both collinear and soft final-state divergences if one combine all the virtual and real diagrams belonging to a certain perturbative order. However, it is important to clarify what it means resolution-indistinguishable final states. The point is that the real diagrams, which have to be added to the virtual ones, contain extra real emissions of QCD particles. Therefore, in principle, they have not the same final state and so they should not be considered together. However, the crucial observation is that, both in the soft and in the collinear limit, the real-emission process becomes experimentally (and theoretically) indistinguishable from the no-emission one and this justifies considering them together.

From the second theorem it is clear that, since summing over the initial degenerate states is not what it is usually done, it is not guaranteed that the initial-state divergences cancel. However, it is possible to show that the soft ones cancel also in the initial state. The conclusion is that only the collinear initial-state divergences remain. For them, a different way of regularization is needed.

In order to clarify this discussion and to introduce the way in which collinear initial-state divergences are regularized, it is advisable to show an example. Consider the two processes in fig. 1.3 in which the bubble σ_0 represent the cross-section of a certain hard-process. In the first diagram the gluon-emission is final with respect to the hard process, while in the second diagram the emission is on the initial state.

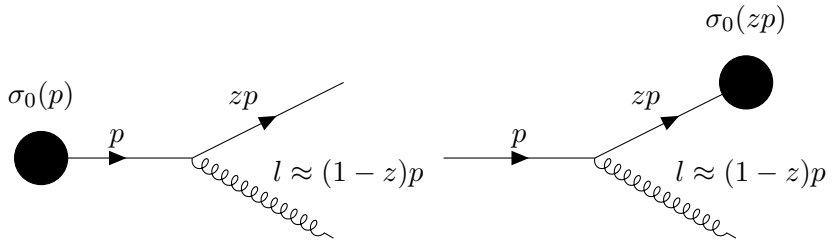

Figure 1.3. Initial and final state gluon emission. Notice that the final state emission does not alter the kinematic of the hard process represented by the bubble σ_0.

Let's focus the attention on the initial state one. Its amplitude can be written as

$$\mathcal{A}_1 = g_s \mathcal{M}_b(p-l)\frac{\not{p} - \not{l}}{(p-l)^2}\gamma^\mu u(p)\epsilon^A_\mu(l)t^A_{ab}, \tag{1.31}$$

where p is the initial quark momentum, $\mathcal{M}_b$ is the amplitude of the bubble and $\epsilon^A_\mu(l)$ is the polarization vector of the emitted gluon. The four-momentum of the gluon l can be parametrized with the so-called Sudakov parametrization. Orienting the spacetime in such a way that $p = p^0(1, 0_\perp, 1)$ and introducing $\overline{p} = p^0(1, 0_\perp, -1)$, it can be written as

$$l = (1-z)p + l_\perp + \xi\overline{p}, \quad \xi = \frac{|l^2_\perp|}{2(p\cdot\overline{p})(1-z)}, \tag{1.32}$$

where the ξ value comes from the on-shell condition $l^2 = 0$. In this parametrization, z represents the longitudinal momentum fraction that is left to the quark (so $(1-z)$ is the part retained by the gluon), $l_\perp$ is the transverse momentum of the gluon and ξ is necessary to respect the on-shell condition. The reason why the Sudakov parametrization is convenient to show divergences regularization is that it makes very explicit the soft and the collinear limits, which are, respectively, $z \to 1$ and $l_\perp \to 0$.

The phase-space for the gluon emission is then given by

$$d\phi = \frac{d|l_\perp|}{(2\pi)^2}\frac{dz}{1-z}, \tag{1.33}$$

which gives, without entering too much in the details of the calculation (which can be found for instance in [15]), the real-emission contribution to the cross-section

$$\sigma_1^{\text{real}}(p) = \int \frac{d|l^2_\perp|}{|l^2_\perp|}\int dz C_F \frac{1+z^2}{1-z}\frac{\alpha_s}{2\pi}\sigma_0(zp). \tag{1.34}$$

Notice that only the singular part in the soft and collinear limits have been written and it has been used the fact that in these limits $(p-l) \approx zp$.

The singular part of the virtual contribution can be written as [15]

$$\sigma_1^{\text{virt}}(p) = -\sigma_0(p) \int \frac{d|l_\perp^2|}{|l_\perp^2|} \int dz C_F \frac{1+z^2}{1-z} \frac{\alpha_s}{2\pi}, \tag{1.35}$$

which, put together with the real one, gives the total singular cross-section

$$\begin{aligned} \sigma_1(p) &= \frac{\alpha_s}{2\pi} \int \frac{d|l_\perp^2|}{|l_\perp^2|} \int dz C_F \frac{1+z^2}{1-z} [\sigma_0(zp) - \sigma_0(p)] \\ &= \frac{\alpha_s}{2\pi} \int \frac{d|l_\perp^2|}{|l_\perp^2|} \int dz C_F \left(\frac{1+z^2}{1-z} \right)_+ \sigma_0(zp), \end{aligned} \tag{1.36}$$

where the definition of the so-called plus-distribution is

$$\int_0^1 dz f(z)[g(z)]_+ \equiv \int_0^1 [f(z) - f(1)]g(z). \tag{1.37}$$

From eq. (1.36) it is clear that the virtual contribution regulates the soft divergence in $z = 1$, while the collinear divergence is still present. This behaviour is exactly the expected one for the initial state splittings, as anticipated at the beginning of this section. Moreover, from eq. (1.36) it is easy to derive the singular expression of the other diagram of fig. 1.3, i.e. the one with the splitting in the final state. In fact, the computation is identical except for the fact that the bubble-momentum remains p instead of becoming zp. In this way, it is clear that the singular part vanishes identically and so both the soft and the collinear divergences cancel. Also this behaviour is exactly what it was expected and its reason is now clear: the final state radiation does not change the kinematics of the hard process, while the initial-state one does.

In the computation above, the actual process was not specified. It can be shown that only the non-singular part of the cross-section is process-dependent, while the singular-part is completely universal. In particular, it has been found that a quark emitting a gluon introduces a collinear divergence proportional, at $\mathcal{O}(\alpha_s)$, to the so-called quark-quark splitting function

$$P_{qq} = \frac{\alpha_s}{2\pi} C_F \left(\frac{1+z^2}{1-z} \right)_+ + \mathcal{O}(\alpha_s^2). \tag{1.38}$$

The other splitting functions come from the computation of other kinds of splitting, specifically a gluon remaining a gluon (P_{gg}), a gluon becoming a quark (P_{qg}) and a quark becoming a gluon (P_{gq}). It is important to underline that, although the splitting functions are process-independent, they are not scheme independent. In this thesis only their $\overline{MS}$ version,

$$\begin{aligned} P_{gg} &= \frac{\alpha_s}{4\pi} \left(4C_A \left[\frac{z}{(1-z)_+} + \frac{1-z}{z} + z(1-z) \right] + \frac{11C_A - 4T_F n_f}{6} \delta(1-z) \right) + \mathcal{O}(\alpha_s^2) \\ P_{qg} &= \frac{\alpha_s}{2\pi} n_f [z^2 + (1-z)^2] + \mathcal{O}(\alpha_s^2) \\ P_{gq} &= \frac{\alpha_s}{2\pi} C_F \frac{1+(1-z)^2}{z} + \mathcal{O}(\alpha_s^2), \end{aligned} \tag{1.39}$$

will be used.

The universality of the splitting functions is the main concept on which the factorization method is based. It is the way in which the collinear divergences are regularized and it plays a central role in this thesis. However, in order to understand how it works, it is necessary to firstly introduce the Feynman parton model. Therefore, its presentation is delayed to section 1.3.1.

1.3 Parton Model

From section 1.2, it should be clear that computing a cross-section of an hadron-initiated process from first-principles only is impossible in standard perturbation theory. The reason is that, even if the centre-of-mass energy is high enough to be in the perturbative region of QCD, the hadrons themself are intrinsically low-energy objects and thus their internal structure is governed by non-perturbative dynamics.

The first solution to this problem was the parton model, conceived by Richard Feynman in the late 1960s. Its basic concept is to factorize the cross-section of an hadron-initiated process in two parts, the cross-section of the high-energy process occurring between the partons (i.e. the quarks and the gluon), called partonic cross-section, and in a process-independent part representing the probability distribution of extracting a certain parton from the hadron. In this way the first part can be computed in perturbation theory, but a method to compute the second part, called parton-distribution function (PDF), is still needed. However, the central argument is that the PDFs can be fitted from data and, once obtained from a certain process, being process-independent, they can be used for all the other processes. In this context, it is worth mentioning that, currently, the most used process for PDF determination is DIS and this is another motivation to apply to it the results of this thesis.

For a process with a single hadron in the initial state, like deep-inelastic scattering, the parton model takes the form

$$\sigma(Q^2) = \sum_q \int_0^1 f_q(x) C_q(x)\, dx + \mathcal{O}\left(\frac{Q^2}{\Lambda^2_{QCD}}\right), \tag{1.40}$$

where C_q are the partonic cross-sections, called coefficients functions in DIS case, f_q is the PDF of the parton q, x is the fraction of the hadron momentum carried by the parton and Q is the energy scale of the process.

The parton model formula of eq. (1.40), as it has been written explicitly, is valid up to corrections of the order Q^2/Λ^2_{QCD}, hence only for energy scales which are in the perturbative region of QCD. From a formal point of view, this has been fully proved only for DIS, but, nevertheless, the parton model is currently used for every QCD process. The graphical interpretation of eq. (1.40) is in fig. 1.4b (which has been applied to the DIS case), while fig. 1.4a represents the two initial hadrons version.

However, this model is only valid at leading order (LO) because it does not include radiative QCD corrections. Including them results in the so-called improved parton model that allows the computation of observables beyond the LO but deprives the PDFs of their probability distribution interpretation. The form of the improved parton model for DIS is

$$\sigma(Q^2, x) = \sum_q \int_0^1 dz \int_0^1 dy f_q(y, \mu_F^2) C_q(z, \frac{\mu_F^2}{Q^2}) \delta(x - zy) + \mathcal{O}\left(\frac{Q^2}{\Lambda^2_{QCD}}\right), \tag{1.41}$$

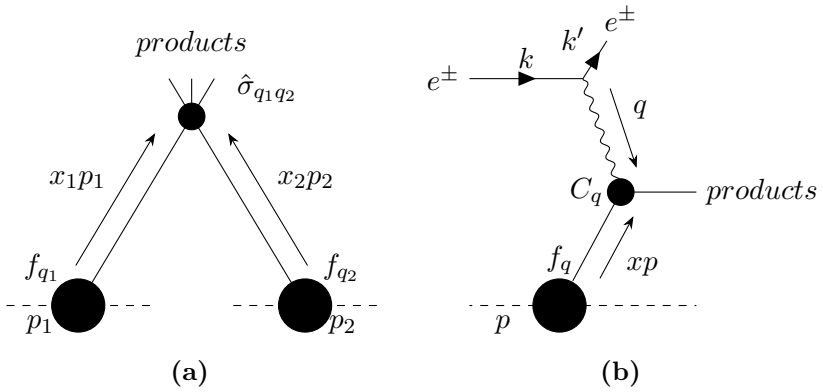

Figure 1.4. Graphical version of the LO parton model formulas applied in both the two initial hadrons (a) and the single-initial hadron (b) cases. The bubbles $\hat{\sigma}$ represent the partonic cross-sections, the other bubbles are the initial hadrons and the f_{q_i} are the PDFs.

where $Q^2 \equiv -q^2$ in DIS case, with q the photon four-momentum, and $x = Q^2/2\nu$, with $\nu = p \cdot q$, is the Bjorken's scaling variable. The energy scale μ_F is called factorization scale and, for the same reason of the renormalization scale, it has to be equal or of the same order of magnitude of the energy scale of the process Q. The graphical interpretation of eq. (1.41) is in fig. 1.5. Using the facts that

$$\delta(zy - x) = \frac{1}{|y|}\delta\left(z - \frac{x}{y}\right) \tag{1.42}$$
$$\int_0^1 dz = \int_{-\infty}^{+\infty} dz(\theta(z)\theta(1-z)),$$

where $\theta(x)$ is the step function which is equal to 1 when its argument is positive and otherwise is 0, one can obtain the expression

$$\sigma(Q^2, x) = \sum_q \int_x^1 \frac{dy}{y} f_q\left(\frac{x}{y}, Q^2\right) C_q(y, Q^2) + \mathcal{O}\left(\frac{Q^2}{\Lambda^2_{QCD}}\right), \tag{1.43}$$

where the factorization scale μ_F has been taken equal to Q. This last equation is the one that will be used in the rest of this thesis.

Beyond the LO, the coefficients functions C_q, as discussed in sec. 1.2.2, contain unregularized IR collinear divergences. However, the PDFs, deprived of their distribution function interpretation, can contain that kind of divergences as well. Therefore, in order to obtain a final finite result from eq. (1.43), the PDFs are assumed to contain IR divergences in a way that compensates the ones contained in the coefficients functions. This is the basic idea of the collinear factorization method, as explained in detail in the following section.

For completeness, the parton model form in the two initial hadrons case is

$$\sigma(Q^2) = \sum_{q_1 q_2} \int_0^1 dx_1 f_{q_1}(x_1, \mu_F^2) \int_0^1 dx_2 f_{q_2}(x_2, \mu_F^2) \hat{\sigma}_{q_1q_2}(x_1p_1, x_2p_2, \frac{\mu_F^2}{Q^2}) + \mathcal{O}\left(\frac{Q^2}{\Lambda^2_{QCD}}\right), \tag{1.44}$$

where f_{q_i} is the PDF of the parton q_i, p_i are the four-momentum of the initial hadrons, x_i is the fraction of the momentum of the hadrons carried by the parton q_i and $\hat{\sigma}_{q_1q_2}$ is the partonic cross-section of the process occuring between q_1 and q_2.

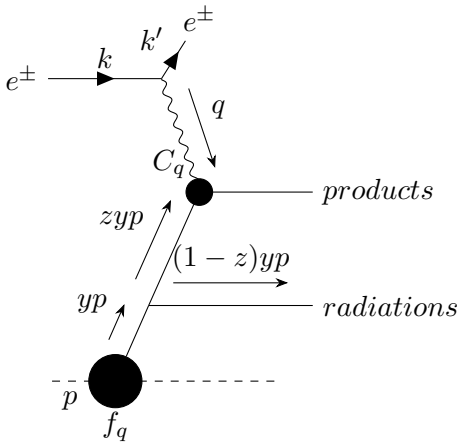

Figure 1.5. Graphical interpretation of the improved parton model applied to the DIS case. The difference from its LO version is the presence of QCD radiations which decrease the momentum of the interacting parton in C_q with respect to the parton extracted from the proton.

1.3.1 Collinear factorization

The Collinear factorization is the method in which the initial state collinear IR divergences are regularized in QCD and it is based on the factorization theorem [16, 17, 18]. Denoting with $\bar{C}_i$ the coefficients functions which still contain the IR singular terms, the theorem, in dimensional regularization, can be written as

$$\bar{C}_i(x, \alpha_s, \epsilon) = \int_x^1 \frac{dz}{z} C_j(\frac{x}{z}, \alpha_s, \epsilon)\Gamma_{ij}(z, \alpha_s, \epsilon), \tag{1.45}$$

where C_i are the IR regularized coefficients functions and the Γ_{ij} terms are called collinear counter-terms and contain the divergent terms. They are both scheme dependent and, in this thesis, their $\overline{MS}$ version will be adopted.

Defining the Mellin transform of a quantity $f(z)$ as

$$f(N) \equiv \int_0^1 dz z^{N-1} f(z), \tag{1.46}$$

the factorization theorem can be equivalently written in Mellin space as

$$\bar{C}_i(N, \alpha_s, \epsilon) = C_j(N, \alpha_s, \epsilon)\Gamma_{ji}(N, \alpha_s, \epsilon), \tag{1.47}$$

where the convolution of eq. (1.45) became a product. This property is the reason why the following expressions will be often written in Mellin space.

The meaning of these last expressions is that it is possible to factorize the universal collinear singularities, i.e. not process-dependent (sec. 1.2.2), contained in Γ_{ij}, from the bare coefficients functions in such a way the remaining parts, C_i, are IR finite. Notice that, from the calculations in sec. 1.2.2, the $\mathcal{O}(\alpha_s)$ expression of Γ_{ij} has already been found and it reads, in $\overline{MS}$,

$$\Gamma_{ij}(z, \alpha_s, \epsilon) = \delta_{ij}\delta(1-z) - \frac{\alpha_s}{\epsilon} P_{ji}^{(0)}(z) + \mathcal{O}(\alpha_s^2), \tag{1.48}$$

where the ϵ pole explicitly represents the collinear divergence.

To summarize the situation, on one side the universal collinear divergences can be factorized from the bare coefficients functions leaving finite the remaining part and, on the other side, the observable are computed through a convolution between the bare coefficients functions and the bare PDFs (sec. 1.3), which in turn can contain IR divergences. It is clear that if the collinear counter-terms could be absorbed in the PDF definition in such a way to make them IR finite, the problem would be solved. In Mellin space this can be written

$$\begin{aligned}\sigma(N,Q^2) &= \bar{C}_i(N,\alpha_s(Q^2),\epsilon)\bar{f}_i(N,\epsilon) \\ &= C_j(N,\alpha_s(Q^2),\epsilon)\Gamma_{ji}(N,\alpha_s(Q^2),\epsilon)\bar{f}_i(N,\epsilon) \\ &= C_j(N,\alpha_s(Q^2),0)f_j(N,Q^2)+\mathcal{O}(\epsilon),\end{aligned} \tag{1.49}$$

where $\bar{f}_i$ are the bare PDFs, f_i are the redefined PDFs and, in the last step, the limit $\epsilon \to 0$ has been taken. This limit can be done only if the divergences in Γ_{ij} actually cancel with the ones in the bare PDFs, as assumed. Although we have not shown this, one can actually prove that this feature is respected and so the initial state IR divergences can be regularized in this way. It is worth mentioning that the procedure to resum the collinear logartihms to all orders, which is the main matter of this thesis and that is presented in chapter 3, is based on a similar method.

1.3.2 Scaling violation: DGLAP evolution

From the explicit expression of the redefinition of the PDFs used in the last step of eq. (1.49),

$$f_j(N,\mu^2) = \lim_{\epsilon\to 0}[\Gamma_{ij}(N,\alpha_s(\mu^2),\epsilon)\bar{f}_i(N,\epsilon)], \tag{1.50}$$

it is possible to notice that the redefined PDFs acquire an energy scale dependence. Since the bare PDFs are assumed to be scale independent one can write

$$\mu^2\frac{d}{d\mu^2}f_i(N,\mu^2) = P_{ij}(N,\alpha_s(\mu^2))f_j(N,\mu^2) \tag{1.51}$$

or, in x-space,

$$\mu^2\frac{d}{d\mu^2}f_i(x,\mu^2) = \int_x^1 \frac{dz}{z}P_{ij}\left(\frac{x}{z},\alpha_s(\mu^2)\right)f_j(z,\mu^2), \tag{1.52}$$

in a similar way to what has been done for the renormalization group equation in sec. 1.2.1.

Notice that the splitting functions P_{ij} take the form

$$P_{ij}(N,\alpha_s) = \lim_{\epsilon\to 0}\left[-\beta(\alpha_s,\epsilon)\Gamma_{ik}(N,\alpha_s,\epsilon)\frac{\partial\Gamma^{-1}_{kj}(N,\alpha_s,\epsilon)}{\partial\alpha_s}\right], \tag{1.53}$$

where the running coupling equation (1.23) has been used. Moreover, thanks to the $SU(n_f)$ flavour simmetry, it is possible to show that

$$\begin{aligned}P_{q_iq_j} &= P_{\bar{q}_i\bar{q}_j} \\ P_{q_i\bar{q}_j} &= P_{\bar{q}_iq_j} \\ P_{q_ig} &= P_{\bar{q}_ig} \equiv P_{qg} \\ P_{gq_i} &= P_{g\bar{q}_i} \equiv P_{gq},\end{aligned} \tag{1.54}$$

which, in turn, allows the definition of the singlet (S) and non-singlet (V) components as

$$\begin{aligned} P_{q_i q_k} &= \delta_{ik} P_{qq}^V + P_{qq}^S \\ P_{q_i \bar{q}_k} &= \delta_{ik} P_{q\bar{q}}^V + P_{q\bar{q}}^S \\ P^{\pm} &\equiv P_{qq}^V \pm P_{q\bar{q}}^V, \end{aligned} \tag{1.55}$$

that will be useful for the last part of this section.

The equations (1.51) and (1.52) are called Dokshitzer–Gribov–Lipatov–Altarelli–Parisi (DGLAP) evolution equations because they implement the energy scale evolution of the PDFs. Therefore, the PDFs are fitted from data, for every x value, at a certain low (but still perturbative) energy and then they are evolved to any other scale using DGLAP, obtaining the final functions of both x and Q^2 (fig. 1.6). Notice that DGLAP equations are written in terms of the splitting functions which are computed in perturbation theory, so, although equations (1.51) and (1.52) are valid to all orders, in practice they are used at a certain finite perturbative order. In particular, the splitting functions are currently fully known only up to $\mathcal{O}(\alpha_s^3)$, hence DGLAP equations are used at most at the same order, called NNLL (next-to-next-to-leading log). The origin of this name for their perturbative order will be clarified in sec. 3.2.1.

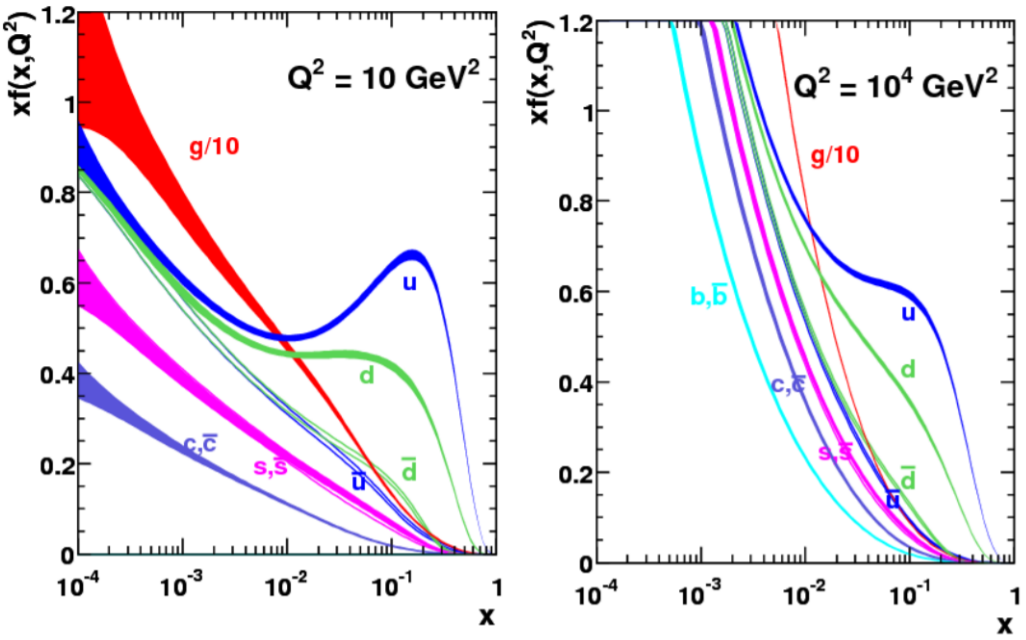

Figure 1.6. Products of x for the proton PDFs as a function of x for two values of the energy scale Q^2. They were extracted by MSTW group in 2008 and evolved with NLO DGLAP equation. Notice that the PDFs of the valence quarks, i.e. u and d, are different from the corresponding anti-quarks PDFs, while, for the others, the sea-quarks, there is no difference, as expected. Notice also that the uncertainties are bigger if x is smaller and this is because the small-x region, which corresponds to an high-energy one, has not been fully explored yet by experiments [19].

DGLAP equations in x-space are six coupled integro-differential equations and thus they are very difficult to solve. In Mellin space they simplify a bit because it

is possible to partially diagonalize the system finding several completely decoupled equations and only a dimension two coupled equation. In particular, following the definitions of the non-singlet combinations [3]

$$\begin{aligned} V_i &= q_i^- \\ T_3 &= u^+ - d^+ \\ T_8 &= u^+ + d^+ - 2s^+ \\ T_{15} &= u^+ + d^+ + s^+ - 3c^+ \\ T_{24} &= u^+ + d^+ + s^+ + c^+ - 4b^+ \\ T_{35} &= u^+ + d^+ + s^+ + c^+ + b^+ - 5t^+, \end{aligned} \tag{1.56}$$

where u,d,s,c,b and t are the PDFs of the corresponding quark-flavour and $q_i^{\pm} \equiv q_i \pm \overline{q}_i$, it is straightforward to show that the V_i and T_i combinations decouple from the others, i.e. evolve following the equations

$$\begin{aligned} \mu^2 \frac{d}{d\mu^2} V_i(x,\mu^2) &= \int_x^1 \frac{dz}{z} P^-\left(\frac{x}{z}, \alpha_s(\mu^2)\right) V_i(z,\mu^2) \\ \mu^2 \frac{d}{d\mu^2} T_i(x,\mu^2) &= \int_x^1 \frac{dz}{z} P^+\left(\frac{x}{z}, \alpha_s(\mu^2)\right) T_i(z,\mu^2). \end{aligned} \tag{1.57}$$

The remaining singlet combination, $\Sigma(x,\mu^2) \equiv \sum_i [q_i(x,\mu^2) + \overline{q}_i(x,\mu^2)]$, is coupled with the gluon PDF via the evolution matrix equation

$$\mu^2 \frac{\partial}{\partial \mu^2} \begin{pmatrix} \Sigma(x,\mu^2) \\ g(x,\mu^2) \end{pmatrix} = \int_x^1 \frac{dz}{z} \times \begin{pmatrix} P_{qq}(\frac{x}{z}, \alpha_s(\mu^2)) & P_{qg}(\frac{x}{z}, \alpha_s(\mu^2)) \\ P_{gq}(\frac{x}{z}, \alpha_s(\mu^2)) & P_{gg}(\frac{x}{z}, \alpha_s(\mu^2)) \end{pmatrix} \begin{pmatrix} \Sigma(x,\mu^2) \\ g(x,\mu^2) \end{pmatrix}$$

with $P_{qq} = P^+ + n_f(P_{qq}^S + P_{q\overline{q}}^S)$.

To conclude, it is important to notice that, as it happened for the running of the coupling α_s, the DGLAP equations have a dependence on the number of active flavour n_f. However, in this case the n_f dependence has a more striking consequence than the β function values variation. In fact, the number of active flavour determines the number of non-zero PDFs, so, adopting a variable-flavour number scheme approach, when a flavour becomes active at a certain energy scale, two new PDFs are born. This feature plays a central role in the context of the main result of this thesis, where the adopted notation will be that $f_i^{[n_f]}$ denotes the PDF of parton i in the scheme in which there are n_f active flavours. In chapter 3, this aspect of PDF evolution will be addressed in greater detail.

This last observation concludes the general aspects of QCD that will be fundamental for the comprehension of the rest of the thesis. In the following chapter the most important notions about deep-inelastic scattering and on its heavy-quark production sector will be presented in order to clarify the notation and an example of a LO calculation will be analyzed in detail to present the central problem addressed in this thesis.

Chapter 2

Deep-inelastic scattering with heavy quark production

The most used process for PDF determination, as well as for QCD validation tests, is deep-inelastic scattering (DIS), i.e. lepton-proton scattering in which the photon that is exchanged between lepton and hadron has large virtuality and can break the internal structure of the hadron. The reason of its importance relies on the fact that there is a single hadron in the initial state and so it is relatively easy to reconstruct one of its event. Moreover, it is also well known from a theoretical point of view.

In this chapter, the fundamental definitions and properties of DIS will be presented and a leading-order calculation will be sketched in order to clarify the adopted notation (sec. 2.1). Then the attention will be devoted to the heavy quark production sector of DIS (sec. 2.2), i.e. the class of its events in which at least one heavy quark is produced, and the full calculation of its leading-order will be analyzed in detail in order to explicitly show the large logarithms problem. The computation will be carried out in both the cases in which the heavy quark is treated as massless (sec. 2.2.1) and in which it is treated as massive (sec. 2.2.2) in such a way to underline the fact that the collinear logarithms, which appear in the massive case, become collinear divergences in the massless case, as mentioned in sec. 1.2.

2.1 The framework

Deep-inelastic scattering is a single-hadron initiated process, hence, as already mentioned in sec. 1.3, its related observables have to be computed using the parton model formalism (fig. 1.5). Denoting k^μ and k'^μ respectively the four-momentum of the incoming and outgoing lepton, p^μ the hadron four-momentum and $q^\mu = k^\mu - k'^\mu$ the exchanged photon four-momentum, the standard kinematic variables of DIS are defined as

$$
\begin{aligned}
&Q^2 = -q^2 && \text{virtuality of the photon} \\
&M^2 = p^2 && \text{hadron mass} \\
&\nu = p \cdot q = M(E' - E) && \\
&x = \frac{Q^2}{2\nu} && \text{Bjorken's scaling variable} \\
&y = \frac{q \cdot p}{k \cdot p} = \frac{Q^2}{2xk \cdot p}, &&
\end{aligned}
\tag{2.1}
$$

where the energy variables, E and E', refer to the hadron rest frame. The Bjorken's x represent the longitudinal momentum fraction of the struck quark in the proton and y is the momentum fraction lost by the lepton.

The fundamental observation, which comes from the diagram 1.5, is that the cross-section can be factorized into a leptonic and a hadronic piece as

$$\frac{d^2\sigma}{dxdy} \propto L_{\alpha\beta}W^{\alpha\beta}, \tag{2.2}$$

where the leptonic piece $L_{\alpha\beta}$ is completely determined by QED and it reads

$$\begin{aligned} L_{\alpha\beta} &= \sum_{pol} \left|e\bar{u}(k')\gamma^\alpha u(k)\right|^2 = e^2 \mathrm{Tr}[\not{k}'\gamma_\alpha \not{k}\gamma_\beta] \\ &= 4e^2(k_\alpha k'_\beta + k_\beta k'_\alpha - g_{\alpha\beta} k\cdot k'). \end{aligned} \tag{2.3}$$

The hadronic piece $W_{\alpha\beta}$, instead, contains all the information about the interaction of the electromagnetic current j_α with the hadron and can be written as

$$\begin{aligned} W_{\alpha\beta}(p,q) &= \frac{1}{4\pi}\sum_X \langle P|\, j^\dagger_\beta(0)\,|X\rangle\,\langle X|\, j_\alpha(0)\,|P\rangle\,(2\pi)^4\delta^4(q+p-p_X) \qquad (2.4)\\ &= \frac{1}{4\pi}\int d^4z e^{iq\cdot x}\,\langle P|\, j^\dagger_\beta(z) j_\alpha(0)\,|P\rangle \\ &= \frac{1}{4\pi}\int d^4z e^{iq\cdot x}\,\langle P|\,[j^\dagger_\beta(z), j_\alpha(0)]\,|P\rangle\,, \qquad (2.5) \end{aligned}$$

where the completeness of the final states X and the integral representation of the delta function have been used.

From this last expression it is clear that, since the electromagnetic current is conserved, $q\cdot W = 0$ and one can write

$$W^{\alpha\beta}(p,q) = \left(g^{\alpha\beta} - \frac{q^\alpha q^\beta}{q^2}\right)W_1(x,Q^2) + \left(p^\alpha + \frac{1}{2x}q^\alpha\right)\left(p^\beta + \frac{1}{2x}q^\beta\right)W_2(x,Q^2), \tag{2.6}$$

which can be derived by requiring also Lorentz invariance.

The DIS cross section, as well as its other observables, can be also written as a function of the so-called electromagnetic structure functions F_i as

$$\frac{d^2\sigma}{dxdy} = \frac{8\pi\alpha_s^2 ME}{Q^4}\left[\left(\frac{1+(1-y)^2}{2}\right)2xF_1 + (1-y)(F_2 - 2xF_1) - \frac{M}{2E}xyF_2\right]. \tag{2.7}$$

The structure functions parametrize the internal structure of the hadron as seen by the virtual photon. They can be linked to the functions W_i comparing this last equation with eq. (2.2) in which the expressions of $L_{\alpha\beta}$ (eq. (2.3)) and $W_{\alpha\beta}$ (eq. (2.6)) are used. By this comparison one gets

$$\begin{aligned} F_1(x,Q^2) &= W_1(x,Q^2) \\ F_2(x,Q^2) &= \nu W_2(x,Q^2) \\ F_L(x,Q^2) &\equiv F_2 - 2xF_1 = \nu W_2 - 2xW_1, \end{aligned} \tag{2.8}$$

where the structure function F_L is often used instead of F_1. Notice that eq. (2.7) can be rewritten as

$$\frac{d^2\sigma}{dxdy} = \frac{8\pi\alpha_s^2 ME}{Q^4}\left[\left(\frac{1+(1-y)^2}{2}\right)F_2 - y^2F_L - \frac{M}{2E}xyF_2\right], \tag{2.9}$$

from which it is possible to notice that F_L becomes a considerable contribution only in the region in which y is large, i.e. in the small-x region.
Since the quantity that is actually computed in perturbation theory is $W_{\alpha\beta}$, it is convenient to define some projectors to obtain directly F_2 and F_L. Defining the light-like four-vectors $\bar{p}$ and $\bar{q}$ such that

$$\begin{aligned} \bar{p}^2 &= \bar{q}^2 = 0 \\ \bar{p}\cdot q &= \bar{q}\cdot p = 0 \\ \bar{p}\cdot p &= \frac{\bar{q}\cdot q}{\nu} = 1, \end{aligned} \tag{2.10}$$

it is easy to show that

$$\begin{aligned} F_2 &= \nu \bar{p}^\alpha \bar{p}^\beta W_{\alpha\beta} \\ F_L &= \frac{4x^2}{\nu} \bar{q}^\alpha \bar{q}^\beta W_{\alpha\beta}, \end{aligned} \tag{2.11}$$

which are the final expressions that will be used in the following.

Before starting to introduce the heavy quark production sector of DIS, it is useful to compute the LO contribution to the structure functions in order to clarify the notation. Notice that the quantities that will be computed in the following, called partonic structure functions, have to be convoluted with the PDFs to obtain the full structure functions.

The leading-order diagram of DIS in the parton model view is the scattering of a free quark off the virtual photon with subsequent production of another free quark (fig. 2.1)

$$\gamma^*(q) + q(\xi p) \to q(l). \tag{2.12}$$

The $0 < \xi \leqslant 1$ variable takes into account the fact that the four-momentum of the quark is less or equal to the one of the hadron from which it is extracted. The

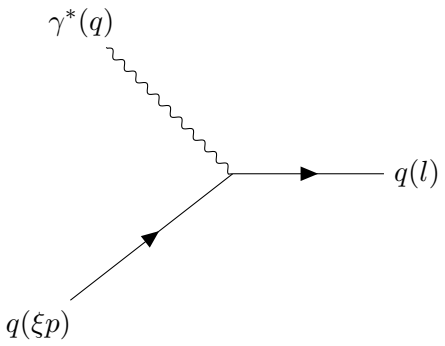

Figure 2.1. Leading order contribution to deep-inelastic scattering. The free quark $q(\xi p)$ scatters off the virtual photon $\gamma^*(q)$ and produce another free quark $q(l)$.

invariant matrix element for this process is

$$M_\alpha = -ie_q \bar{u}(l)\gamma_\alpha u(\xi p), \tag{2.13}$$

with e_q the electric charge of the interacting quark. Squaring eq. (2.13) results in

$$\begin{aligned} \overline{\sum} |M|_{\alpha\beta} &= \frac{e_q^2}{2} \xi \mathrm{Tr}[(\not{l})\gamma_\alpha(\not{p})\gamma_\beta] \\ &= 2e_q^2 \xi (l_\alpha p_\beta + l_\beta p_\alpha - g_{\alpha\beta}(l\cdot p)), \end{aligned} \tag{2.14}$$

where the quark mass has been neglected and $\overline{\sum}$ means that one has to average over the initial polarizations, as well as summing on the final ones. Using the projectors as in eq. (2.11) leads to

$$\begin{aligned} \bar{p}^{\alpha}\bar{p}^{\beta}\overline{\sum}|M|_{\alpha\beta} &= 4e_q^2\xi(\bar{p}\cdot l) \\ \bar{q}^{\alpha}\bar{q}^{\beta}\overline{\sum}|M|_{\alpha\beta} &= 0, \end{aligned} \tag{2.15}$$

where it can be noticed that F_L is equal to zero at leading order. In order to compute $\bar{p}\cdot l$, one has, in principle, to choose a parametrization for the four-momentum l in a certain reference frame (as it will be done in secs. 2.2.1 and 2.2.2). However, in this case, it is enough to notice that from four-momentum conservation

$$\xi p + q = l \tag{2.16}$$

one can get

$$\xi = \bar{p}\cdot l \tag{2.17}$$

simply making the dot product of $\bar{p}$ from both sides of momentum conservation equation and using the definition of the projector in eq. (2.10).

Therefore, the final squared matrix element is

$$\overline{\sum}|M|_{\alpha\beta} = 4e_q^2\xi^2, \tag{2.18}$$

so, integrating over the one-dimensional phase space

$$d\phi = 2\pi\delta((\xi p + q)^2) = 2\pi\delta(2\xi pq - Q^2) \tag{2.19}$$

and inserting the flux factor $1/4\pi$, it is possible to obtain the final $\hat{F}_2$ expression at parton level [3]

$$\hat{F}_2(\xi) = e_q^2\xi^2\delta\left(1 - \frac{x}{\xi}\right). \tag{2.20}$$

There are several important aspects related to this LO final result which have to be underlined. First of all, $\hat{F}_2$ at leading-order does not depend on the energy scale of the process, i.e. on the virtuality of the photon Q^2. This feature is not surprising because the computed diagram (fig. 2.1) is exactly the naive (leading-order) parton model of fig. 1.4b while, as mentioned in sec. 1.3, the scale dependence comes from QCD corrections and thus it starts at $\mathcal{O}(\alpha_s)$ (fig. 2.2).

Another important leading-order trait, which derives from this calculation, is the so-called Callan-Gross relation

$$F_2 = 2xF_1 \tag{2.21}$$

that follows from $F_L = 0$. This relation can be also derived from more general naive parton model arguments and it is a direct consequence of the spin-$\frac{1}{2}$ property of the quarks.

Finally, it is also important to notice that the computed diagram belongs to the heavy quark production sector only if the interacting quark is the one considered as heavy. Therefore, a very similar calculation leads to the leading-order contribution of the final result constructed in chapter 4.

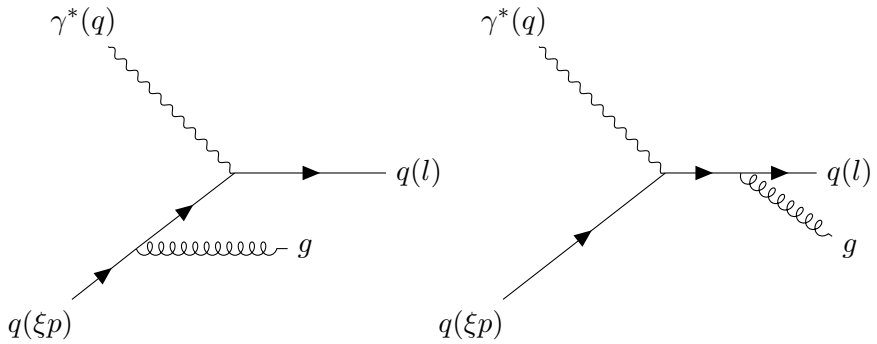

Figure 2.2. Corrections at $\mathcal{O}(\alpha_s)$ to deep-inelastic scattering off a quark.

2.2 Heavy quark production

The heavy quark production sector of deep-inelastic scattering is one of the main tool exploited to study the nucleon structure. From an experimental point of view it is advantageous with respect to other categories of processes because the relatively large masses of the final heavy quarks facilitate the separation of the produced particles [20]. Moreover, from a theoretical point of view, the large mass makes possible the adoption of perturbative QCD for the calculation of the coefficients functions. In fact, the bottom is the quark that will be considered as heavy in the following chapters and its mass is way bigger than 1 GeV.

In the context of the goals of this thesis, there is another reason to choose heavy quark production: the mass of the heavy quark has a central role in the proposed scheme, both when the mass-logarithms are resummed and when the result starts to include mass corrections, so, considering only the processes in which bottom quarks are produced, will underline the improvements given by the proposed procedure.

However, the definition of what it is meant by heavy quark production is somewhat ambiguous. The most adopted one is to include all the diagrams in which the bottom quark interacts with the photon, i.e. every diagram which include the term e_b. This is the convention adopted also in this thesis, but it is important to underline that, experimentally, it is not always possible to distinguish between a bottom quark produced by the interaction with the photon and one produced by an emitted gluon, especially if the emission is soft. This is the reason why there are other alternative conventions which facilitates the comparison of the theoretical predictions with the experimental data.

The dominant mechanism of an heavy quark production process is boson-gluon fusion (BGF): the photon interacts with a gluon extracted from the hadron to form an heavy quark-antiquark pair [21]. The calculation of the contribution of this diagram (fig. 2.3) is the argument of the next two sections in which it will be addressed both in the massless case (2.2.1) and in the massive case (2.2.2). The obtained results will be not only useful as ingredients for the construction of the final result, but also to show explicitly the large logarithms problem and its similarity to the collinear divergences one.

2.2.1 Leading order calculation in the massless case

In this section, the computation of $\hat{F}_2$ and $\hat{F}_L$ for the leading order diagram of fig. 2.3 will be carried out in the massless case, i.e. neglecting the mass of the produced bottom quark and anti-quark. Since, in this case, the result is expected to contain

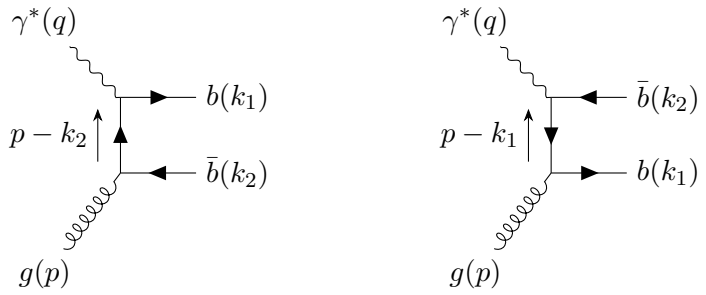

Figure 2.3. Boson-gluon fusion diagrams for bottom quarks production. Since they have the same final state, they have to be summed incoherently to obtain the total amplitude.

collinear divergences (1.2.2), the computation will be done in $d \neq 4$ dimensions (in dimensional regularization) with the $\overline{MS}$ prescription. Therefore, the coupling will be written as (eq. (1.19))

$$\alpha_s^b = \alpha_s(\mu)\left(\frac{\mu^2 e^\gamma}{4\pi}\right)^\epsilon \tag{2.22}$$

with $\epsilon = (4-d)/2$ and γ the Euler's gamma.

The two contributions of fig. 2.3a and fig. 2.3b have the same final state so they have to be summed incoherently one to the other to obtain the total amplitude. This results in

$$M^\mu = g_s e_q t^C \bar{u}(k_1)\left[\gamma^\mu \frac{\not{p} - \not{k}_2}{(p-k_2)^2}\not{\epsilon}(p) - \not{\epsilon}(p)\frac{\not{p} - \not{k}_1}{(p-k_1)^2}\gamma^\mu\right]v(k_2), \tag{2.23}$$

where t^C comes from the feynman rule of fig. 1.1a, $\epsilon(p)$ is the polarization four-vector of the gluon and it has been used the fact that $k_1^2 = k_2^2 = 0$ in the massless case. The minus sign comes from the opposite direction of the momentum $(p - k_1)$ with respect to the spinor arrow direction in the second diagram.

It is convenient to express every expression that will be obtained from now on in terms of the so-called Mandlestam variables, which in this case are defined as

$$\begin{aligned} s &= (q+p)^2 = -Q^2 + 2p\cdot q = (k_1+k_2)^2 = 2k_1\cdot k_2 \\ t &= (q-k_1)^2 = -Q^2 - 2k_1\cdot q = (k_2-p)^2 = -2k_2\cdot p \\ u &= (q-k_2)^2 = -Q^2 - 2k_2\cdot q = (k_1-p)^2 = -2k_1\cdot p \end{aligned} \tag{2.24}$$

in which $q^2 = -Q^2$ and $p^2 = 0$ have been used. From momentum conservation $p + q = k_1 + k_2$ and from the properties of the projectors $\bar{p}$ and $\bar{q}$, it is also possible to obtain the important relations

$$\begin{aligned} s + t + u + Q^2 &= 0 \\ \bar{p}\cdot k_1 + \bar{p}\cdot k_2 &= 1 \\ \bar{q}\cdot k_1 + \bar{q}\cdot k_2 &= \frac{Q^2}{2x} \end{aligned} \tag{2.25}$$

which will be used in the following.

The amplitude expression of eq. (2.23) is still valid for both $\hat{F}_2$ and $\hat{F}_L$ and from it, it is possible to obtain the hadronic tensor as

$$W^{\mu\nu} = \overline{\sum}(M^\mu)^* M^\nu, \tag{2.26}$$

which still needs to be integrated over the phase-space.

The following steps will consist in applying the relations of eq. (2.11) to get first $\hat{F}_2$ and then $\hat{F}_L$.

$\hat{F}_2$ calculation

Using $\bar{p}$ on eq. (2.26) and averaging over the $d-2$ gluon polarizations results in

$$W_2 = \frac{g_s^2 e_q^2 T_R}{(1-\epsilon)} \bar{p}_\mu \bar{p}_\nu \sum \left[\frac{1}{t^2} A^{\mu\nu} + \frac{1}{u^2} B^{\mu\nu} - \frac{2}{ut} C^{\mu\nu} \right], \tag{2.27}$$

where

$$\begin{aligned} A^{\mu\nu} &= \mathrm{Tr}(\not{k}_1 \gamma^\mu (\not{p} - \not{k}_2) \not{\epsilon}(\mathrm{p}) \not{k}_2 \not{\epsilon}(\mathrm{p})^* (\not{p} - \not{k}_2) \gamma^\nu) \\ B^{\mu\nu} &= \mathrm{Tr}(\not{k}_1 \not{\epsilon}(\mathrm{p}) (\not{p} - \not{k}_1) \gamma^\mu \not{k}_2 \gamma^\nu (\not{p} - \not{k}_1) \not{\epsilon}(\mathrm{p})^*) \\ C^{\mu\nu} &= \mathrm{Tr}(\not{k}_1 \gamma^\mu (\not{p} - \not{k}_2) \not{\epsilon}(\mathrm{p}) \not{k}_2 \gamma^\nu (\not{p} - \not{k}_1) \not{\epsilon}(\mathrm{p})^*). \end{aligned} \tag{2.28}$$

In order to compute the traces in the A, B and C definitions, it is essential to choose the gauge in which performing the calculation. In this case the most convenient is the Feynman gauge (sec. 1.1), which fixes $\sum_{\mathrm{pol}} (\epsilon_\nu)^* \epsilon_\mu = -g_{\mu\nu}$ (valid only at this perturbative order), because it gives the simplest expression for the gluon polarizations sum and, since at this perturbative order the ghost contribution is not present yet, it has no disadvantages. With this choice and after some manipulations, one can get

$$\begin{aligned} A^{\mu\nu} &= -4t(1-\epsilon)(u g^{\mu\nu} + 2k_1^\mu p^\nu + 2k_1^\nu p^\mu) \\ B^{\mu\nu} &= -4u(1-\epsilon)(t g^{\mu\nu} + 2k_2^\mu p^\nu + 2k_2^\nu p^\mu) \\ C^{\mu\nu} &= 4g^{\mu\nu}(s^2 + s(t+u) - tu\epsilon) - 8(k_1^\nu(-tk_1^\mu + k_2^\mu(s+t+u) + \epsilon t p^\mu) \\ &\quad + k_2^\nu(s k_1^\mu - u k_2^\mu - s p^\mu) \\ &\quad + p^\nu(-s k_1^\mu + \epsilon u k_2^\mu + \epsilon s p^\mu)), \end{aligned} \tag{2.29}$$

where the definitions of the Mandelstam variables and the d-dimensional relations

$$\begin{aligned} g^{\mu\nu} g_{\mu\nu} &= d \\ \gamma^\mu \gamma_\mu &= d \\ \gamma^\mu \gamma^\rho \gamma_\mu &= -(d-2)\gamma^\rho \\ \gamma^\mu \gamma^\rho \gamma^\sigma \gamma_\mu &= 4g^{\rho\sigma} - 2\epsilon \gamma^\rho \gamma^\sigma \\ \gamma^\mu \gamma^\rho \gamma^\sigma \gamma^\nu \gamma_\mu &= -2\gamma^\nu \gamma^\sigma \gamma^\rho + 2\epsilon \gamma^\rho \gamma^\sigma \gamma^\nu \end{aligned} \tag{2.30}$$

have been used.

Plugging these expressions in eq. (2.27) and exploiting the properties of the projectors result in

$$W_2 = 8g_s^2 e_q^2 T_R \Big[-\frac{\bar{p}\cdot k_1}{t} - \frac{\bar{p}\cdot k_2}{u} + \\ + \frac{1}{ut(1-\epsilon)}((\bar{p}\cdot k_1)(\bar{p}\cdot k_2)(s-Q^2) - t(\bar{p}\cdot k_1)^2 - u(\bar{p}\cdot k_2)^2 + s\epsilon + \\ + (\bar{p}\cdot k_1)(t\epsilon - s) + (\bar{p}\cdot k_2)(u\epsilon - s))\Big] \tag{2.31}$$

that becomes

$$W_2 = 8g_s^2 e_q^2 T_R \Big[\frac{-\bar{p}\cdot k_1 u + \bar{p}\cdot k_1 t - t}{ut} + \\ + \frac{1}{ut(1-\epsilon)}((u+s)(\epsilon-1) + (\bar{p}\cdot k_1)(s - Q^2 + t\epsilon + u(2-\epsilon)) + \\ + 2(\bar{p}\cdot k_1)^2 Q^2)\Big] \tag{2.32}$$

if one writes $\bar{p}\cdot k_2$ as a function of $\bar{p}\cdot k_1$ using the relation of eq. (2.25).

From the last expression, with some algebraic manipulations, it is possible to obtain

$$W_2 = \frac{8g_s^2 e_q^2 T_R Q^2}{ut(1-\epsilon)}\Big[2(\bar{p}\cdot k_1)^2 - 2(\bar{p}\cdot k_1) + 1 - \epsilon\Big], \tag{2.33}$$

which is the final expression that can be written in terms of Lorentz invariants.

In order to proceed to the phase-space integration, it is necessary to write this expression in a chosen reference frame. A possible convenient choice is the center-of-mass frame of the gluon-photon system with the gluon and photon momenta along the third direction, in such a way they can be written as

$$p = p_0 n, \quad q = \alpha n + (p_0 + \alpha)\bar{n} \tag{2.34}$$

where

$$n = (1,0,0,1), \quad \bar{n} = (1,0,0,-1). \tag{2.35}$$

Moreover, it is possible to find an expression of the coefficients p_0 and α, written in terms of s and Q^2, imposing

$$\begin{aligned} Q^2 &= -q^2 = -4\alpha(p_0+\alpha) \\ s &= (p+q)^2 = 4(p_0+\alpha)^2, \end{aligned} \tag{2.36}$$

from which one gets

$$\alpha = -\frac{Q^2}{2\sqrt{s}}, \quad p_0 = \frac{s+Q^2}{2\sqrt{s}}. \tag{2.37}$$

In order to find the expression of $\bar{p}\cdot k_1$ in this reference frame, it is necessary to parameterize also the four-vectors $\bar{p}$, k_1 and k_2 in terms of n and $\bar{n}$. Writing them as

$$\begin{aligned} \bar{p} &= A_{\bar{p}} n + B_{\bar{p}}\bar{n} + \bar{p}_t \\ k_1 &= A_1 n + B_1 \bar{n} + k_t \\ k_2 &= A_2 n + B_2 \bar{n} - k_t, \end{aligned} \tag{2.38}$$

where the four-vectors k_t and $\bar{p}_t$ have only the two transverse spatial components, and imposing $k_1^2 = k_2^2 = 0$ in addition to the relations of eq. (2.24) and eq. (2.10), it is possible to obtain

$$\begin{aligned} \bar{p} &= \frac{Q^2/\sqrt{s}}{s+Q^2} n + \frac{\sqrt{s}}{s+Q^2}\bar{n} + \bar{p}_t \\ k_1 &= -\frac{K^2}{u}\frac{s+Q^2}{\sqrt{s}} n - \frac{u}{2}\frac{\sqrt{s}}{s+Q^2}\bar{n} + k_t \\ k_2 &= -\frac{K^2}{t}\frac{s+Q^2}{\sqrt{s}} n - \frac{t}{2}\frac{\sqrt{s}}{s+Q^2}\bar{n} - k_t, \end{aligned} \tag{2.39}$$

where

$$\begin{aligned} \bar{p}_t^2 &= -\frac{4x^2}{Q^2} \\ k_t^2 &= -2K^2 \\ K^2 &= -\frac{t(1-x)}{2Q^2}(Q^2 + tx). \end{aligned} \tag{2.40}$$

Using this parameterization it is possible to obtain the expression

$$\bar{p} \cdot k_1 = \frac{x}{Q^2}(t(2x-1) + Q^2) + k_t \cdot \bar{p}_t, \tag{2.41}$$

where the $k_t \cdot \bar{p}_t$ term is equal to $-\left|\vec{k}_t\right||\vec{p}_t|\cos\phi$ with $\vec{k}_t$ and $\vec{p}_t$ the spatial vectors linked to the namesakes four-vectors and ϕ the azimuthal angle between the two vectors. Since

$$\frac{1}{2\pi}\int_0^{2\pi} \cos\phi\, d\phi = 0, \quad \frac{1}{2\pi}\int_0^{2\pi} \cos^2\phi\, d\phi = \frac{1}{2}, \tag{2.42}$$

the term $k_t \cdot \bar{p}_t$ contributes only in the quadratic term in eq. (2.33), which thus becomes

$$\frac{1}{2\pi}\int_0^{2\pi} (k_t \cdot \bar{p}_t)^2\, d\phi = -\frac{4x^2}{Q^2}\frac{t(1-x)(Q^2+tx)}{Q^2}. \tag{2.43}$$

It is now possible to proceed to the phase-space integration over the d-dimensional phase-space (APP. A)

$$d\phi_2 = \frac{1}{8\pi}\frac{(4\pi)^\epsilon}{\Gamma(1-\epsilon)}\left(\frac{1-x}{x}\right)^{-\epsilon} Q^{-2\epsilon} y^{-\epsilon}(1-y)^{-\epsilon} dy, \tag{2.44}$$

where y has been defined as $y = -xt/Q^2 = (1-\cos\theta)/2$ with θ the angle of k_1 with respect to the z axis.

Plugging eq. (2.41) and eq. (2.43) in eq. (2.33) and integrating in the phase-space result in

$$\hat{F}_2 = x\frac{2e_q^2 T_R \alpha_s e^{\gamma\epsilon}}{\Gamma(1-\epsilon)(1-\epsilon)}\left(\frac{1-x}{x}\right)^{-\epsilon}\int_0^1 \frac{-2(6x^2-6x+1)y(1-y) + (1-\epsilon) + 2x(x-1))}{y^{\epsilon+1}(1-y)^{\epsilon+1}}\, dy \tag{2.45}$$

where the term $\nu = Q^2/2x$ has been also included. In obtaining the last equation, it has been also used the relation $s = Q^2(1-x)/x$ and the $\overline{MS}$ scale μ^2 has been fixed equal to the scale of the process Q^2. Notice that in the $\epsilon \to 0$ limit, i.e. the limit

in which the space-time dimensions become 4, the integral has a divergent part. In particular

$$\int_0^1 \frac{1+2x(x-1)}{y(1-y)}\,dy \tag{2.46}$$

is divergent in both the $y \to 0$ and $y \to 1$ limits, which correspond respectively to $\theta \to 0$ and $\theta \to \pi$. Hence, these divergences are related, as expected, to the collinearity of one or the other emitted quark with the initial state gluon.

In dimensional regularization the integrals can be computed using the general expression

$$\int_0^1 y^{a-1}(1-y)^{b-1}\,dy = \frac{\Gamma(a)\Gamma(b)}{\Gamma(a+b)}, \tag{2.47}$$

which, applied to the integral in eq. (2.45), gives

$$\begin{aligned} &2(6x^2-6x+1)\int_0^1 y^{-\epsilon}(1-y)^{-\epsilon}\,dy - (1-\epsilon+2x(x-1))\int_0^1 y^{-\epsilon-1}(1-y)^{-\epsilon-1}\,dy = \\ &=(1-\epsilon+2x(x-1))\frac{\Gamma^2(-\epsilon)}{\Gamma(-2\epsilon)} - 2(6x^2-6x+1)\frac{\Gamma^2(1-\epsilon)}{\Gamma(2-2\epsilon)}. \end{aligned} \tag{2.48}$$

This expression, plugged in eq. (2.45), can be expanded in powers of ϵ using the expansions

$$\begin{aligned} \Gamma(\epsilon) &= \frac{1}{\epsilon} - \gamma + o(\epsilon) \\ e^{\gamma\epsilon} &= 1 + \gamma\epsilon + o(\epsilon^2) \\ \left(\frac{1-x}{x}\right)^{-\epsilon} &= 1 - \epsilon \ln\left(\frac{1-x}{x}\right) + o(\epsilon^2), \end{aligned} \tag{2.49}$$

which result in

$$\begin{aligned} \hat{F}_2 = 4xe_q^2 T_R \alpha_s \Bigg(&-8x^2+8x-1 \\ &+ \ln\left(\frac{1-x}{x}\right)(x^2+(1-x)^2) - \frac{1}{\epsilon}(x^2+(1-x)^2)\Bigg), \end{aligned} \tag{2.50}$$

where orders beyond $\mathcal{O}(\epsilon^0)$ have been neglected since they go to zero in the $\epsilon \to 0$ limit.

This final result, which is actually the $\mathcal{O}(\alpha_s)$ gluon coefficients function $C_g^{(1)}$ for F_2, shows many of the feature which were mentioned so far. First of all, the collinear divergence, which was in the integral of eq. (2.45), became a pole $1/\epsilon$ in dimensional regularization. The fact that there are no finite contributions proportional to γ and to $\ln(4\pi)$ is precisely due to the adoption of the modified minimal subtraction scheme but, regardless the particular scheme adopted, the divergence would still have become an ϵ pole in dimensional regularization. Moreover, the term which multiplies the pole is exactly the P_{qg} splitting function, eq. (1.39), as expected (sec. 1.2.2). This is the direct consequence of the universality of the collinear divergences.

It is also important to notice the presence of the logarithmic term $\ln((1-x)/x)$. This term becomes large in the $x \to 0$ and $x \to 1$ limits and so it is an example of a kind of log terms which can spoil the perturbative series just like the collinear one.

$\hat{F}_L$ calculation

In order to obtain the $\hat{F_L}$ expression, it is enough to apply $\bar{q}$ on the hadronic tensor following eq. (2.11). This results in

$$W_L = \frac{4x^2}{\nu}\frac{g_s^2 e_q^2 T_R}{(1-\epsilon)}\bar{q}_\mu \bar{q}_\nu \sum\left[\frac{1}{t^2}A^{\mu\nu} + \frac{1}{u^2}B^{\mu\nu} - \frac{2}{ut}C^{\mu\nu}\right], \tag{2.51}$$

where A, B and C are given by eq. (2.29).

Using the properties of the projector $\bar{q}$ it is possible to obtain

$$W_L = \frac{4x^2}{\nu}\frac{4g_s^2 e_q^2 T_R}{ut(1-\epsilon)}\left[-2(\bar{q}\cdot k_2)^2 u - 2(\bar{q}\cdot k_1)^2 t + 2(\bar{q}\cdot k_1)(\bar{q}\cdot k_2)(s-Q^2)\right],$$

which can be written as

$$W_L = \frac{4x^2}{\nu}\frac{4g_s^2 e_q^2 T_R Q^2}{ut(1-\epsilon)}\left[4(\bar{q}\cdot k_1)^2 + (\bar{q}\cdot k_1)\frac{2u+s-Q^2}{x} - \frac{Q^2}{2x^2}u\right] \tag{2.52}$$

using eq. (2.25).

This is the most simplified Lorentz invariant expression so, in order to integrate it on the phase space, it is necessary to choose a reference frame and find an expression for $\bar{q}\cdot k_1$. Choosing the centre-of-mass frame of the photon-gluon system, as in the $\hat{F}_2$ case, it is enough to find a parameterization for the four-vector $\bar{q}$. Writing it as

$$\bar{q} = A_{\bar{q}} n + B_{\bar{q}}\bar{n} + \bar{q}_t, \tag{2.53}$$

where the four-vector $\bar{q}_t$ has only the two transverse spatial components, and imposing the relations of eq. (2.10)

$$\begin{aligned} \bar{q}\cdot p &= 2p_0 B_{\bar{q}} = 0 \\ \bar{q}\cdot q &= 2A_{\bar{q}}(p_0+\alpha) = \nu \\ \bar{q}^2 &= \bar{q}_t^2 + 4A_{\bar{q}}B_{\bar{q}} = 0, \end{aligned} \tag{2.54}$$

it is possible to find

$$\begin{aligned} A_{\bar{q}} &= \frac{Q^2}{2x\sqrt{s}} \\ B_{\bar{q}} &= 0 \\ \bar{q}_t^2 &= 0 \rightarrow \bar{q}_t = 0. \end{aligned} \tag{2.55}$$

Therefore, $\bar{q} = \frac{Q^2}{2x\sqrt{s}}n$, so, using also the k_1 parameterization of eq. (2.39), one can get

$$\bar{q}\cdot k_1 = -\frac{Q^2 u}{2x(s+Q^2)}, \tag{2.56}$$

which, plugged in eq. (2.52), gives

$$W_L = \frac{16 g_s^2 e_q^2 T_R}{1-\epsilon}x^2(1-x). \tag{2.57}$$

It is now possible to proceed to the integration over the phase space of eq. (2.44), obtaining

$$\hat{F}_L = x\frac{16\alpha_s e_q^2 T_R e^{\gamma\epsilon}}{(1-\epsilon)\Gamma(1-\epsilon)}\left(\frac{1-x}{x}\right)^{-\epsilon} x(1-x)\int_0^1 y^{-\epsilon}(1-y)^{-\epsilon}\,dy, \tag{2.58}$$

which becomes

$$\hat{F}_L = 16 e_q^2 T_R \alpha_s x^2(1-x) \tag{2.59}$$

if one exploits the integral of eq. (2.47) and the expansions of eq. (2.49).

Equation (2.59) is the final result for the $\mathcal{O}(\alpha_s)$ gluon coefficients function of the structure function F_L and, unlike the expression of $\hat{F}_2$ (2.50), it does not contain ϵ poles. This means that it is not divergent in the collinear limit, as indeed it was possible to notice from the integral of eq. (2.58).

In the next section the same calculation will be carried out in the massive case, i.e. considering different from zero the masses of the final bottom quarks. In this way the collinear logarithms will appear in place of the ϵ poles and the problem that is related to them will be clarified.

2.2.2 Leading order calculation in the massive case

In the massive case the collinear divergences are no longer expected, since the mass acts as an IR regulator, so the computation will be carried out in 4 dimensions. The procedure, other than rather small differences in the computation itself, will be very similar to the massless case. The only major changes will be in the phase space, which will be more complicated, and the parametrization of the four-vectors in the centre-of-mass frame.

The amplitude expression in the massive case is

$$M^\mu = g_s e_q t^C \bar{u}(k_1)\left[\gamma^\mu \frac{\not{p} - \not{k}_2 + m}{(p-k_2)^2 - m^2}\not{\epsilon}(p) - \not{\epsilon}(p)\frac{\not{p} - \not{k}_1 - m}{(p-k_1)^2 - m^2}\gamma^\mu\right] v(k_2). \tag{2.60}$$

The Mandelstam variables are

$$\begin{aligned} s &= (q+p)^2 = -Q^2 + 2p\cdot q = (k_1+k_2)^2 = 2m^2 + 2k_1\cdot k_2 \\ t &= (q-k_1)^2 = m^2 - Q^2 - 2k_1\cdot q = (k_2-p)^2 = m^2 - 2k_2\cdot p \\ u &= (q-k_2)^2 = m^2 - Q^2 - 2k_2\cdot q = (k_1-p)^2 = m^2 - 2k_1\cdot p \end{aligned} \tag{2.61}$$

and from momentum conservation the following relations hold:

$$\begin{aligned} &s + t + u + Q^2 - 2m^2 = 0 \\ &\bar{p}\cdot k_1 + \bar{p}\cdot k_2 = 1 \\ &\bar{q}\cdot k_1 + \bar{q}\cdot k_2 = \frac{Q^2}{2x} \end{aligned} \tag{2.62}$$

$\hat{F}_2$ calculation

From the hadronic tensor definition and from the amplitude of eq. (2.60), it is possible to get

$$W_2 = g_s^2 e_q^2 T_R \bar{p}_\mu \bar{p}_\nu \sum\left[\frac{1}{(t-m^2)^2}A^{\mu\nu} + \frac{1}{(u-m^2)^2}B^{\mu\nu} - \frac{2}{(u-m^2)(t-m^2)}C^{\mu\nu}\right], \tag{2.63}$$

where

$$\begin{aligned} A^{\mu\nu} &= \mathrm{Tr}((\not{k}_1 + \mathrm{m})\gamma^\mu(\not{p} - \not{k}_2 + \mathrm{m})\not{\epsilon}(\mathrm{p})(\not{k}_2 - \mathrm{m})\not{\epsilon}(\mathrm{p})^*(\not{p} - \not{k}_2 + \mathrm{m})\gamma^\nu) \\ B^{\mu\nu} &= \mathrm{Tr}((\not{k}_1 + \mathrm{m})\not{\epsilon}(\mathrm{p})(\not{p} - \not{k}_1 - \mathrm{m})\gamma^\mu(\not{k}_2 - \mathrm{m})\gamma^\nu(\not{p} - \not{k}_1 - \mathrm{m})\not{\epsilon}(\mathrm{p})^*) \\ C^{\mu\nu} &= \mathrm{Tr}((\not{k}_1 + \mathrm{m})\gamma^\mu(\not{p} - \not{k}_2 + \mathrm{m})\not{\epsilon}(\mathrm{p})(\not{k}_2 - \mathrm{m})\gamma^\nu(\not{p} - \not{k}_1 - \mathrm{m})\not{\epsilon}(\mathrm{p})^*). \end{aligned} \tag{2.64}$$

Computing A, B and C in Feynman gauge and plugging their value in equation (2.63) leads to

$$\begin{aligned} W_2 = 8g_s^2 e_q^2 T_R \Bigg[&-\frac{a(t + m^2(2b-3))}{(m^2-t)^2} - \frac{b(m^2(2a-3)+u)}{(m^2-u)^2} + \\ &+ \frac{m^2(a^2 + a(2-6b) + b(b+2) - 2) - a^2 t + as(2b-1) + ab(t+u) - b(s+bu)}{(m^2-t)(m^2-u)} \Bigg] \end{aligned} \tag{2.65}$$

where $a = \bar{p} \cdot k_1$ and $b = \bar{p} \cdot k_2$ have been used for ease of notation.

Using equation (2.62) to write b as a function of a and u as a function of s, Q^2 and t, it is possible to obtain

$$\begin{aligned} W_2 = 8g_s^2 e_q^2 T_R \Bigg[&\frac{m^2(4a^2 - 2a + 1) - t(2a(a-1)+1)}{(m^2-t)^2} + \frac{2m^2(a-1)^2)}{(s+t+Q^2-m^2)^2} \\ &+ \frac{m^2(6a(a-1)+1) - (s+t)(2a(a-1)+1)}{(m^2-t)(s+t+Q^2-m^2)} \Bigg], \end{aligned} \tag{2.66}$$

which becomes

$$\begin{aligned} W_2 = \frac{-8g_s^2 e_q^2 T_R}{(m^2-t)^2(x(t-m^2)+Q^2)^2} \Big[&2aQ^2 x(m^2-t)(m^2(2-x)+Q^2+tx) \\ &+ 2a^2Q^2(-m^2(Q^2(x+1)+2tx^2) + m^4 x + xt(Q^2+tx)) + \\ &- x(m^2-t)(Q^2x(t-m^2) + 2m^2x(m^2-t) + Q^4) \Big] \end{aligned} \tag{2.67}$$

using $s = Q^2(1-x)/x$.

Equation (2.67) is the final equation which can be written in terms of Lorentz invariants so it is now necessary to write it in a chosen reference frame and proceed to the phase-space integration. In order to do that, following the same approach adopted in the massless case, an expression of the four-vectors involved in the process in the gluon-photon center-of-mass frame is needed.

With respect to the massless case, only the k_1 and k_2 expressions change and become

$$\begin{aligned} k_1 &= -\frac{K^2}{u-m^2}\frac{s+Q^2}{\sqrt{s}}n - \frac{u-m^2}{2}\frac{\sqrt{s}}{s+Q^2}\bar{n} + k_t \\ k_2 &= -\frac{K^2}{t-m^2}\frac{s+Q^2}{\sqrt{s}}n - \frac{t-m^2}{2}\frac{\sqrt{s}}{s+Q^2}\bar{n} - k_t, \end{aligned} \tag{2.68}$$

where

$$k_t^2 = m^2 - 2K^2, \quad K^2 = -\frac{(t-m^2)(1-x)}{2Q^2}(Q^2 + x(t-m^2)). \tag{2.69}$$

From these last expressions and from the parameterization of $\bar{p}$ (eq. (2.39)) it is possible to obtain

$$\bar{p} \cdot k_1 = \frac{x}{Q^2}((t-m^2)(2x-1)+Q^2) + k_t \cdot \bar{p}_t, \tag{2.70}$$

where, as in the massless case, the term $k_t \cdot \bar{p}_t$ contributes only if squared and its expression is

$$\frac{1}{2\pi}\int_0^{2\pi}(k_t \cdot \bar{p}_t)^2\, d\phi = -\frac{4x^2}{Q^2}\frac{(t-m^2)(1-x)(Q^2+x(t-m^2))+Q^2m^2}{Q^2}. \tag{2.71}$$

From the t definition, instead, it is possible to obtain

$$t = m^2 - 2k_2 \cdot p = m^2 - 2(k_2^0 p^0 - \left|\vec{k}_2\right||\vec{p}|\cos\theta) = m^2 - 2k_2^0 p^0\left(1 - \frac{\left|\vec{k}_2\right|}{k_2^0}\cos\theta\right) \tag{2.72}$$

from which it is natural to define

$$y = \frac{1}{2}(1 - v\cos\theta), \tag{2.73}$$

with

$$v = \sqrt{1 - \frac{4m^2x}{Q^2(1-x)}}, \tag{2.74}$$

in such a way $t - m^2 = -Q^2y/x$.

It is now enough to plug equation (2.70) in the expression of W_2 (eq. (2.67)) and integrate in the two-body phase-space (APP. A)

$$d\phi_2 = \frac{\lambda^{1/2}(s,m^2,m^2)}{32\pi^2 s}d\Omega = \frac{2}{v}\frac{\sqrt{s}\sqrt{s-4m^2}}{16\pi s} = \frac{1}{8\pi}dy, \tag{2.75}$$

where

$$\lambda(l,m,n) \equiv l^2 + m^2 + n^2 - 2lm - 2ln - 2mn \tag{2.76}$$

is the triangular function and the integration is done from $y_1 = (1+v)/2$ to $y_2 = (1-v)/2$.

So, writing t as a function of y and including all the proper factors it is possible to write

$$\begin{aligned}\hat{F}_2 = \frac{4g_s^2e_q^2T_Rx}{\pi Q^2}\int_{\frac{1+v}{2}}^{\frac{1-v}{2}}\frac{1}{y^2(1-y)^2}\Big[&-\frac{4m^4x^2}{Q^2} \\ &+ 2xm^2(x(y^2+(1-y)^2) - 2y(1-y)(3x-1)) \\ &+ Q^2y(1-y)((2x^2-2x+1) - 2y(1-y)(6x^2-6x+1))\Big]\,dy,\end{aligned} \tag{2.77}$$

which gives the final result

$$\begin{aligned}\hat{F}_2 = 4x\alpha_s e_q^2 T_R\Big[&\ln\frac{1+v}{1-v}(x^2+(1-x)^2+4\tau x(1-3x)-8\tau^2x^2) \\ &+ v(8x(1-x)-1-4\tau x(1-x))\Big],\end{aligned} \tag{2.78}$$

where $\tau = m^2/Q^2$.

The final massive result of eq. (2.78) correctly becomes the massless one in the limit $\tau \to 0$. In fact, in this limit, $v \to 1$ and both the non-divergent and the divergent part of eq. (2.50) are recovered. The term $\ln((1+v)/(1-v))$ is exactly the collinear logarithm, in fact it diverges in the region $Q \gg m$ and multiplies exactly the splitting function P_{qg}. As mentioned at the beginning of this section, it exactly takes the place of the ϵ pole of the massless case and this feature is the reason why the solution of the collinear logarithms problem follows the same track of the collinear divergences factorization.

The fact that there is only one collinear logarithm raised at the same power of the coupling α_s is not accidental but it is related to the general behaviour of these terms. In fact, they appear in the perturbative series in a single-log enhancement form, i.e. they appear always raised to all the possible powers i which are less or equal to the power k of the coupling. Therefore, the perturbative series of a certain observable can be written schematically as

$$\alpha_s(L + L^0) \tag{2.79}$$
$$+\alpha_s^2(L^2 + L + L^0)$$
$$+\alpha_s^3(L^3 + L^2 + L + L^0)$$
$$+\mathcal{O}(\alpha_s^4), \tag{2.80}$$

where L represent the collinear logarithm. It is then clear that, in the kinematic region in which L is large, i.e. the $Q \gg m$ region such that $\alpha_s L \sim 1$, the $(\alpha_s L)^i$ terms become of comparable size whatever the value of the power i and so, truncating the series at a certain finite order, the neglected terms are of the same size of those included. Notice that, as in the massless case, the same problem arises in the small-x limit.

$\hat{F}_L$ computation

The amplitude of $\hat{F_L}$ is

$$W_L = \frac{8x^3}{Q^2} g_s^2 e_q^2 T_R \bar{q}_\mu \bar{q}_\nu \sum \left[\frac{1}{(t-m^2)^2} A^{\mu\nu} + \frac{1}{(u-m^2)^2} B^{\mu\nu} - \frac{2}{(u-m^2)(t-m^2)} C^{\mu\nu} \right], \tag{2.81}$$

where A, B and C are given by eq. (2.64).

Using the properties of $\bar{q}$ and equation (2.62), it is possible to obtain

$$W_L = \frac{32x^3}{Q^2} \frac{g_s^2 e_q^2 T_R}{x^2} \left[\frac{(Q^2 - 2\rho x)(m^2(Q^2 - 8\rho x) - t(Q^2 - 4\rho x))}{(m^2 - t)^2} + \frac{4\rho m^2 x(2\rho x - Q^2)}{(m^2 - u)^2} \right. \tag{2.82}$$
$$\left. + \frac{2\rho x(Q^2(-5m^2 + 2s + t) - 4\rho x(-3m^2 + s + t))}{(m^2 - t)(m^2 - u)} \right],$$

where $\rho = \bar{q} \cdot k_1$ has been used for ease of notation.

Writing now u as a function of s, Q^2 and m^2 (eq. (2.62)) and using $s = Q^2(1 -$

$x)/x$, one can obtain

$$W_L = \frac{32x^3}{Q^2}\frac{g_s^2 e_q^2 T_R}{x^2}\Bigg[\frac{(Q^2-2\rho x)(m^2(Q^2-8\rho x)-t(Q^2-4\rho x))}{(m^2-t)^2} + \frac{4\rho m^2 x^3(2\rho x-Q^2)}{(Q^2+x(t-m^2))^2} + \frac{2\rho x(-Q^2x(4\rho(x-1)-5m^2+t)+4\rho x^2(t-3m^2)+2Q^4(x-1))}{(m^2-t)(x(m^2-t)-Q^2)}\Bigg], \tag{2.83}$$

which is the final expression that can be written in terms of Lorentz invariants.

From the parametrization of eqs. (2.68) and (2.53), it is possible to get the expression

$$\rho = \bar{q}\cdot k_1 = \frac{1}{2x}(Q^2+x(t-m^2)) \tag{2.84}$$

in the centre of mass of the photon-gluon system. Plugging it in (2.82) results in

$$\hat{F}_L = -\frac{x^3}{Q^2}8g_s^2e_q^2T_R\int_{(1+v)/2}^{(1-v)/2}\left[\frac{m^2}{y(y-1)}+Q^2\frac{1-x}{x}\right]dy, \tag{2.85}$$

where $y = x(m^2-t)/Q^2$ has been used and the integration on the phase space has been made explicit.

Performing the integral leads to the final result

$$\hat{F}_L = 16x^3\alpha_s e_q^2 T_R\left[-2\frac{m^2}{Q^2}\ln\frac{1+v}{1-v}+v\frac{1-x}{x}\right]. \tag{2.86}$$

It is important to notice that, although there is the term $\ln\left((1+v)/(1-v)\right)$ which already appeared in the $\hat{F}_2$ expression, in this case it is not a problematic collinear logarithm. In fact, in the limit $Q \gg m$, in which the logarithm diverges, the term m^2/Q^2 tends to zero fast enough to make the whole term converge to zero. This is exactly the expected behaviour because in the massless limit, which is equivalent to $Q \gg m$, the expression of eq. (2.59) has to be recovered and it did not contain ϵ poles.

To summarize, two classes of results have been obtained: massless and massive. The massless results have been computed assuming the mass of the produced b-quark to be zero and this made, in $\hat{F}_2$ case (eq. (2.50)), the integral on the phase space divergent in the collinear region. In order to regulate it, dimensional regularization has been adopted, i.e. the calculation has been performed in $d = 4-2\epsilon$ dimensions, which converts the collinear divergence in an ϵ pole. The factor of this pole was exactly the P_{qg} splitting function, as expected, and this confirmed the applicability of the factorization procedure. The same method has been applied also to $\hat{F}_L$ but it has been found that its phase-space integral is not divergent and so its final expression (eq. (2.59)) is free of ϵ poles.

In the massive case, instead, the computation has been carried out in the standard 4 dimensions because the mass acts as an IR regulator and so collinear divergences were expected to be regularized. In $\hat{F}_2$ case this results in a conversion of the ϵ pole in a mass logarithm, i.e. a log term which becomes large in the limit $Q \gg m$, and, of course, in the appearance of mass power corrections (eq. (2.78)). The fact that the ϵ pole is precisely converted in the mass logarithm is the reason of the analogy between the factorization method and the strategy adopted to resum to all

orders such logarithm terms, as described in the next chapter. In $\hat{F}_L$ case, collinear logarithms have not been found (eq. (2.86)), as expected from the absence of ϵ poles in the massless result.

In the next chapter the strategy adopted to achieve the resummation of collinear logarithms to all orders will be presented in the most general possible way, while, in chapter 4, it will be applied specifically to heavy quark production in DIS and explicit expressions order by order in perturbation theory will be provided.

Chapter 3

Resummation strategy

In this chapter, the way in which it is possible to solve the mass logarithms problem presented in the previous chapters will be analyzed. From what has been discussed so far, it should be clear that, in order to obtain reliable predictions in the kinematic region where the typical energy scale of the process is higher than the bottom mass, it is necessary to resum to all orders the mass logarithms which appear in the perturbative series. The goal of this thesis, however, is to construct a reliable prediction in a wider kinematic region, including also $Q \approx m_b$. In order to achieve that, it will be necessary to construct a matched result which correctly implements the log resummation in the $Q \gg m_b$ region but includes mass power corrections in the $Q \approx m_b$ region.

From a more general and formal point of view, in the computation of a DIS observable, there are at least two energy scales, the factorization scale μ_F, which is set equal to Q, and the soft scale $\mu_\Lambda \sim \Lambda_{QCD} \sim 1GeV$, which separates the perturbative and the non-perturbative regimes. These two scales govern the applicability of the standard QCD factorization theorem, as seen in chapter 1.

Besides these two, there are the energy scales given by the masses of the quarks and that will be denoted as $\mu_q \sim m_q$. These scales, as already discussed, are often taken exactly equal to m_q but, in principle, as long as they are kept of the same order, one is free to separate them. In particular in this work the variations of the results given by the variation of μ_b around m_b are used to estimate the intrinsic resummation uncertainties.

The typical DIS energy scales are of the order of some GeV so the masses of the first four quarks can be safely considered equal to zero, while, since the mass of the top-quark is $\approx 170\,\text{GeV}$, it is completely decoupled from the theory adopting the decoupling scheme (1.2.1). For the sake of completeness it is also worth to mention that, since the mass of the c-quark sits exactly at the border between perturbative and non-perturbative regimes, in some cases also the charm quark can be treated as we will treat the bottom quark in this work [9].

Therefore, the only relevant scales one is left with are m_b, Q and μ_Λ. The hierarchy between Q and m_b determines the way of computation in which the observable has the best approximation. In particular there are three main cases:

I $Q \ll m_b$: In this case the b quark can be ignored as the t quark. Therefore it is renormalized trough the decoupling scheme and the computation is done considering only four massless quarks.

II $Q \sim m_b$: In this case there is only one energy scale in addition to μ_Λ. The b quark never appears as initial state of the process but can be produced by

the hard interaction. Therefore the partonic calculation contains the exact dependence on m_b but the b quark is still considered a non-active flavour and does not contribute to the evolutions (DGLAP and running coupling). Moreover, m_b acts as an IR regulator and so the collinear singularities, given by the gluon splitting in a b-pair, produce $\ln(m_b^2/Q^2)$ terms, which, in this regime, are considered small and so included in the fixed order expansion.

III $Q \gg m_b$: In this case there are two separate scales in addition to μ_Λ. The b quark is considered an active flavour so its renormalization scheme is switched from decoupling to $\overline{MS}$ and it also contributes to DGLAP evolution. The collinear logarithms are not small in this regime and so they spoil the accuracy of the fixed order expansion, hence they are resummed to all orders in an effective b quark PDF. In this case the calculation is carried out in the $m_b \to 0$ limit because the finite-mass effects are power correction $\mathcal{O}(m_b/Q)$ and thus can be safely neglected.

In this work, the result obtained following the approach of the second case will be called fixed-order (FO) result, while the one obtained following the third case will be called resummed (R) result. The first case is a trivial limit of the FO case and so it will not be treated in this thesis.

Therefore, as mentioned at the beginning of this chapter, in order to obtain a theoretical prediction that is valid in a wide range of energy, it is often desirable to construct a 5FS matched result which includes the right mass-dependence for scales near the b quark mass and the resummation of collinear logarithms in the region $Q \gg m_b$. How this combination is carried out will be explained in section 3.3. This matched result is then combined with the four active flavour (4FS) result of the FO approach trough a variable flavour number scheme (VFNS). In contrast, the result obtained following only one of the two approaches, in particular the FO one in the bottom quark case, is referred to as obtained in a fixed-flavour number scheme (FFNS).

The way in which the FO result can be constructed will be explained in the following section (3.1), while the adopted strategy for the construction of the R result will be presented in 3.2. In both cases, the obtained expressions will always be at all orders and only in sec. 3.1.1 some truncations at finite order will be analyzed. This means that, since when an observable is constructed in two different ways, they can differ from each other only if the perturbative series is truncated, the expressions obtained in the following are expected to be equivalent to the analogous ones from [5, 6, 7, 8]. In sec. 3.4, this equivalence, in particular with FONLL and ACOT constructions, will be explicitly verified.

3.1 Fixed Order (FO) result

In the kinematic region in which $Q \sim m_b$, the best way to construct a prediction for a DIS observable is to consider the 4FS in which only the light quarks, which are treated as massless, contribute to the evolutions and the b quark is treated as a massive non-active flavour. Therefore, one has to reabsorb the poles $1/\epsilon$ which come from the collinear divergences of the massless quarks in the PDFs, but leave the $\ln(m_b^2/Q^2)$ unresummed. This is exactly the factorization procedure presented in sec. 1.3.1 but, for the sake of completeness and to clarify the notation, it will be recalled in this section.

According to the parton model in Mellin space, a certain DIS observable can be

written as

$$F = \sum_{i=q,\bar{q},g} C_i^B(m_b,\epsilon) f_i^{B[4]}, \tag{3.1}$$

where $C_i^B(\epsilon, m_b)$ are the bare coefficients functions for the observable F, $f_i^{B[4]}$ are the bare PDFs in the 4FS and the sum runs over the number of active flavours ($n_f = 4$). The objects denoted with the apex B are bare in the sense that the factorization procedure has not been applied yet. Therefore, the coefficients functions are IR divergent in the collinear region and, being regularized via dimensional regularization, contain ϵ poles. From now on, the number in the square parenthesis denotes the adopted flavour scheme and the dependencies on the scales will not always be explicitly written for ease of notation.

Adopting the factorization procedure, it is possible to factorize the $1/\epsilon$ terms from the coefficients functions as

$$\begin{aligned} C_i^B(\epsilon, m_b) &= \sum_{j=q,\bar{q},g} C_j^{[4]}(m_b,\epsilon)\Gamma_{ji}^{[4]}(\epsilon) \\ C_j^{[4]}(m_b) &= \lim_{\epsilon\to 0} \sum_{i=q,\bar{q},g} C_i^B(\epsilon, m_b)(\Gamma^{[4]})_{ij}^{-1}(\epsilon), \end{aligned} \tag{3.2}$$

where $C_j^{[4]}(m_b)$ are the new coefficients functions in which there are no poles and $\Gamma_{ji}^{[4]}(\epsilon)$ are the collinear counter-terms. Notice that eq. (3.2) has been written in Mellin space, as it will be done in the following as well. The collinear counter-terms contain the poles $1/\epsilon$ and, as already mentioned, can be written in terms of the Altarelli-Parisi splitting functions P_{ij} as

$$\Gamma_{ij}^{[4]}(\epsilon) = \delta_{ij} - \frac{\alpha_s^{[4]}}{\epsilon} P_{ij}^{(0)}(z) + \mathcal{O}(\alpha_s^2), \tag{3.3}$$

where the square bracket above the coupling denotes that, as mentioned in sec. 1.2.1, the UV renormalization scheme is $\overline{MS}$ for the light quarks and the decoupling scheme for the b and t quarks. Notice that the number inside the round brackets denotes the expansion order of the term they refer to and this convention will be used in the rest of the thesis as well.

The $C_j^{[4]}(m_b)$ contains the exact bottom mass dependence and also the collinear logarithm terms which, in this region are not large and so do not spoil the perturbative expansion. They can be computed expanding in $\alpha_s^{[4]}$ both sides of eq. (3.2) order by order in perturbation theory, as it is done in sec. 3.1.1 up to $\mathcal{O}(\alpha_s^2)$.

Therefore, plugging the coefficients function definition of eq. (3.2) in eq. (3.1), the observable F computed at fixed order takes the form

$$F^{FO} = \sum_{i,j=q,\bar{q},g} C_j^{[4]}(m_b,\epsilon)\Gamma_{ji}^{[4]}(\epsilon) f_i^{B[4]}, \tag{3.4}$$

so, defining the new PDFs as

$$f_j^{[4]}(\epsilon) = \sum_{i=q,\bar{q},g} \Gamma_{ji}^{[4]}(\epsilon) f_i^{B[4]}, \tag{3.5}$$

one can obtain its final expression

$$F^{FO} = \sum_{i=q,\bar{q},g} C_j^{[4]}(m_b) f_j^{[4]}, \tag{3.6}$$

which has been obtained in the $\epsilon \to 0$ limit.

It is important to notice that, since the observable expression must be finite and since the $C_j^{[4]}(m_b)$ do not contain ϵ pole, also the new PDFs are free from IR divergences. However, they are defined at a low energy scale $\mu_\Lambda \approx 1\,\text{GeV}$, so they must be evolved to the scale Q using DGLAP equations (1.3.2) as

$$f_i^{[4]}(Q) = \sum_{j=q,\bar{q},g} U_{ij}^{[4]}(Q,\mu_\Lambda) f_j^{[4]}(\mu_\Lambda), \tag{3.7}$$

where $U_{ij}^{[4]}(Q,\mu_\Lambda)$ are called DGLAP evolution functions and, being the solutions of the DGLAP equation, implement the PDF evolution from the scale μ_Λ to Q.

Therefore, the final FO expression becomes

$$F^{FO}(Q,m_b) = \sum_{i,j=q,\bar{q},g} C_i(Q,m_b) U_{ij}^{[4]}(Q,\mu_\Lambda) f_j^{[4]}(\mu_\Lambda), \tag{3.8}$$

where all the scale dependencies have been written explicitly.

3.1.1 Coefficients function expressions up to $\mathcal{O}(\alpha_s^2)$ in the FO scheme

The 4FS coefficients functions for heavy-quark production are determined in perturbation theory expanding both sides of eq. (3.2) in $\alpha_s^{[4]}$. Adopting the convention for the expansions

$$\begin{aligned} C_i^B(m_b,\epsilon) &= \sum_{k=1} C_i^{(k)B}(m_b,\epsilon)\left[\frac{\alpha_s^{[4]}(Q)}{2\pi}\right]^k \\ C_i^{[4]}(m_b,\epsilon) &= \sum_{k=1} C_i^{(k)[4]}(m_b,\epsilon)\left[\frac{\alpha_s^{[4]}(Q)}{2\pi}\right]^k \\ \Gamma_{ij}^{[4]}(\epsilon) &= \sum_{k=0} \Gamma_{ij}^{(k)[4]}(\epsilon)\left[\frac{\alpha_s^{[4]}(Q)}{2\pi}\right]^k, \end{aligned} \tag{3.9}$$

and knowing that there are no $\mathcal{O}(1)$ Feynman diagrams for heavy-quark production in the 4FS, it is clear that $C_i^{(0)B}(\epsilon,m_b) = 0$ and so $C_i^{(0)[4]}(m_b) = 0$.

At NLO, i.e $\mathcal{O}(\alpha_s)$, since

$$\Gamma_{ij}^{(0)[4]}(\epsilon) = \delta_{ij}\delta(1-z), \tag{3.10}$$

one obtains simply

$$\begin{aligned} C_g^{(1)[4]}(m_b,\epsilon) &= C_g^{(1)B}(m_b,\epsilon) \\ C_q^{(1)[4]}(m_b) &= 0, \end{aligned} \tag{3.11}$$

where the $C_g^{(1)B}(m_b,\epsilon)$ is given by the Feynman diagram computed in sec. 2.2.2 and it is exactly the expression of eq. (2.78) or eq. (2.86) depending on whether the observable in computation is respectively F_2 or F_L. Notice that, in this case, the bare gluon coefficients function is equal to the redefined one. This is exactly the expected behaviour since it does not contain ϵ poles and since its collinear logarithms are retained in the series at fixed-order. Notice also that eqs. (2.78) and

(2.86) contain the exact bottom mass dependence, as desired, and that the quark coefficients function is zero since the only way to produce a b quark extracting a quark from the proton at $\mathcal{O}(\alpha_s)$ is that the extracted quark itself is the bottom (fig. 2.1), but this can not happen in the 4FS.

At NNLO, since

$$\begin{aligned}\Gamma_{gg}^{(1)[4]}(\epsilon, z) &= -\frac{\alpha_s}{\epsilon} P_{gg}^{(1)}(z) \\ \Gamma_{gq}^{(1)[4]}(\epsilon, z) &= -\frac{\alpha_s}{\epsilon} P_{gq}^{(1)}(z),\end{aligned} \tag{3.12}$$

where the one-loop splitting functions are defined in eq. (1.39), one obtains

$$\begin{aligned}C_g^{(2)[4]}(m_b, \epsilon) &= C_g^{(2)B}(m_b, \epsilon) - C_g^{(1)[4]}(m_b, \epsilon)\Gamma_{gg}^{(1)[4]}(\epsilon, z) \\ C_q^{(2)[4]}(m_b, \epsilon) &= C_q^{(2)B}(m_b, \epsilon) - C_g^{(1)[4]}(m_b, \epsilon)\Gamma_{gq}^{(1)[4]}(\epsilon, z).\end{aligned} \tag{3.13}$$

The $C_g^{(2)B}(m_b, \epsilon)$ and the $C_q^{(2)B}(m_b, \epsilon)$ come respectively from the Feynman diagrams of fig. 3.1 and fig. 3.2.

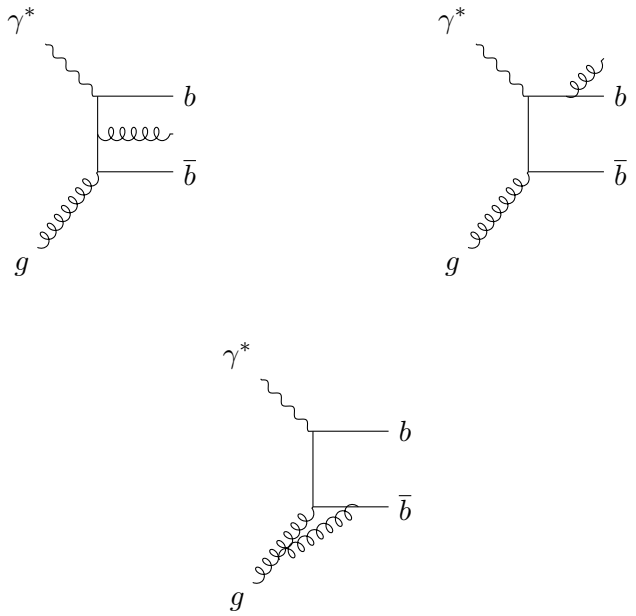

Figure 3.1. The three gluon-initiated Feynman diagrams contributing to the $\mathcal{O}(\alpha_s^2)$ DIS with heavy-quark production. Notice that in the final products are included also other particles (in this case gluons) other than the b quarks. This is a direct consequence of the heavy-quark process definition adopted in this thesis (2.2).

In this case they are affected by collinear divergences in the form of ϵ poles and so they must be subtracted by the collinear counter-terms. The collinear logarithms, instead, are not subtracted and they are retained, together with the exact m_b dependence, in the perturbative series.

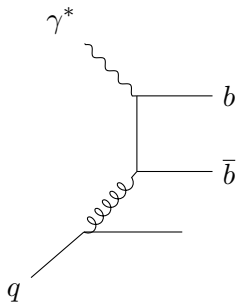

Figure 3.2. Quark-initiated Feynman diagram contributing to the $\mathcal{O}(\alpha_s^2)$ DIS with heavy-quark production. Notice that in the final products are included also other particles (in this case light quarks) other than the b quarks. This is a direct consequence of the heavy-quark process definition adopted in this thesis (2.2).

3.2 Resummed (R) result

In the $Q \gg m_b$ kinematic region, the $\ln(m_b^2/Q^2)$ terms are large and they would spoil the accuracy of the perturbative series if included at fixed order. Hence, they have to be resummed to all orders adopting the 5FS. The coefficients functions should be computed in the massless limit, since power mass corrections can be completely neglected in this region, and the b quark should be treated as an active flavour and thus included in the running of the coupling and in DGLAP evolution equations. As already mentioned, the resummation is achieved through a factorization of the collinear logarithms and a redefinition of the PDFs which includes them, in such a way DGLAP equation resums them in the evolution. This property of DGLAP equations is discussed in sec. 3.2.1.

Therefore, the 5FS result can be written as

$$F^R = \sum_{i,j=q,\bar{q},b,\bar{b},g} C_j^{[5]} \Gamma_{ji}^{[5]}(\epsilon) f_i^{B[5]} = \sum_{j=q,\bar{q},b,\bar{b},g} C_j^{[5]} f_j^{[5]}, \tag{3.14}$$

where the $C_j^{[5]}$ are massless and have been regularized trough the standard collinear factorization, as in the 4FS case. Notice that, as in the rest of this chapter, the fact that the sum runs also over the b quark is explicitly written.

However, the 5FS PDFs $f_j^{[5]}$ and the 4FS set $f_j^{[4]}$ come from the same underlying PDFs, so it must be possible linking one to the other. This can be done using the bottom mass m_b as IR regulator. In this way, as mentioned in the previous chapter, the collinear divergences become mass logarithms which can be factorized in the so-called matching functions $K_{ij}^{[5]\to[4]}$. This is the content of the Collins factorization theorem ([22, 23]) that can be stated as

$$C_j^{[4]}(Q, m_b) = \sum_{k=q,\bar{q},b,\bar{b},g} C_k^{[5]} K_{kj}^{[5]\leftarrow[4]}(m_b, \mu_b) + \mathcal{O}\left(\frac{m_b^2}{Q^2}\right), \tag{3.15}$$

where the $C_k^{[5]}$ contain no collinear logarithms and no power corrections, as explicitly written. The apex above the matching functions denotes the fact that they link the 4FS coefficients functions with the 5FS ones.

The matching functions $K_{ij}^{[5]\leftarrow[4]}$ contain the collinear logarithms and they are the massive version of the collinear counter-terms Γ_{ij}, which contain the ϵ poles

coming from the regularized collinear divergences. Actually, they are the same object but, while the matching functions are obtained when the mass is used as IR regulator, the collinear counter-terms are obtained when adopting dimensional regularization. Notice that, while the collinear counter-terms are terms of a square matrix, the matching functions are terms of a rectangular matrix, as it is possibile to see from eq. (3.15). This feature will play an important role in the matched result construction addressed in section 3.3.

From eq. (3.15), it is then clear that the 5FS PDFs can be linked to the 4FS PDFs as

$$f_k^{[5]}(m_b,\mu_b) = \sum_{j=q,\bar{q},g} K_{kj}^{[5]\leftarrow[4]}(m_b,\mu_b) f_j^{[4]}(\mu_b). \tag{3.16}$$

Notice that the contributions to the bottom PDF $f_b^{[5]}$ come only from the off-diagonal $K_{bj}^{[5]\leftarrow[4]}$ terms. Since the matching function perturbative expansion is in the form

$$K_{ij}^{[5]\leftarrow[4]} = \delta_{ij}\delta(1-z) + \alpha_s k_{ij}^{(1)} + \mathcal{O}(\alpha_s^2), \tag{3.17}$$

and so the off-diagonal terms are at least of $\mathcal{O}(\alpha_s)$, the bottom PDF is said to be only perturbatively generated. This means that, unlike the other PDFs, which have an intrinsic component of $\mathcal{O}(1)$, the $f_b^{[5]}$ leading order is of order α_s. This feature will have a strong impact on the perturbative counting adopted in the final results which will be discussed in the next chapter.

However, it is important to underline that, in principle, one is free to consider an intrinsic component also for the heavy quark PDF and this is what it has been done for instance in [9] in the charm case. In the bottom case, instead, this is usually not done because its intrinsic PDF is expected to be very small or even zero because of its high mass with respect to the proton mass.

Moreover, it is also important to notice that the fact that $K_{ij}^{[5]\leftarrow[4]}$ is a rectangular matrix is exactly caused by the absence of intrinsic bottom component. In fact, if there had been $f_b^{[4]}$ in eq. (3.16), the sum would have run also over the b quark and $K_{ij}^{[5]\leftarrow[4]}$ would have been a square matrix.

In order to obtain the observable expression at a certain scale Q, it is necessary to evolve the 5FS PDFs using DGLAP evolution equations, as it has been already done in the 4FS case. However, in this case, one has also to include the matching functions, so the evolved PDFs take the form

$$f_k^{[5]}(Q,m_b) = \sum_{j=q,\bar{q},b,\bar{b},g} \sum_{i,p=q,\bar{q},g} U_{kj}^{[5]}(Q,\mu_b) K_{jp}^{[5]\leftarrow[4]}(m_b,\mu_b) U_{pi}^{[4]}(\mu_b,\mu_\Lambda) f_i^{[4]}(\mu_\Lambda), \tag{3.18}$$

where the apex above the DGLAP kernels denotes the number of flavours which take part to the evolution and all the scale dependencies have been explicitly written. In eq. (3.18) the starting PDFs $f_i^{[4]}(\mu_\Lambda)$ are firstly evolved to the μ_b scale with $U_{pi}^{[4]}(\mu_b,\mu_\Lambda)$, then they are converted to their 5FS version thanks to $K_{jp}^{[5]\leftarrow[4]}(m_b,\mu_b)$ and finally they are evolved to the final scale Q with $U_{kj}^{[5]}(Q,\mu_b)$. Notice that the latter is exactly the term which resums the logarithms $\ln(Q^2/m_b^2)$, as explained in the next section.

Plugging the last equation in (3.14) leads to

$$F^R(Q,m_b) = \sum_{k,j=q,\bar{q},b,\bar{p},g} \sum_{i,p=q,\bar{q},g} C_k^{[5]}(Q) U_{kj}^{[5]}(Q,\mu_b) K_{jp}^{[5]\leftarrow[4]}(m_b,\mu_b) U_{pi}^{[4]}(\mu_b,\mu_\Lambda) f_i^{[4]}(\mu_\Lambda), \tag{3.19}$$

which represents the final resummed result.

Notice that the observable F^R does not depend on the scale μ_b because eq. (3.19) is an all-order expression but, if it was truncated at a certain finite order, it would have a residual dependence. This dependence is expected to decrease as the perturbative order increases and so it can be used as a validation test of the adopted perturbative counting and to estimate the theoretical uncertainties linked to the missing orders. This is exactly what will be done in the numerical implementation in chapter 5.

3.2.1 Resummation and DGLAP evolution equations

The whole resummation strategy explained in the previous section works thanks to the property of the DGLAP evolution kernel $U_{ij}^{[5]}(\mu, \mu_0)$ of resumming the logarithmic terms of the form $L = \ln(\mu^2/\mu_0^2)$ to all orders. In particular, if its $\mathcal{O}(\alpha_s^i)$ version is used, all the logarithmic terms like $\alpha_s^k L^k, \alpha_s^k L^{k-1}, \dots \alpha_s^k L^{k-i}$ are resummed to all orders (i.e. for every k value). For instance, taking the leading-log (LL) expression, i.e. the $\mathcal{O}(1)$, of the DGLAP kernel, it resums all the terms in which the power of the coupling and the power of the collinear logarithm coincide, i.e the first coloumn of eq. (2.79). Therefore, the results obtained in this way are called leading-log (LL) results.

This property of DGLAP equations follows from the fact that it is equivalent to an RGE equation, such as the running coupling one (eq. (1.23)), which has the property of resumming logarithms of the evolution scales as well. The goal of this section is to give the basic idea of how this feature works at LL in the most simplified scenario.

Starting from any of the decoupled DGLAP equations in Mellin space

$$\mu^2 \frac{d}{d\mu^2} f(N, \mu^2) = P(N, \alpha_s(\mu^2)) f(N, \mu^2), \tag{3.20}$$

its solution can be written as

$$f(N, \mu_F^2) = f(N, \mu_0^2) \exp\left\{ \int_{\mu_0^2}^{\mu_F^2} P(N, \alpha_s(\mu^2)) \frac{d\mu^2}{\mu^2} \right\}, \tag{3.21}$$

where μ_0^2 and μ_F^2 are respectively the initial and the final evolution scales. Considering only the lowest order of the splitting function expansion,

$$P(N, \alpha_s(\mu^2)) = P^{(1)}(N) \alpha_s(\mu^2), \tag{3.22}$$

and neglecting the dependence on μ^2 of the coupling, since it gives an higher order contribution, results in

$$\begin{aligned} f(N, \mu_F^2) &= f(N, \mu_0^2) \exp\left\{ P^{(1)}(N) \alpha_s \ln \frac{\mu_F^2}{\mu_0^2} \right\} \\ &= f(N, \mu_0^2) \sum_{k=0}^{\infty} \frac{(P^{(1)}(N))^k}{k!} \left(\alpha_s \ln \frac{\mu_F^2}{\mu_0^2} \right)^k. \end{aligned} \tag{3.23}$$

From the last equation it is clear that every term of the form $(\alpha_s \ln(\mu_F^2/\mu_0^2))^k$ is resummed to all orders in α_s and this is exactly what it has to be shown. Clearly, the choice of considering only a decoupled, i.e. non singlet, DGLAP equation has been

made for the sake of simplicity, but the same conclusion would have been obtained if the singlet equations were considered.

An analogous calculation can be carried out at the next perturbative order to show the resummation of also the terms $\alpha_s^k(\ln(\mu_F^2/\mu_0^2))^{k-1}$, but it is more complicated because the running coupling must be considered in this case. However, other techniques can be exploited in order to get an explicit expression of the NLO evolution kernels and thus recognize the next-to-leading log resummation. Although they are not treated in this thesis, one may refer to [24] for a detailed description.

3.3 Matched result: combination of the 4FS with the 5FS

The final 4FS and 5FS results obtained in the previous sections represent the best approximation for a certain observable respectively in the $Q \sim m_b$ and in the $Q \gg m_b$ regions. In order to match these two expressions and obtain a reliable prediction on the whole considered kinematic region, it is necessary to construct the 5FS matched result which combines the 4FS result and the 5FS resummed result in such a way to retain the mass power corrections in the threshold region, i.e. the $Q \sim m_b$ region, and to resum the collinear logarithms in the high-energy one.

The standard approach [25] for combining a resummation with its corresponding fixed-order result is to write the full observable as

$$F = F^R + F^{nons}, \tag{3.24}$$

where F^R is the 5FS R result of eq. (3.19) and F^{nons} contains all the mass power corrections and thus vanishes in the limit $m_b \to 0$. This last condition ensures that eq. (3.24) correctly implements the resummed 5FS result in the high-energy limit.

In order to get the mass power corrections of the 4FS result in the threshold region, it is necessary to require that the fixed-order expansion of eq. (3.24) reproduces the correct FO result of eq. (3.8). This means to impose

$$F^{nons} = F^{FO} - F^{sing}, \tag{3.25}$$

where F^{FO} is exactly the final FO result of eq. (3.8), while $F^{sing} = F^R|_{FO}$ is the fixed-order expansion of the resummed result at a certain α_s order. In order to make F^{nons} actually vanish in the $m_b \to 0$ limit, F^{sing} must contain all singular terms which are present in F^{FO}, i.e. all the contributions which do not vanish in the massless limit. Clearly, this last condition is a meaningful definition only if the 5FS resummed result at a given order incorporates all these fixed-order singular terms and, therefore, the perturbative counting of the two result must be consistent. The final expanded results presented in the next chapter exactly respect this needed feature.

Moreover, the 4FS result is naturally expanded in terms of $\alpha_s^{[4]}$, while the 5FS result is in terms of its $n_f = 5$ version but, in order to get a consistent comparison between FO and R results, it is advisable to expand them in terms of the same coupling. In this thesis we choose to use $\alpha_s^{[5]}$ in both cases. Therefore, for F^{FO}, it is enough to use the matching equation (1.30) in the expressions of the $C_i^{[4]}(Q, m_b, \alpha_s^{[4]})$, obtaining the converted 4FS coefficients functions $D_i^{[4]}(Q, m_b, \alpha_s^{[5]})$. Notice that, although they are denoted with different symbols for the sake of clarity, they are the same object and only the terms of their perturbative expansions differ.

Thanks to the consistent construction of the 5FS resummed result with respect to the 4FS result, it is possible to obtain F^{sing} simply evaluating the resummed result at $\mu_b = Q$, as

$$F^{sing} = F^{resum}|_{FO} = F^{resum}|_{\mu_b=Q} \tag{3.26}$$
$$= \sum_{i,j,k=q,\overline{q},g} [C_j^{[5]}(Q,m_b)K_{ji}^{[5]\leftarrow[4]}(m_b,Q) + C_b^{[5]}(Q,m_b)K_{bi}^{[5]\leftarrow[4]}(m_b,Q)]U_{ik}^{[4]}(Q,\mu_\Lambda)f_k^{[4]}(\mu_\Lambda),$$

which, plugged in the definition of F^{nons}, gives

$$F^{nons} = F^{FO} - F^{sing} \tag{3.27}$$
$$= \sum_{i,j=q,\overline{q},g} [D_i^{[4]}(Q,m_b) - C_j^{[5]}(Q,m_b)K_{ji}^{[5]\leftarrow[4]}(m_b,Q) - C_b^{[5]}(Q,m_b)K_{bi}^{[5]\leftarrow[4]}(m_b,Q)]\, f_i^{[4]}(Q),$$

with

$$f_i^{[4]}(Q) = \sum_{k=q,\overline{q},g} U_{ik}^{[4]}(Q,\mu_\Lambda)f_k^{[4]}(\mu_\Lambda). \tag{3.28}$$

Notice that, in this case, the sum runs only on the light flavours because the bottom terms have been explicitly separated from the light-quark terms.

The F^{nons} expression of eq. (3.27) is free of collinear logarithms, which are exactly cancelled by the singular terms order by order in perturbation theory. Moreover, it vanishes for $m_b \to 0$, as required.

However, this F^{nons} expression is expressed in terms of the 4FS PDFs computed at the scale Q, while the resummed result is necessarily expressed in terms of the 5FS PDFs $f_i^{[5]}(Q,m_b)$. This is not advisable from an implementation point of view because it makes necessary to construct and evolve two different sets of PDFs. Therefore, the most simple solution is to write the nonsingular contributions in terms of the 5FS PDFs, imposing

$$F^{nons} = \delta C_i^{nons}(Q,m_b)f_i^{[5]}(Q,m_b), \tag{3.29}$$

where the $\delta C_i^{nons}(Q,m_b)$ are fixed comparing the last equation with eq. (3.27). In order to express $f_i^{[4]}$ in terms of $f_i^{[5]}$, one has to invert eq. (3.16) as

$$f_i^{[4]}(\mu_b) = \sum_{j=q,\overline{q},b,\overline{b},g} (K^{[5]\leftarrow[4]})_{ij}^{-1}(m_b,\mu_b)f_j^{[5]}(m_b,\mu_b) \tag{3.30}$$
$$= \sum_{j=q,\overline{q},b,\overline{b},g} K_{ij}^{[4]\leftarrow[5]}(m_b,\mu_b)f_j^{[5]}(m_b,\mu_b),$$

which can be exploited in the comparison between eq. (3.27) and eq. (3.29) to obtain

$$\delta C_i^{nons} = \sum_{j=q,\overline{q},g} [D_j^{[4]}(Q,m_b) - \sum_{k=q,\overline{q},b,\overline{b},g} [C_k^{[5]}(Q)K_{kj}^{[5]\leftarrow[4]}(m_b,Q)]]\, K_{ji}^{[4]\leftarrow[5]}(m_b,Q), \tag{3.31}$$

where $i = q,\overline{q},b,\overline{b},g$.

Since $K_{ij}^{[5]\leftarrow[4]}$ is a rectangular matrix, its inverse $K_{ij}^{[4]\leftarrow[5]}$ is ambiguous and so the last expression is a set of under-constrained equations. This ambiguity has been treated in different ways in the various schemes available in literature. In this thesis,

it has been chosen to exploit it to simplify the construction of the matched result. In particular, one can choose to fix the two exceeding degrees of freedom imposing

$$\delta C_b^{nons}(Q, m_b) = \delta C_{\overline{b}}^{nons}(Q, m_b) = 0 \tag{3.32}$$

in such a way to avoid including the power-mass corrections in the bottom coefficients function (the same choice has been also made in S-ACOT [7], FONLL [5], TR [8] and BPT [25] schemes). It is important to notice that this is only a matter of choice and, therefore, does not imply that any kind of approximation has been adopted.

It is then possible to absorb the nonsingular contributions into the redefinition of the coefficients functions as

$$\begin{aligned} \tilde{C}_i(Q, m_b) &= C_i^{[5]}(Q) + \delta C_i^{nons}(Q, m_b) \quad i = q, \overline{q}, g \\ \tilde{C}_b(Q, m_b) &= C_b^{[5]}(Q), \end{aligned} \tag{3.33}$$

which, in practice, includes the mass power corrections of $\delta C_i^{nons}(Q, m_b)$ in the massless light-quark coefficients functions $C_i^{[5]}(Q)$, while leaving untouched the bottom coefficients function $C_b^{[5]}(Q)$, as desired.

Exploiting the definitions of eq. (3.33) in eq. (3.31), it is also possible to obtain

$$\sum_{i=q,\overline{q},g} \tilde{C}_i(Q, m_b) K_{ij}^{[5]\leftarrow[4]}(Q, m_b) = D_j^{[4]}(Q, m_b) - C_b^{[5]}(Q) K_{bj}^{[5]\leftarrow[4]}(Q, m_b), \tag{3.34}$$

where $j = q, \overline{q}, g$. This last equation means that the nonsingular contributions can be absorbed into the resummed result just computing the matching functions at the scale Q.

The final all-order expression for the matched result is then

$$F = \sum_{i=q,\overline{q},g} \tilde{C}_i(Q, m_b) f_i^{[5]}(Q) + C_b(Q) f_b^{[5]}(Q). \tag{3.35}$$

As mentioned at the beginning of this chapter, this matched result provides reliable predictions in both the threshold region ($Q \sim m_b$) and the high-energy region ($Q \gg m_b$) and, in the final numerical results presented in chapter 5, it is combined to the 4FS FO result trough a VFNS, in such a way to include also the $Q \lesssim m_b$ region. [1]

For the sake of completeness, it is worth to report the truncated at NLO and NNLO expression of the $\tilde{C}_i(Q, m_b)$. Expanding at NLO eq. (3.34) results in

$$\begin{aligned} \tilde{C}_{g,2}^{(1)}(Q, m_b) &= D_{g,2}^{[4](1)}(Q, m_b) - C_{b,2}^{[5](0)}(Q) K_{bg}^{[5]\leftarrow[4](1)}(m_b, \mu_b) \\ \tilde{C}_{g,L}^{(1)}(Q, m_b) &= D_{g,L}^{[4](1)}(Q, m_b) \\ \tilde{C}_{q,2}^{(1)}(Q, m_b) &= D_{q,2}^{[4](1)}(Q, m_b) - C_{b,2}^{[5](0)}(Q) K_{bq}^{[5]\leftarrow[4](1)}(m_b, \mu_b) = 0 \\ \tilde{C}_{q,L}^{(1)}(Q, m_b) &= D_{q,L}^{[4](1)}(Q, m_b) = 0, \end{aligned} \tag{3.36}$$

where the subscripts denote the structure function to which the coefficients functions are referring. Notice that $\tilde{C}_{q,2}^{(1)}(Q, m_b)$ is zero because both $D_{q,2}^{[4](1)}(Q, m_b)$ and

[1] Actually, although the two energy regions, $Q \sim m_b$ and $Q \gg m_b$, are described both by the matched result, the perturbative counting which has to be adopted for each of them is different, as it will be shown in chapter 4

$K_{bq}^{[5]\leftarrow[4](1)}(m_b,\mu_b)$ are zero and that $\tilde{C}_{g,L}^{(1)}(Q,m_b) = D_{g,L}^{[4](1)}(Q,m_b)$ exactly reflects the fact that in $D_{g,L}^{[4](1)}(Q,m_b)$ there are no collinear logarithms to subtract.

At NNLO they read

$$\begin{aligned}
\tilde{C}_{g,2}^{(2)}(Q,m_b) &= D_{g,2}^{[4](2)}(Q,m_b) - C_{b,2}^{[5](0)}(Q)K_{bg}^{[5]\leftarrow[4](2)}(m_b,\mu_b) \\
&\quad - C_{b,2}^{[5](1)}(Q)K_{bg}^{[5]\leftarrow[4](1)}(m_b,\mu_b) - C_{g,2}^{[5](1)}(Q)K_{gg}^{[5]\leftarrow[4](1)}(m_b,\mu_b) \\
\tilde{C}_{g,L}^{(2)}(Q,m_b) &= D_{g,L}^{[4](2)}(Q,m_b) - C_{b,L}^{[5](1)}(Q)K_{bg}^{[5]\leftarrow[4](1)}(m_b,\mu_b) - C_{g,L}^{[5](1)}(Q)K_{gg}^{[5]\leftarrow[4](1)}(m_b,\mu_b) \\
\tilde{C}_{q,2}^{(2)}(Q,m_b) &= D_{q,2}^{[4](2)}(Q,m_b) - C_{b,2}^{[5](0)}(Q)K_{bq}^{[5]\leftarrow[4](2)}(m_b,\mu_b) - C_{g,2}^{[5](1)}(Q)K_{gq}^{[5]\leftarrow[4](1)}(m_b,\mu_b) \\
\tilde{C}_{q,L}^{(2)}(Q,m_b) &= D_{q,L}^{[4](2)}(Q,m_b) - C_{g,L}^{[5](1)}(Q)K_{gq}^{[5]\leftarrow[4](1)}(m_b,\mu_b).
\end{aligned} \tag{3.37}$$

In the next section, the matched result all-order expression of eq. (3.35) will be compared to the analogous expressions proposed by FONLL and S-ACOT schemes, in order to verify their equivalence.

3.4 All-order equivalence with FONLL and S-ACOT constructions

The matched result expression of eq. (3.35) is the all-order result proposed in this thesis (obtained following the procedure presented in [25]) and it will be the one which will be expanded in perturbation theory and thus implemented. Being an all-order expression, it has to be equivalent to the analogous final results which are available in literature, as mentioned at the beginning of this chapter. This section's goal is to verify this equivalence, in particular with FONLL and S-ACOT schemes.

The first necessary step is to recall the FONLL construction and notation. In the following they will be briefly summarized but the complete construction can be found in [5].

The FONLL result is constructed summing the 4FS massive result with the resummed massless 5FS one and subtracting any double counted terms. Therefore, for a generic observable F, the FONLL result can be written as

$$F_{\text{FONLL}}(Q,m_b) = F^{[4]}(Q,m_b) + F^{[5]}(Q,0) - F^{[4,0]}(Q,m_b), \tag{3.38}$$

where in $F^{[4,0]}(Q,m_b)$ the double counted terms are included and hence it can be obtained as the massless limit of the 4FS result. However, this limit is divergent, so a proper definition of it is given by

$$F^{[4,0]}(Q,m_b) = \sum_{i=g,q,\bar{q},b,\bar{b}} C_i^{[4,0]}(m_b,Q) f_i^{[4]}(Q), \tag{3.39}$$

where the $C_i^{[4,0]}(m_b,Q)$ are called massive-zero coefficients functions and are obtained as the massless limit of the 4FS result leaving the log terms untouched. Notice that, as usual, all the expressions are written in Mellin space and that, so far, no assumptions on the intrinsic b quark PDF have been made. Therefore, its existence is admitted.

In this way it is clear that, when $Q \gg m_b$, the term $F^{[4]}(Q,m_b) - F^{[4,0]}(Q,m_b)$ vanishes as powers of m_b/Q and the 5FS massless result is recovered, while, when $Q \sim m_b$, the term $F^{[d]} = F^{[5]}(Q,0) - F^{[4,0]}(Q,m_b)$ becomes sub-leading in α_s, since there are no large logarithms, and so the massive 4FS result is recovered.

In order to obtain the massive-zero limit order by order in perturbation theory, it is necessary to express the 4FS result in terms of the 5FS PDFs and coupling, as it has been already done in the previous section. The PDFs in the 5FS are related to the 4FS ones by

$$f_i^{[5]} = \sum_{j=g,q,\bar{q},b,\bar{b}} K_{ij}^{[5]\leftarrow[4]}(m_b,\mu_b) f_j^{[4]}, \tag{3.40}$$

while the $n_f = 4$ and the $n_f = 5$ running couplings are related by the matching equation (1.30).

Using these expressions it is possible to get

$$F^{[4]}(Q,m_b) = \sum_{i,j=g,q,\bar{q},b,\bar{b}} C_i^{[4]} K_{ij}^{[4]\leftarrow[5]}(m_b,\mu_b) f_j^{[5]} \tag{3.41}$$

for the massive 4FS result, while, for the massive-zero result one gets

$$F^{[4,0]}(Q,m_b) = \sum_{i,j=g,q,\bar{q},b,\bar{b}} C_i^{[4,0]} K_{ij}^{[4]\leftarrow[5]}(m_b,\mu_b) f_j^{[5]}, \tag{3.42}$$

which lead to the observable expression in the FONLL scheme

$$\begin{aligned} F_{\text{FONLL}}(Q,m_b) = & \sum_{i,j=g,q,\bar{q},b,\bar{b}} [C_i^{[4]} - C_i^{[4,0]}] K_{ij}^{[4]\leftarrow[5]}(m_b,\mu_b) f_j^{[5]} \\ & + \sum_{i=g,q,\bar{q},b,\bar{b}} C_i^{[5]} f_i^{[5]}. \end{aligned} \tag{3.43}$$

It is now simple to see that, since

$$\sum_{i=g,q,\bar{q},b,\bar{b}} C_i^{[5]} K_{ij}^{[5]\leftarrow[4]}(m_b,\mu_b) = C_j^{[4,0]}, \tag{3.44}$$

the massive-zero contribution cancels exactly with the 5FS term, and so the final result becomes

$$\begin{aligned} F_{\text{FONLL}}(Q,m_b) &= \sum_{i,j=g,q,\bar{q},b,\bar{b}} C_i^{[4]} K_{ij}^{[4]\leftarrow[5]}(m_b,\mu_b) f_j^{[5]} \\ &= \sum_{i=g,q,\bar{q},b,\bar{b}} C_i^{[5]} f_i^{[5]}, \end{aligned} \tag{3.45}$$

which shows that, when one does not make assumption on the 5FS PDFs at the initial scale, i.e. does not assume zero intrinsic heavy-quark, the FONLL construction is equivalent to the ACOT [6] one at all orders.

However, in order to compare the FONLL construction with the one proposed in this thesis, it is now necessary to assume zero intrinsic heavy-quark as it has been done in the previous sections.

With this assumption, the 4FS FONLL result becomes

$$\begin{aligned} F^{[4]}(Q,m_b) &= \sum_{i=g,q,\bar{q}} C_i^{[4]} f_i^{[4]} \\ &= \sum_{i,j=g,q,\bar{q}} C_i^{[4]} \tilde{K}_{ij}^{[4]\leftarrow[5]}(m_b,\mu_b) f_j^{[5]} \\ &= \sum_{i=g,q,\bar{q}} B_i^{[5]} f_i^{[5]}, \end{aligned} \tag{3.46}$$

where the massive coefficients functions $B_i^{[5]}$ have been implicitly defined as

$$B_i^{[5]} = C_i^{[4]} \tilde{K}_{ij}^{[4]\leftarrow[5]}(m_b, \mu_b) \tag{3.47}$$

and the $\tilde{K}_{ij}^{[4]\leftarrow[5]}$ denotes the matching matrix inverted only on the subspace of the light partons.

Using eq. (3.46), it is then possible to obtain the expression of the FONLL result with zero intrinsic bottom

$$\begin{aligned} F_{\text{FONLL}}(Q, m_b) = &\sum_{i=g,q,\overline{q}} [B_i^{[5]} - B_i^{[5,0]} + C_i^{[5]}] f_i^{[5]} \\ &+ \sum_{b,\overline{b}} C_i^{[5]} f_i^{[5]}, \end{aligned} \tag{3.48}$$

where

$$\begin{aligned} B_i^{[5,0]} &= \sum_{j=g,q,\overline{q}} C_j^{[4,0]} \tilde{K}_{ji}^{[4]\leftarrow[5]}(m_b, \mu_b) \\ &= \sum_{j=g,q,\overline{q}} \sum_{k=g,q,\overline{q},b,\overline{b}} C_k^{[5]} K_{kj}^{[5]\leftarrow[4]}(m_b, \mu_b) \tilde{K}_{ji}^{[4]\leftarrow[5]}(m_b, \mu_b) \\ &= C_i^{[5]} + \sum_{k=b,\overline{b}} \sum_{j=g,q,\overline{q}} C_k^{[5]} K_{kj}^{[5]\leftarrow[4]}(m_b, \mu_b) \tilde{K}_{ji}^{[4]\leftarrow[5]}(m_b, \mu_b). \end{aligned} \tag{3.49}$$

Notice that, in the last step, both the relation between 4FS and 5FS coefficients functions (eq. (3.44)) and the identity

$$\sum_{k=g,q,\overline{q}} (\tilde{K}^{-1})_{ik} \tilde{K}_{kj} = \sum_{k=g,q,\overline{q}} \tilde{K}_{ik} (\tilde{K}^{-1})_{kj} = \delta_{ij} \qquad i,j = g,q,\overline{q} \tag{3.50}$$

have been used.

Finally, substituting the $B_i^{[5,0]}$ expression of eq. (3.49) in the FONLL result of eq. (3.48), it is possible to get the final result

$$\begin{aligned} F_{\text{FONLL}}(Q, m_b) = &\sum_{i=g,q,\overline{q}} B_i^{[5]} f_i^{[5]} + \sum_{i=b,\overline{b}} C_i^{[5]} f_i^{[5]} \\ &- \sum_{k=b,\overline{b}} \sum_{j=g,q,\overline{q}} C_k^{[5]} K_{kj}^{[5]\leftarrow[4]}(m_b, \mu_b) \tilde{K}_{ji}^{[4]\leftarrow[5]}(m_b, \mu_b) f_i^{[5]}. \end{aligned} \tag{3.51}$$

It is now possible to show the equivalence between the FONLL result of the last equation and the result of eq. (3.35), which, in turn, is equivalent also to S-ACOT [7]. In fact, the S-ACOT final result can be written as

$$F_{\text{S-ACOT}}(Q, m_b) = \sum_{i=g,q,\overline{q},b,\overline{b}} C_i^{\text{S-ACOT}} f_i^{[5]}, \tag{3.52}$$

where

$$C_i^{[4]} = \sum_{j=g,q,\overline{q},b,\overline{b}} C_j^{\text{S-ACOT}} K_{ji}^{[5]\leftarrow[4]}, \tag{3.53}$$

which, with the same choice that has been done in sec. 3.2 of exploiting the ambiguity of the matching matrix inversion, gives

$$C_i^{\text{S-ACOT}} = \sum_{j=g,q,\overline{q}} [C_j^{[4]} - \sum_{k=b,\overline{b}} C_k^{[5]} K_{kj}^{[5]\leftarrow[4]}] \tilde{K}_{ji}^{[4]\leftarrow[5]} \quad i = q, \overline{q}, g$$
$$C_b^{\text{S-ACOT}} = C_b^{[5]}. \tag{3.54}$$

It is then simple to recognize the equivalence of the latter with the $\tilde{C}_i$ defined in eq. (3.34) and hence recognize the equivalence to all orders between S-ACOT and the construction proposed in this thesis. Therefore, to show that this equivalence holds also with FONLL, it is enough to prove that it holds for S-ACOT.

From (3.52) and (3.48) it is clear that, in order FONLL to be equivalent to all orders to S-ACOT, it has to hold

$$C_i^{\text{S-ACOT}} = B_i^{[5]} - B_i^{[5,0]} + C_i^{[5]} \quad i = g, q, \overline{q}, \tag{3.55}$$

while, for the bottom coefficients function, the equivalence is automatically given by $C_b^{\text{S-ACOT}}(m_b) = C_b^{[5]}(0)$.

The equality of eq. (3.55) is indeed satisfied, in fact, from eq. (3.49) and from eq. (3.46), it is possible to obtain

$$C_i^{[5]} - B_i^{[5,0]} = \sum_{k=b,\overline{b}} \sum_{j=g,q,\overline{q}} C_k^{[5]} K_{kj}^{[5]\leftarrow[4]} \tilde{K}_{ji}^{[4]\leftarrow[5]} \tag{3.56}$$

and

$$B_i^{[5]} = \sum_{j=g,q,\overline{q}} C_j^{[4]} \tilde{K}_{ji}^{[4]\leftarrow[5]}, \tag{3.57}$$

which show exactly the correctness of eq. (3.55) and so the all order equivalence between S-ACOT and FONLL.

To summarize, although the different methodologies get to the final result following different ways, they obtain, as expected, final expressions that are equivalent to all orders. However, the various schemes adopt different countings to truncate the perturbative series at a certain finite order in α_s and so the final numerical results are different. The counting proposed in this thesis will be presented in the next chapter and it will be explicitly compared with the FONLL one. The numerical consequences caused by the different countings will instead be analyzed in chapter 5.

Chapter 4

Phenomenological applications

In this chapter, the all-order expressions obtained in the previous chapter will be applied explicitly to the structure functions F_2 and F_L related to the heavy-quark production sector of DIS, and the proposed perturbative counting for the NLO and NNLO results will be presented. However, depending on the considered kinematic region, the most appropriate scheme and counting to adopt can change. In particular, there are three kinematic regions of interest:

- $Q \lesssim \mu_b$: in this region, as already mentioned, the best approximation is provided by the 4FS FO result. Since the gluon and the light-quark PDFs at the scale μ_Λ will always be considered non-perturbative objects and thus included in the counting as $\mathcal{O}(1)$ quantities, the FO counting will be carried out simply combining together the 4FS coefficients functions with the same number in the round bracket apex. It is treated in more details in sec. 4.1.

- $Q \gtrsim \mu_b$: in this region, the matched result provides the best approximation. Its counting is less trivial than the FO counting because, as already mentioned, the effective bottom PDF is perturbatively generated and so it should be counted as an $\mathcal{O}(\alpha_s)$ quantity. This is equivalent to say that the perturbative counting must be applied also to the DGLAP kernel and to the matching coefficients at μ_b, which are part of the effective PDF definition. In sec. 4.2 it will be shown that, for this kinematic region, this is indeed the case.

- $Q \gg \mu_b$: in this region, the most appropriate result is still the matched result but, as explained in more detail in the first part of sec. 4.2, for this energy scale the bottom PDF should be considered as an $\mathcal{O}(1)$ quantity like the other PDFs. This means that the way in which the counting is carried out changes and becomes equivalent to the counting that is commonly adopted in literature.

Therefore, these three versions of the result must be combined together to construct a prediction which is reliable in a wide kinematic region. As already mentioned, a VFNS approach has been adopted to switch from the FO result to the matched result of the second case. Instead, the combination of the two countings of the second and third cases has been carried out trough an energy damping function (see secs. 4.3 and 5.3).

Notice that, in this case, the energy scale of the process Q has been compared to μ_b and not to m_b. This is justified by the fact that Q and μ_b, as it will be shown in sec. 4.2, are the scales which are present in the DGLAP kernel responsible for the alternative counting. However, since $m_b \sim \mu_b$, the comparison could have been equivalently done with m_b without essential variations.

The final expressions of the matched results, truncated at NLO and NNLO, will be also explicitly compared to the FONLL expressions in sec. 4.3.

4.1 FO counting: result in the $Q \lesssim \mu_b$ region

The expansion of the FO expression of eq. (3.8) is done considering the 4FS PDFs as external $\mathcal{O}(1)$ quantities. This is justified by the fact that the DGLAP kernels $U_{ij}^{[4]}(\mu, \mu_\Lambda)$, which evolve them from an initial scale μ_Λ to the final scale μ, resum single logarithms L of the ratio μ/μ_Λ to all-orders in α_s (sec. 3.2.1) and so their perturbative counting can be written as

$$U_{ij}^{[4]}(\mu, \mu_\Lambda) = U^{LL}(\alpha_s L) + \alpha_s U^{NLL}(\alpha_s L) + \alpha_s^2 U^{NNLL}(\alpha_s L) + \cdots , \tag{4.1}$$

where the terms $U^{N^kLL}(\alpha_s L)$ are functions of $\alpha_s L$ to all orders in α_s. This means that, counting $\alpha_s L \approx 1$, the 4FS PDFs at a generic scale μ are

$$f_i^{[4]}(\mu) = \sum_{j=q,\bar{q},g} U_{ij}^{[4]}(\mu, \mu_\Lambda) f_j^{[4]}(\mu_\Lambda) \approx \mathcal{O}(1) \tag{4.2}$$

and so they can be counted as external $\mathcal{O}(1)$ quantities. Notice that this feature is independent of how large the logarithms $\ln(\mu/\mu_\Lambda)$ actually are because the DGLAP evolution kernels do not introduce a parametric difference between the light-quark PDFs, even if they mix them. This is the standard praxis and it will be applied to the 5FS PDFs at μ_b as well in the next section.

The perturbative counting for the FO structure functions is then directly applied to the 4FS coefficients functions. This results in

$$\begin{aligned}
&\text{NLO} && F_2^{FO} = \alpha_s^{[5]}(Q) D_{g,2}^{[4](1)}(Q, m_b) f_g^{[4]}(Q) \\
&\text{NNLO} && \quad + \alpha_s^{[5]2}(Q) [D_{g,2}^{[4](2)}(Q, m_b) f_g^{[4]}(Q) + D_{q,2}^{[4](2)}(Q, m_b) f_q^{[4]}(Q)] \\
&\text{N}^3\text{LO} && \quad + \cdots ,
\end{aligned} \tag{4.3}$$

for F_2 and in

$$\begin{aligned}
&\text{NLO} && F_L^{FO} = \alpha_s^{[5]}(Q) D_{g,L}^{[4](1)}(Q, m_b) f_g^{[4]}(Q) \\
&\text{NNLO} && \quad + \alpha_s^{[5]2}(Q) [D_{g,L}^{[4](2)}(Q, m_b) f_g^{[4]}(Q) + D_{q,L}^{[4](2)}(Q, m_b) f_q^{[4]}(Q)] \\
&\text{N}^3\text{LO} && \quad + \cdots ,
\end{aligned} \tag{4.4}$$

for F_L. Notice that, as in the rest of this chapter, the subscript below a coefficients function denotes the structure function to which it is referred.

As mentioned in the previous section, the perturbative counting has been performed in terms of the 5FS coupling $\alpha_s^{[5]}$ in order to simplify the combination of the FO result with the R result, and this means one has to use the converted coefficients functions $D_i^{[4]}$.

From eqs. (4.3) and (4.4), it is clear that, in order to obtain the structure functions with an $\mathcal{O}(\alpha_s^k)$ accuracy, it is necessary to use the PDFs evolved at N^{k}LO, i.e. the ones obtained using the $\mathcal{O}(\alpha_s^k)$ DGLAP kernels. However, it is important to notice that one has, in principle, to reexpand eqs. (4.3) and (4.4) taking into account the DGLAP kernel expansion of eq. (4.1). In practice, this is usually not done,

because, as already mentioned, the standard praxis is to consider the 4FS PDFs as external $\mathcal{O}(1)$ quantities. In this way, spurious terms of higher order will be present in the result expressions. These terms, however, can have a not small contribution because some cancellations, which would occur if all the terms necessary to form the correct perturbative order were included, do not necessarily occur in this case. In this thesis, the consequences on the numerical results due to this cross-expansion procedure have been studied and they are presented in the next chapter.

4.2 Matched result countings: results in the $Q \gtrsim \mu_b$ and in the $Q \gg \mu_b$ regions

The perturbative expansion of the matched result is more subtle than the FO one because of the perturbative nature of the bottom 5FS PDF. Since

$$f_i^{[5]}(Q) = \sum_{j=q,\overline{q},b,\overline{b},g} \sum_{k=q,\overline{q},g} U_{ij}^{[5]}(Q,\mu_b) K_{jk}^{[5]\leftarrow[4]}(m_b,\mu_b) f_k^{[4]}(\mu_b), \tag{4.5}$$

it is clear that, due to the presence of the additional scale μ_b, the way in which the counting has to be performed is not trivial as in the FO case. In fact, while the 4FS PDFs at μ_b,

$$f_k^{[4]}(\mu_b) = \sum_{l=q,\overline{q},g} U_{kl}^{[4]}(\mu_b,\mu_\Lambda) f_l^{[4]}(\mu_\Lambda), \tag{4.6}$$

can be counted as $\mathcal{O}(1)$ quantities, as follow from the same arguments given in the previous section, there are two options for the DGLAP kernel $U_{ij}^{[5]}(Q,\mu_b)$ expansion depending on the hierarchy between Q and μ_b.

In particular, as mentioned at the beginning of this chapter, in the kinematic region of interest for the matched result there are two possibilities:

- In the high energy (H.E.) limit, i.e. $Q \gg \mu_b$, $\alpha_s L \approx 1$ and so it is possible to adopt the same logarithmic counting applied for $U_{ij}^{[4]}(Q,\mu_\Lambda)$ in the FO case. This means that one has to count

  $$U_{ij}^{[5]} \sim U_{bj}^{[5]} \sim U_{ib}^{[5]} \sim U_{bb}^{[5]} \sim 1 \tag{4.7}$$

  and so every 5FS PDFs has to be counted as an $\mathcal{O}(1)$ quantity.

- In the intermediate energy (I.E.) region, i.e. $Q \gtrsim \mu_b$, one has to take into account that the fixed-order expansion of the off-diagonal evolution kernels $U_{bi}^{[5]}$ and $U_{ib}^{[5]}$ starts at order $\alpha_s L$ rather than at $\mathcal{O}(1)$. This means that they are suppressed by a factor $\alpha_s L$ with respect to the diagonal ones and vanish in the limit $Q \to \mu_b$. Therefore, in this case, it is necessary to count

  $$\begin{aligned} U_{ij}^{[5]}(Q,\mu_b) &\sim U_{bb}^{[5]}(Q,\mu_b) \sim 1 \quad i,j = q,\overline{q},g \\ U_{bi}^{[5]}(Q,\mu_b) &\sim U_{ib}^{[5]}(Q,\mu_b) \sim \alpha_s \quad i = q,\overline{q},g. \end{aligned} \tag{4.8}$$

Adopting the counting described in eq. (4.7), the 5FS PDFs up to $\mathcal{O}(\alpha_s)$ are

$$\begin{aligned}
f_g^{[5]}(m_b,Q) &= \left[U_{gg}^{[5]} + \alpha_s[U_{gb}^{[5]}K_{bg}^{(1)} + U_{gg}^{[5]}K_{gg}^{(1)} + \cdots]\right] f_g^{[4]}(\mu_b) + \left[U_{gq}^{[5]} + \cdots\right] f_q^{[4]}(\mu_b) \\
f_q^{[5]}(m_b,Q) &= \left[U_{qq}^{[5]} + \cdots\right] f_q^{[4]}(\mu_b) + \left[U_{qg}^{[5]} + \alpha_s[U_{qb}^{[5]}K_{bg}^{(1)} + U_{qg}^{[5]}K_{gg}^{(1)} + \cdots]\right] f_g^{[4]}(\mu_b) \\
f_b^{[5]}(m_b,Q) &= \left[U_{bg}^{[5]} + \alpha_s[U_{bb}^{[5]}K_{bg}^{(1)} + U_{bg}^{[5]}K_{gg}^{(1)} + \cdots]\right] f_g^{[4]}(\mu_b) + \left[U_{bq}^{[5]} + \cdots\right] f_q^{[4]}(\mu_b),
\end{aligned} \tag{4.9}$$

and so they all can be treated as external $\mathcal{O}(1)$ quantities. Notice that the $U_{ij}^{[5]}$ perturbative order is not explicitly written, as in the rest of this chapter, but it is clear that, in order to construct the 5FS PDFs up to $\mathcal{O}(\alpha_s)$, they must be taken at NLO.

Then, the matched result counting for a generic structure function becomes

$$\begin{aligned}
\text{LO} \quad F^{\text{H.E.}} &= C_b^{[5](0)} f_b^{[5]}(Q,m_b) \\
\text{NLO} \quad &+ \alpha_s^{[5]}(Q)\left[C_g^{[5](1)}(Q) f_g^{[5]}(Q,m_b) + C_b^{[5](1)}(Q) f_b^{[5]}(Q,m_b)\right] \\
\text{NNLO} \quad &+ \alpha_s^{[5]2}(Q)\left[C_g^{[5](2)}(Q) f_g^{[5]}(Q) + C_b^{[5](2)}(Q) f_b^{[5]}(Q,m_b) + C_q^{[5](2)}(Q) f_q^{[5]}(Q)\right] \\
\text{N}^3\text{LO} \quad &+ \cdots,
\end{aligned} \tag{4.10}$$

which, as explicitly denoted, is valid in the high-energy region, i.e. when $Q \gg \mu_b$, in which the mass power corrections are completely negligible and this is the reason why the coefficients functions in eq. (4.10) are taken in the massless limit. Notice that this is the most adopted counting in literature and that it is also used in the intermediate energy region, as discussed in section 4.3.

This counting, however, applies when one can count $\alpha_s L \sim 1$ and, taking $\mu_b \approx m_b \approx 5\,\text{GeV}$, it is possible to roughly estimate that this happens for $Q \gtrsim 1\,\text{TeV}$. Therefore, for the usually explored kinematic region in a DIS experiment, it is more appropriate to adopt the second counting. Another possibility, as already mentioned at the beginning of this chapter, is to combine the results obtained with the two countings through an energy damping function, see (secs. 4.3 and 5.3).

The matched result counting for a generic structure function, obtained adopting the second choice, is instead

$$\begin{aligned}
&\text{LO} \quad F^{\text{I.E.}} = \\
&\text{NLO} \\
&\qquad \left[\alpha_s(Q)\tilde{C}_g^{(1)}(Q)U_{gg}^{[5]} + C_b^{[5](0)}(Q)[U_{bg}^{[5]} + \alpha_s(\mu_b)U_{bb}^{[5]}K_{bg}^{(1)}]\right] f_g^{[4]}(\mu_b) \\
&\text{NNLO} \\
&\qquad + \alpha_s(Q)\left[\alpha_s(Q)\tilde{C}_g^{(2)}(Q)U_{gg}^{[5]} + C_b^{[5](1)}(Q)[U_{bg}^{[5]} + \alpha_s(\mu_b)U_{bb}^{[5]}K_{bg}^{(1)}]\right] f_g^{[4]}(\mu_b) \\
&\qquad + \alpha_s(\mu_b)\left[\alpha_s(Q)\tilde{C}_g^{(1)}(Q)U_{gg}^{[5]}K_{gg}^{(1)} + C_b^{[5](0)}(Q)[U_{bg}^{[5]}K_{gg}^{(1)} + \alpha_s(\mu_b)U_{bb}^{[5]}K_{bg}^{(2)}]\right] f_g^{[4]}(\mu_b) \\
&\qquad + \left[\alpha_s^2(Q)\tilde{C}_q^{(2)}(Q)U_{qq}^{[5]} + \alpha_s(Q)\tilde{C}_g^{(1)}(Q)U_{gq}^{[5]} + C_b^{[5](0)}(Q)[U_{bq}^{[5]} + \alpha_s^2(\mu_b)U_{bb}^{[5]}K_{bq}^{(2)}]\right] f_q^{[4]}(\mu_b)
\end{aligned} \tag{4.11}$$

where the coupling is always in the 5FS and some of the arguments have been neglected for ease of notation. As explicitly denoted, this counting is valid in the

intermediate energy region, i.e. when $Q \gtrsim \mu_b$, where the mass power corrections are not negligible and this is why the tilde version of the coefficients functions has been used.

Notice also that, in this case, coefficients functions with different numbers in the round brackets are combined together to construct the same perturbative order of the structure function. For instance, the NLO contribution of the first line is constructed combining the NLO gluon coefficients function, $\tilde{C}_g^{[5](1)}$, with the LO bottom coefficients function, $C_b^{[5](0)}$. This is a direct consequence of counting the kernel $U_{bg}^{[5]}$ as an $\mathcal{O}(\alpha_s)$ object and, although it may seem counterintuitive, it makes perfectly sense from a physical point of view. In fact, in absence of intrinsic component of the bottom PDF, it is impossible to extract a b quark from the proton unless it is produced by a gluon. This pair-production provides at least one α_s term that exactly fills the ostensible mismatch between $C_b^{[5](0)}$ and $\tilde{C}_g^{[5](1)}$. Moreover, in the FO result of eqs. (4.3) and (4.4) there are no terms contributing at LO and, since the resummation provides a correction to the FO result, it cannot introduce such terms. However, in eq. (4.10), the $C_b^{[5](0)}$ coefficients function contributes at LO and this is another proof of correctness, in the $Q \gtrsim \mu_b$ region, of the counting in eq. (4.11) which has no LO contributions.

The expression of eq. (4.11) is quite involved but it is possible to collect some of the terms into the definition of effective PDFs as

$$\begin{aligned}
\tilde{f}_g^{(0)}(m_b, Q) &= U_{gg}^{[5]}(Q, \mu_b) f_g^{[4]}(\mu_b) + U_{gq}^{[5]}(Q, \mu_b) f_q^{[4]}(\mu_b) \\
\tilde{f}_g^{(1)}(m_b, Q) &= \alpha_s(\mu_b) U_{gg}^{[5]}(Q, \mu_b) K_{gg}^{(1)}(m_b, \mu_b) f_g^{[4]}(\mu_b)
\end{aligned} \tag{4.12}$$

$$\begin{aligned}
\tilde{f}_q^{(0)}(m_b, Q) &= U_{qq}^{[5]}(Q, \mu_b) f_q^{[4]}(\mu_b) + U_{qg}^{[5]}(Q, \mu_b) f_g^{[4]}(\mu_b) \\
\tilde{f}_q^{(1)}(m_b, Q) &= \alpha_s(\mu_b) U_{qg}^{[5]}(Q, \mu_b) K_{gg}^{(1)}(m_b, \mu_b) f_g^{[4]}(\mu_b)
\end{aligned}$$

$$\begin{aligned}
\tilde{f}_b^{(1)}(m_b, Q) &= \left[U_{bg}^{[5]}(Q, \mu_b) + \alpha_s(\mu_b) U_{bb}^{[5]}(Q, \mu_b) K_{bg}^{(1)}(m_b, \mu_b)\right] f_g^{[4]}(\mu_b) + U_{bq}^{[5]}(Q, \mu_b) f_q^{[4]}(\mu_b) \\
\tilde{f}_b^{(2)}(m_b, Q) &= \alpha_s(\mu_b) \left[U_{bg}^{[5]}(Q, \mu_b) K_{gg}^{(1)}(m_b, \mu_b) + \alpha_s(\mu_b) U_{bb}^{[5]}(Q, \mu_b) K_{bg}^{(2)}(m_b, \mu_b)\right] f_g^{[4]}(\mu_b) \\
&\quad + \alpha_s^2(\mu_b) U_{bb}^{[5]}(Q, \mu_b) K_{bq}^{(2)}(m_b, \mu_b) f_q^{[4]}(\mu_b),
\end{aligned}$$

which has been written order by order adopting the standard notation but explicitly retaining the α_s terms. Again, it is easy to recognize the perturbative nature of the bottom PDF given by the kernels $U_{bg}^{[5]}(Q, \mu_b)$ and $U_{bq}^{[5]}(Q, \mu_b)$, that is also the reason of the $\tilde{f}_b^{(0)}(m_b, Q)$ absence.

It is important to notice that the effective PDFs of eq. (4.12) are different from the standard 5FS ones of eq. (4.9). In particular, every off-diagonal matching function that involves the bottom quark is delayed of one order in the effective PDFs with respect to the standard ones. For instance, the $U_{gb}^{[5]} K_{bg}^{(1)}$ term counts as $\mathcal{O}(\alpha_s)$ in the standard PDFs but as $\mathcal{O}(\alpha_s^2)$ in the effective PDFs and, in fact, it is not in eq. (4.12). This alternative version of the PDFs, which is part of the original proposal of this thesis, has been constructed and evolved using the APFEL++ framework [26, 27] and the numerical result have been computed using both them and the standard ones (cha. 5). Some details on how the alternative PDFs have been constructed are provided in Appendix B.

Exploiting the alternative PDF expressions, it is possible to write the final truncated at NNLO matched result as

$$\begin{aligned} F_2^{\text{I.E.}} &= \alpha_s \tilde{C}_{g,2}^{[5](1)}(Q) \tilde{f}_g^{\{1\}}(m_b, Q) + C_{b,2}^{[5](0)}(Q) \tilde{f}_b^{\{2\}}(m_b, Q) \\ &+ \alpha_s^2 \tilde{C}_{i,2}^{[5](2)}(Q) \tilde{f}_i^{\{0\}}(m_b, Q) + \alpha_s C_{b,2}^{[5](1)}(Q) \tilde{f}_b^{\{1\}}(m_b, Q) \end{aligned} \tag{4.13}$$

for F_2 and

$$\begin{aligned} F_L^{\text{I.E.}} &= \alpha_s \tilde{C}_{g,L}^{[5](1)}(Q) \tilde{f}_g^{\{1\}}(m_b, Q) \\ &+ \alpha_s^2 \tilde{C}_{i,L}^{[5](2)}(Q) \tilde{f}_i^{\{0\}}(m_b, Q) + \alpha_s C_{b,L}^{[5](1)}(Q) \tilde{f}_b^{\{1\}}(m_b, Q) \end{aligned} \tag{4.14}$$

for F_L, where, in the last equation, the fact that $C_{b,L}^{[5](1)}(Q) = 0$ has been used.

Notice that, as in the FO case, the correct procedure is to expand also the PDFs and thus truncate the PDF series at different perturbative order for every term, as it has been done in the equations above. In fact, the brace notation adopted in eqs. (4.13) and (4.14) denotes the fact that $f_i^{\{k\}}$ are the PDFs truncated at $\mathcal{O}(\alpha_s^i)$. In other words, they can be obtained from eq. (4.12) as

$$\tilde{f}_i^{\{k\}} = \sum_{p=0}^{k} \tilde{f}_i^{(p)}. \tag{4.15}$$

However, as already mentioned, from an implementation point of view, it is simpler to use a single PDF set evolved to the highest order required by the result under construction. In this way, the NNLO result for a general structure function would be

$$\begin{aligned} F^{\text{I.E.}} &= \alpha_s \tilde{C}_g^{[5](1)}(Q) \tilde{f}_g^{\{1\}}(m_b, Q) + C_b^{[5](0)}(Q) \tilde{f}_b^{\{2\}}(m_b, Q) \\ &+ {\alpha_s}^2 \tilde{C}_i^{[5](2)}(Q) \tilde{f}_i^{\{1\}}(m_b, Q) + \alpha_s C_b^{[5](1)}(Q) \tilde{f}_b^{\{2\}}(m_b, Q). \end{aligned} \tag{4.16}$$

Notice that $\tilde{f}_g^{\{1\}}$, $\tilde{f}_q^{\{1\}}$ and $\tilde{f}_b^{\{2\}}$ are all evolved at NNLO and thus they are implemented in such a way to belong to the same set (see appendix B). In the same way, the $\tilde{f}_g^{\{0\}}$, $\tilde{f}_q^{\{0\}}$ and $\tilde{f}_b^{\{1\}}$ PDFs are evolved at NLO and thus they are part of the NLO results.

In this thesis, the numerical results have been constructed following both the cross-counting and the standard approach, in order to study the benefits given by the more expensive procedure of cross-expansion (cha. 5).

4.3 Comparison with FONLL

In this section the perturbative countings presented in the previous section will be compared with the counting proposed by the FONLL scheme. The differences that will be found are the cause of the different quality of the final results, mostly on the uncertainties, that will be presented in the next chapter.

In particular, there are three different final results proposed by the FONLL scheme. Two of them, FONLL-A and FONLL-C, are canonical in the sense that they are constructed in a way analogous to the standard counting of eq. (4.10). They account respectively for the α_s and for the α_s^2 orders and thus they are used respectively together with NLO and NNLO PDFs. The third, FONLL-B, is a modified version meant to improve the final results given by FONLL-A, through the anticipation of

the massive contributions of one perturbative order. In particular, this means to take $F^{[5]}(Q,0)$ at $\mathcal{O}(\alpha_s)$ while taking $F^{[4]}(Q,m_b)$ at $\mathcal{O}(\alpha_s^2)$ and consequently modify the double-counted terms in $F^{[4,0]}(Q,m_b)$ (see eq. (3.38)). Since FONLL-B is considered an improvement of FONLL-A, it is used together with NLO PDFs.

Here, we argue that FONLL-B method is the correct way to construct the NNLO result if the considered energy scale is such as to justify the adoption of the counting of eq. (4.11), i.e. it is in the $Q \gtrsim \mu_b$ region. In fact, as it will be explicitly shown in sec. 4.3.3, FONLL-B is equivalent to the $F^{\text{I.E.}}$ NNLO result obtained in the previous section [1]. Instead, as explicitly shown in sec. 4.3.4, FONLL-C is equivalent to the $F^{\text{H.E.}}$ NNLO result. This means that, as already mentioned at the beginning of this chapter, in order to construct an NNLO result which is reliable in both the $Q \gtrsim \mu_b$ and $Q \gg \mu_b$ regions, one should combine FONLL-B and FONLL-C trough an energy damping function. This ultimate version of the result is implemented in sec. 5.3.

However, in this thesis, also other versions of the FONLL results have been considered. These versions are never mentioned in [5] but they can be obtained as simple generalizations of the methods of construction of FONLL-A, FONLL-B and FONLL-C. In particular, following the same nomenclature of FONLL, they are called FONLL-0, FONLL-D, FONLL-E and FONLL-F. Following the notation, it should be clear that, in FONLL's way of thinking, only FONLL-E represents a canonical result (in particular at $\mathcal{O}(\alpha_s^3)$), while the others are improvement versions.

In particular, FONLL-0 is analogous to FONLL-B, but for the NLO. Therefore, it is constructed taking $F^{[5]}(Q,0)$ at $\mathcal{O}(1)$ and $F^{[4]}(Q,m_b)$ at $\mathcal{O}(\alpha_s)$. In FONLL's way of thinking, it provides an improvement of the standard $\mathcal{O}(1)$ result and so it has to be used together with LO PDFs. In this thesis, instead, it is used together with FONLL-A to construct the NLO of the ultimate version of the result (sec. 5.3), in an analogous way of FONLL-B and FONLL-C which are used together to construct its NNLO.

The other versions are never actually implemented in this thesis because, with the currently available perturbative orders of the coefficients functions, it is not possible yet. However, since only a few of the necessary ingredients for FONLL-D and FONLL-E are currently missing, and some reliable approximation of them can be found in literature yet [28], the way of construction proposed in this thesis will soon allow to treat the N^{3}LO DIS and so it will soon give access to the N^{3}LO PDFs. The summary of what has been mentioned so far is given in table 4.1.

	FONLL	Impr. FONLL	Our proposal
NLO	FONLL-A	FONLL-B	FONLL-0 $+\chi(Q)\big[\text{FONLL-A} - \text{FONLL-0}\big]$
NNLO	FONLL-C	FONLL-D	FONLL-B $+\chi(Q)\big[\text{FONLL-C} - \text{FONLL-B}\big]$
N^{3}LO	FONLL-E	FONLL-F	FONLL-D $+\chi(Q)\big[\text{FONLL-E} - \text{FONLL-D}\big]$

Table 4.1. Summary of FONLL standard and improved results and of the prescription proposed in this thesis. Notice that both FONLL-E and FONLL-F are needed for the N^{3}LO in FONLL prescription, while our proposal makes use only of FONLL-D and FONLL-E. The damping function $\chi(Q)$ is discussed in detail in sec. 5.3.

In the next sections, the expressions of FONLL-0, FONLL-A, FONLL-B and FONLL-C will be obtained and compared with the NLO and NNLO results proposed in this thesis. In particular, the NLO results will be compared to FONLL-0 (4.3.1)

[1] Actually, as shown in sec. 4.3.3, they have some different terms which come from the fact that $F^{\text{I.E.}}$ is used together with NNLO PDFs, while FONLL-B is meant to be used together NLO PDFs.

and FONLL-A (4.3.2), while the NNLO results to FONLL-B (4.3.3) and FONLL-C (4.3.4).

4.3.1 FONLL-0

The way in which FONLL-0 and FONLL-B results are constructed relies in a redefinition of the massive-zero coefficients functions which exclude the constant terms from the subtraction. This is because the massive-zero coefficients functions are meant to subtract any double-counted terms (see sec. 3.4) which come from the sum of massive and massless part. However, in order to construct FONLL-0 and FONLL-B, they are taken to different perturbative orders. In particular, for FONLL-0, the massive part is taken at most at order α_s and the massless part is taken at most at order α_s^0. Therefore, this redefinition is

$$\overline{B}_i^{[0]}\left(\frac{m_b}{Q}\right) = B_i^{[0]}\left(\frac{m_b}{Q}\right) - B_i^{[0]}(1), \tag{4.17}$$

where $B_i^{[0]}(m_b/Q)$ and $B_i^{[0]}(1)$ are the standard massive-zero functions computed respectively with $m_b \neq Q$ and $m_b = Q$.

Adopting eq. (3.48) and truncating it at first order, the F_2 expression becomes

$$F_2^{(0)} = C_{b,2}^{(0)} f_b + \alpha_s \left[B_{g,2}^{(1)} - \overline{B}_{g,2}^{[0](1)}\left(\frac{m_b}{Q}\right)\right] f_g, \tag{4.18}$$

where it should be noted that $B_{g,2}^{(1)}$ is exactly equal to the 4FS coefficients function $D_{g,2}^{[4](1)}$.

However, the expression of $B_{g,2}^{[0](1)}(m_b/Q)$ in terms of the 5FS coefficients functions can be easily obtained truncating at first order eq. (3.49). This results in

$$B_{g,2}^{[0]}\left(\frac{m_b}{Q}\right) = C_{g,2}^{(1)} + 2C_{b,2}^{(0)} K_{bg}^{(1)}\left(\frac{m_b}{Q}\right), \tag{4.19}$$

from which it is possible to get

$$B_{g,2}^{[0](1)}(1) = C_{g,2}^{(1)} + 2C_{b,2}^{(0)} K_{bg}^{(1)}(1) = C_{g,2}^{(1)}, \tag{4.20}$$

where the fact that $K_{bg}^{(1)}(1) = 0$, since it contains no constant terms, has been used. Notice that, taking $m_b = Q$ has no impact on the 5FS coefficients functions because they do not depend on m_b, but it acts on the matching functions and so on the subtraction of the collinear logarithms. From these last two equations it is possible to get the expression of the first order modified massive-zero gluon coefficients function, which reads

$$\overline{B}_{g,2}^{[0]}\left(\frac{m_b}{Q}\right) = 2C_{b,2}^{(0)} K_{bg}^{(1)}\left(\frac{m_b}{Q}\right). \tag{4.21}$$

Putting everything together one gets

$$\begin{aligned} F_2^{(0)} &= C_{b,2}^{(0)} f_b + \alpha_s \left[B_{g,2}^{(1)} - 2C_{b,2}^{(0)} K_{bg}^{(1)}\left(\frac{m_b}{Q}\right)\right] f_g \\ &= C_{b,2}^{(0)} f_b + \alpha_s \tilde{C}_{g,2}^{(1)} f_g, \end{aligned} \tag{4.22}$$

where, in the last step, the definition of the gluon tilde coefficients function has been recognized.

Following the same road-map, it is possible to obtain the F_L expression. In this case, the massive-zero coefficients function assumes the simple form

$$B^{[0]}_{g,L}\left(\frac{m_b}{Q}\right) = C^{(1)}_{g,L} = B^{[0]}_{g,L}(1), \tag{4.23}$$

which means that $\overline{B}^{[0]}_{g,L}(m_b/Q) = 0$. Therefore, one gets

$$F^{(0)}_L = \alpha_s B^{(1)}_{g,L} f_g, \tag{4.24}$$

which is equal to the $F^{\text{I.E.}}$ NLO result proposed in this thesis, since $\tilde{C}^{(1)}_{g,L}(Q, m_b) = D^{[4](1)}_{g,L}(Q, m_b)$.

Eqs. (4.24) and (4.22) show that the counting proposed in this thesis for the $F^{\text{I.E.}}$ NLO result and the counting adopted for the construction of FONLL-0 coincide. However, it is important to note that the two schemes are not exactly equivalent due to the different perturbative order to which the PDFs are evolved. In fact, FONLL-0 is meant to be used together with LO PDFs unlike the proposed $F^{\text{I.E.}}$ NLO result which uses NLO PDFs. This difference, rather than being of a practical nature, is conceptual. In fact, the reason why FONLL-0 adopts LO PDFs relies on considering the $C^{(0)}_b$ term of $\mathcal{O}(1)$, while, as already discussed, it should be counted as an $\mathcal{O}(\alpha_s)$.

4.3.2 FONLL-A

The FONLL-A scheme is constructed simply taking both the massive and the massless coefficients functions at most at order α_s. So

$$\begin{aligned} F^{(A)}_2 &= C^{(0)}_{b,2} f_b \\ &\quad + \alpha_s \left[C^{(1)}_{b,2} f_b + \left(B^{(1)}_{g,2} - B^{[0](1)}_{g,2}\left(\frac{m_b}{Q}\right) + C^{(1)}_{g,2} \right) f_g \right], \end{aligned} \tag{4.25}$$

which, using the definition of $B^{[0](1)}_{g,2}(m_b/Q)$ in eq. (4.20), becomes

$$\begin{aligned} F^{(A)}_2 &= C^{(0)}_{b,2} f_b \\ &\quad + \alpha_s \left[C^{(1)}_{b,2} f_b + \left(B^{(1)}_{g,2} - 2C^{(0)}_{b,2} K^{(1)}_{bg}\left(\frac{m_b}{Q}\right) \right) f_g \right]. \end{aligned} \tag{4.26}$$

It is then possible to recognize the last two terms to be exactly $\tilde{C}^{(1)}_{g,2}$ and so one gets

$$\begin{aligned} F^{(A)}_2 &= C^{(0)}_{b,2} f_b \\ &\quad + \alpha_s [C^{(1)}_{b,2} f_b + \tilde{C}^{(1)}_{g,2} f_g]. \end{aligned} \tag{4.27}$$

Notice that this expression differs from the $F^{\text{I.E.}}$ NLO result proposed in this thesis (while it is equal to $F^{\text{H.E.}}$) because the bottom coefficients function is included at $\mathcal{O}(\alpha_s)$ rather than at $\mathcal{O}(1)$ and so, being f_b of order α_s, the bottom contribution is mismatched with respect to the gluon contribution. In the $Q \gtrsim \mu_b$ region, this

will cause the numerical result to be strongly dependent on the scale μ_b and so the uncertainties will increase, as it will be shown in the next chapter.

Repeating the same procedure for F_L it is possible to get

$$F_L^{(A)} = \alpha_s[C_{b,L}^{(1)} f_b + B_{g,L}^{(1)} f_g] = \alpha_s[C_{b,L}^{(1)} f_b + \tilde{C}_{g,L}^{(1)} f_g], \tag{4.28}$$

in which the same difference of the F_2 case arises.

4.3.3 FONLL-B

In order to construct FONLL-B, it is necessary to take the massive part at most at order α_s^2, the massless part at most at order α_s and change the massive-zero definition as in eq. (4.17).

Following this procedure, it is possible to get

$$\begin{aligned} F_2^{(B)} &= C_{b,2}^{(0)} f_b \\ &+ \alpha_s[C_{b,2}^{(1)} f_b + \tilde{C}_{g,2}^{(1)} f_g] \\ &+ \alpha_s^2 \Bigg[\left(B_{g,2}^{(2)} - \overline{B}_{g,2}^{[0](2)}\left(\frac{m_b}{Q}\right) - \left(B_{g,2}^{(1)} - B_{g,2}^{[0](1)}\left(\frac{m_b}{Q}\right)\right) K_{gg}^{(1)}\left(\frac{m_b}{Q}\right)\right) f_g \\ &+ \left(B_{q,2}^{(2)} - \overline{B}_{q,2}^{[0](2)}\left(\frac{m_b}{Q}\right)\right) f_q \Bigg], \end{aligned} \tag{4.29}$$

where the expressions of the massive-zero functions can be obtained by their definition of eq. (3.56) and they read

$$\begin{aligned} B_{g,2}^{[0](2)}\left(\frac{m_b}{Q}\right) &= C_{g,2}^{(2)} + C_{g,2}^{(1)} K_{gg}^{(1)}\left(\frac{m_b}{Q}\right) + 2C_{b,2}^{(1)} K_{bg}^{(1)}\left(\frac{m_b}{Q}\right) \\ &+ 2C_{b,2}^{(0)} K_{bg}^{(2)}\left(\frac{m_b}{Q}\right) \end{aligned} \tag{4.30}$$

and

$$B_{q,2}^{[0](2)}\left(\frac{m_b}{Q}\right) = C_{q,2}^{(2)} + 2C_{b,2}^{(0)} K_{bq}^{(2)}\left(\frac{m_b}{Q}\right). \tag{4.31}$$

From the last two equations it is possible to get

$$\begin{aligned} B_{g,2}^{[0](2)}(1) &= C_{g,2}^{(2)} + 2C_{b,2}^{(0)} K_{bg}^{(2)}(1) \\ B_{q,2}^{[0](2)}(1) &= C_{q,2}^{(2)} + 2C_{b,2}^{(0)} K_{bq}^{(2)}(1), \end{aligned} \tag{4.32}$$

from which follow the expressions of the overlined massive-zero coefficients functions

$$\begin{aligned} \overline{B}_{g,2}^{[0](2)}\left(\frac{m_b}{Q}\right) &= C_{g,2}^{(1)} K_{gg}^{(1)}\left(\frac{m_b}{Q}\right) + 2C_{b,2}^{(1)} K_{bg}^{(1)}\left(\frac{m_b}{Q}\right) + 2C_{b,2}^{(0)}\left(K_{bg}^{(2)}\left(\frac{m_b}{Q}\right) - K_{bg}^{(2)}(1)\right) \\ \overline{B}_{q,2}^{[0](2)}\left(\frac{m_b}{Q}\right) &= 2C_{b,2}^{(0)}\left(K_{bq}^{(2)}\left(\frac{m_b}{Q}\right) - K_{bq}^{(2)}(1)\right). \end{aligned} \tag{4.33}$$

Notice that, in this case, $K_{bg}^{(2)}(1)$ and $K_{bq}^{(2)}(1)$ are not zero because they contain also constant terms. Putting everything together it is possible to get the final F_2^B

expression

$$
\begin{aligned}
F_2^{(B)} &= C_{b,2}^{(0)} f_b \\
&+ \alpha_s [C_{b,2}^{(1)} f_b + \tilde{C}_{g,2}^{(1)} f_g] \\
&+ \alpha_s^2 \Bigg[\left(B_{g,2}^{(2)} - 2C_{b,2}^{(1)} K_{bg}^{(1)} \left(\frac{m_b}{Q} \right) - 2C_{b,2}^{(0)} \left(K_{bg}^{(2)} \left(\frac{m_b}{Q} \right) - K_{bg}^{(2)}(1) \right) \right. \\
&- B_{g,2}^{(1)} K_{gg}^{(1)} \left(\frac{m_b}{Q} \right) + 2C_{b,2}^{(0)} K_{bg}^{(1)} \left(\frac{m_b}{Q} \right) K_{gg}^{(1)} \left(\frac{m_b}{Q} \right) \Bigg) f_g \\
&+ \left. \left(B_{q,2}^{(2)} - 2C_{b,2}^{(0)} \left(K_{bq}^{(2)} \left(\frac{m_b}{Q} \right) - K_{bq}^{(2)}(1) \right) \right) f_q \Bigg]
\end{aligned}
\tag{4.34}
$$

that can be written in terms of the tilde coefficient functions as

$$
\begin{aligned}
F_2^{(B)} &= C_{b,2}^{(0)} f_b \\
&+ \alpha_s [C_{b,2}^{(1)} f_b + \tilde{C}_{g,2}^{(1)} f_g] \\
&+ \alpha_s^2 \Big[(\tilde{C}_{g,2}^{(2)} + 2C_{b,2}^{(0)} K_{bg}^{(2)}(1)) f_g \\
&+ (\tilde{C}_{q,2}^{(2)} + 2C_{b,2}^{(0)} K_{bq}^{(2)}(1)) f_q \Big].
\end{aligned}
\tag{4.35}
$$

The last expression is not exactly equal to the $F^{\text{I.E.}}$ NNLO result proposed in this thesis due to the presence of the non-zero matching function terms $K_{bg}^{(2)}(1)$ and $K_{bq}^{(2)}(1)$. This is a symptom of the different order of the PDFs used in the two schemes. In fact, those terms are naturally included in the PDF definition if they are evolved at NNLO. However, FONLL-B is meant to be used together with NLO PDFs and so those terms explicitly appear in the perturbative series. Therefore, as in the FONLL-0 case, the countings of FONLL-B and of the $F^{\text{I.E.}}$ NNLO result of eq. (4.13) are equivalent but the resulting numerical results will differ due to the different PDF order adopted.

Regarding F_L one can get

$$
\begin{aligned}
F_L^{(B)} &= \alpha_s [C_{b,L}^{(1)} f_b + B_{g,L}^{(1)} f_g] \\
&+ \alpha_s^2 \Big[(B_{g,L}^{(2)} - \overline{B}_{g,L}^{[0](2)} \left(\frac{m_b}{Q} \right) - (B_{g,L}^{(1)} - B_{g,L}^{[0](1)} \left(\frac{m_b}{Q} \right)) K_{gg}^{(1)} \left(\frac{m_b}{Q} \right)) f_g \\
&+ (B_{q,L}^{(2)} - \overline{B}_{q,L}^{[0](2)} \left(\frac{m_b}{Q} \right)) f_q \Big],
\end{aligned}
\tag{4.36}
$$

where the massive-zero coefficients functions read

$$
\begin{aligned}
B_{g,L}^{[0](2)} \left(\frac{m_b}{Q} \right) &= C_{g,L}^{(2)} + C_{g,L}^{(1)} K_{gg}^{(1)} \left(\frac{m_b}{Q} \right) + 2C_{b,L}^{(1)} K_{bg}^{(1)} \left(\frac{m_b}{Q} \right) \\
B_{g,L}^{[0](2)}(1) &= C_{g,L}^{(2)} \\
B_{q,L}^{[0](2)} \left(\frac{m_b}{Q} \right) &= C_{q,L}^{(2)} \\
B_{q,L}^{[0](2)}(1) &= C_{q,L}^{(2)}.
\end{aligned}
\tag{4.37}
$$

From the last equation, it follows

$$\overline{B}^{[0](2)}_{g,L}\left(\frac{m_b}{Q}\right) = C^{(1)}_{g,L}K^{(1)}_{gg}\left(\frac{m_b}{Q}\right) + 2C^{(1)}_{b,L}K^{(1)}_{bg}\left(\frac{m_b}{Q}\right) \tag{4.38}$$
$$\overline{B}^{[0](2)}_{q,L}\left(\frac{m_b}{Q}\right) = 0,$$

and so, after some manipulations, it is possible to obtain the final F_L expression

$$\begin{aligned} F_L^{(B)} &= \alpha_s[C^{(1)}_{b,L}f_b + B^{(1)}_{g,L}f_g] \\ &+ \alpha_s^2[\tilde{C}^{(2)}_{g,L}f_g + B^{(2)}_{q,L}f_q] \end{aligned} \tag{4.39}$$

written in terms of the tilde coefficients functions.

To summarize, it has been shown that FONLL-0 and FONLL-B are respectively equivalent, except for the PDF evolution orders, to the NLO and NNLO of the $F^{\text{I.E.}}$ results proposed in this thesis. This is the reason why, in chapter 5, FONLL-0 and FONLL-B are never mentioned and, in particular, in sec. 5.3 where the ultimate versions of the results are constructed (tab. 4.1), they are replaced by the $F^{\text{I.E.}}$ results.

This equivalence is not surprising because it is straightforward to show that the all-order equivalence shown in eq. (3.55) is valid also order by order in perturbation theory if one uses the FONLL prescription for the construction of the B and the 0 versions. In fact, this means to take eq. (3.56) at order α_s for FONLL-0 and at order α_s^2 for FONLL-B while taking the massless $C_k^{[5]}$ at order α_s at most. It is easy to show that this is equivalent to take the piece

$$\sum_{j=g,q,\bar{q}}\sum_{k=b,\bar{b}} C_k^{[5]}K_{kj}^{[5]\leftarrow[4]}\tilde{K}_{ji}^{[4]\rightarrow[5]} \tag{4.40}$$

of eq. (3.54) respectively at order α_s and at order α_s^2. In fact, $K_{kj}^{[5]\leftarrow[4]}$ is at least of order α_s, since it cannot be diagonal (j is a light-quark while k is the heavy-quark), and so the other terms are forced to be of the correct order.

4.3.4 FONLL-C

The FONLL-C scheme is constructed simply taking both the massive and the massless coefficients functions at most at order α_s^2. So

$$\begin{aligned} F_2^{(C)} &= C^{(0)}_{b,2}f_b \\ &+ \alpha_s[C^{(1)}_{b,2}f_b + \tilde{C}^{(1)}_{g,2}f_g] \\ &+ \alpha_s^2\Bigg[C^{(2)}_{b,2}f_b + \left(B^{(2)}_{q,2} - B^{[0](2)}_{q,2}\left(\frac{m_b}{Q}\right) + C^{(2)}_{q,2}\right)f_q \\ &+ \left(B^{(2)}_{g,2} - B^{[0](2)}_{g,2}\left(\frac{m_b}{Q}\right) + C^{(2)}_{g,2} - \left(B^{(1)}_{g,2} - B^{[0](1)}_{g,2}\left(\frac{m_b}{Q}\right)\right)K^{(1)}_{gg}\left(\frac{m_b}{Q}\right)\right)f_g\Bigg] \end{aligned} \tag{4.41}$$

which, using the definition of $B^{[0](2)}_{g,2}(m_b/Q)$ in eq. (4.30), becomes

$$\begin{aligned} F_2^{(C)} &= C^{(0)}_{b,2}f_b \\ &+ \alpha_s[C^{(1)}_{b,2}f_b + \tilde{C}^{(1)}_{g,2}f_g] \\ &+ \alpha_s^2[C^{(2)}_{b,2}f_b + \tilde{C}^{(2)}_{g,2}f_g + \tilde{C}^{(2)}_{q,2}f_q]. \end{aligned} \tag{4.42}$$

Following the same steps for F_L, it is possible to get

$$F_L^{(C)} = \alpha_s[C_{b,L}^{(1)} f_b + B_{g,L}^{(1)} f_g] + \alpha_s^2[C_{b,L}^{(2)} f_b + \tilde{C}_{g,L}^{(2)} f_g + \tilde{C}_{q,L}^{(2)} f_q]. \tag{4.43}$$

Notice that, as expected, in both the F_2 and the F_L cases, the bottom coefficients function appears at an exceeding order with respect to the $F^{\text{I.E.}}$ NNLO results of eqs. (4.13) and (4.14). Again, this means that, in the $Q \gtrsim \mu_b$ region, the resulting numerical results will have a strong dependence on the μ_b scale even if, in this case, it will be suppressed by a factor α_s with respect to FONLL-A case.

From the expressions obtained so far, it is also interesting to note that, in order to construct FONLL-D and FONLL-E, the only currently missing coefficients functions are the gluon and light quark massive ones at N^3LO, for which some reliable approximations already exist in literature [29]. The other missing ingredients, regarding either the matching and the splitting functions at N^3LO, are currently under calculation and they will be probably available soon. Therefore, following the proposal of this thesis (table 4.1), it will soon be possible to make theoretical predictions on the N^3LO DIS and so the access to the N^3LO PDFs will be got for the first time.

Chapter 5

Results

In this chapter, the numerical results, in their different versions linked to the expressions obtained in chapter 4, will be presented. However, the content of this chapter is not limited to the presentation of the results alone, rather it is a detailed account of the consequences related to the adoption of the scheme proposed in this thesis. In particular, after having shown the correctness of the procedure adopted for the construction of the matched result, the final results, for $F_2^{\text{I.E.}}$ and $F_L^{\text{I.E.}}$ at NLO and NNLO, will be constructed using both the standard 5FS PDFs and the alternative PDFs of eq. (4.12), in both the cross-expanded and the standard way. In this way, it will be possible to determine if the more expensive procedures, related to alternative PDFs and cross-expansion, are advantageous compared to those usually adopted or not.

The final results will be then also compared with the FONLL ones, in such a way to underline the numerical consequences resulting from the adoption of different countings. Finally, the ultimate version of the results will be constructed combining the two different countings through an energy damping function, as mentioned in sec. 4.3.

The complete road-map of this chapter is then the following:

- In section 5.1, the NLO results for both $F_2^{\text{I.E.}}$ and $F_L^{\text{I.E.}}$ will be presented. First, the correctness of the matched result, in particular regarding the combination of the resummed massless result with the fixed-order massive result, and the way in which the uncertainties are estimated, will be shown. This will be done for both the standard and the alternative 5FS PDFs versions and the comparison between them will be presented. Then, the NLO intermediate energy result proposed in this thesis will be compared to FONLL-A.

- In section 5.2, the same structure of the previous one will be followed but for the NNLO results. In this case, it will be also possible to analyze the differences which arise from the adoption of the PDF cross-expansion. At the end of the section, the NLO and NNLO intermediate energy results will be shown together, in order to analyze the differences that an extra perturbative order entails.

- In section 5.3 the ultimate version of the result will be constructed combining the two different countings through an energy damping function (tab. 4.1). As mentioned in chapter 4, this is the correct procedure if the considered energy scale ranges in a very wide kinematic region and so the result obtained following it can be considered the extension of the previous results to higher energies.

5.1 NLO results

In this section, the numerical results for the NLO structure functions, in their different versions, will be presented as a function of the energy scale Q for four different values of the Bjorken's x. The latter are chosen in such a way to show the structure function behaviour in all the meaningful kinematic regions. In particular, they are $x = 0.0001$, which can be considered in the small-x region, $x = 0.001$ and $x = 0.01$, which are in the intermediate region, and $x = 0.1$, which is in the large-x region. These values are the same for all the plots shown in this chapter.

In figs. 5.1 and 5.2, the matched results at NLO, together with the FO and the R results, respectively for $F_2^{\text{I.E.}}$ and $F_L^{\text{I.E.}}$ and computed using the alternative 5FS PDFs of eq. (4.12) are shown.

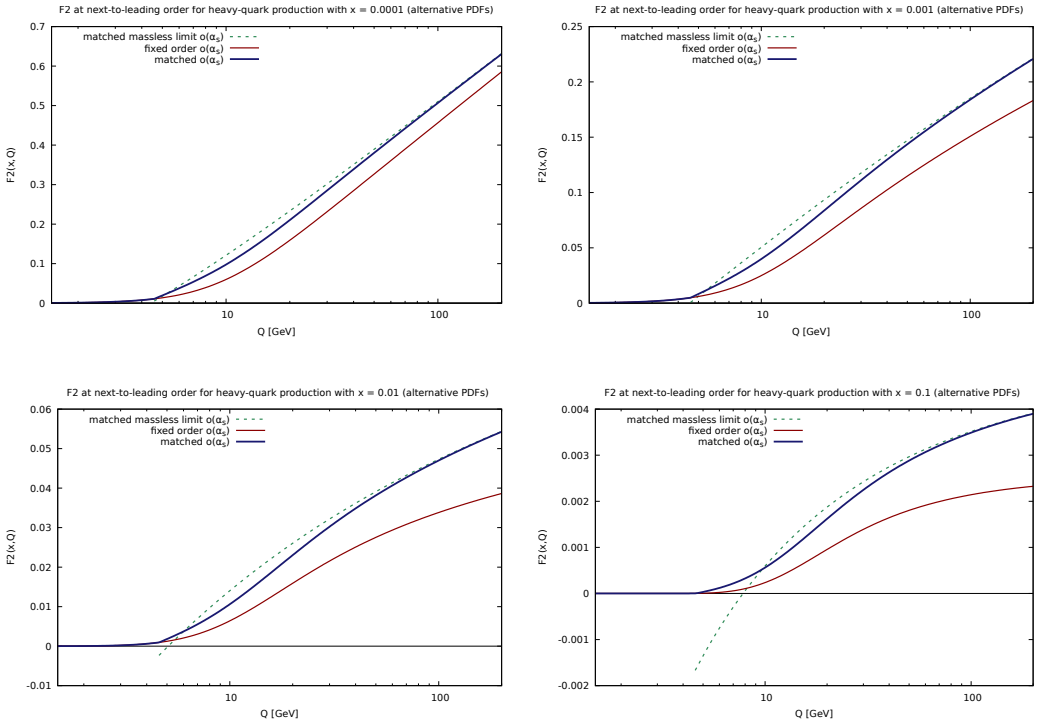

Figure 5.1. $F_2^{\text{I.E.}}$ at NLO as a function of Q for different values of the Bjorken's x. In this case the results have been constructed using the alternative version of the 5FS PDFs.

In both cases, and for every x value, it is possible to note that the matched result tends to the FO result in the threshold region and to the R result when $Q \gg m_b$. This is exactly the expected behaviour that confirms the correctness of the adopted procedure for the FO and R combination. Notice that, at this order, the FO result of F_L is equal to the matched one [1]. This is because F_L, at $\mathcal{O}(\alpha_s)$, has no collinear logarithms to resum, as discussed in the previous chapters, and so there are no resummation corrections to be added to the matched result.

It is also important to notice that the matched $F_2^{\text{I.E.}}$ result has a discontinuity on the slope in the threshold region, for every x value, caused by the transition from 4FS to 5FS. As it will be shown in sec. 5.2, this slope discontinuity will still be present in the NNLO results, even if it will be less pronounced. In appendix C,

[1] Actually they are not exactly identical due to the adoption of 5FS PDFs for the matched result and of 4FS PDFs for the FO result.

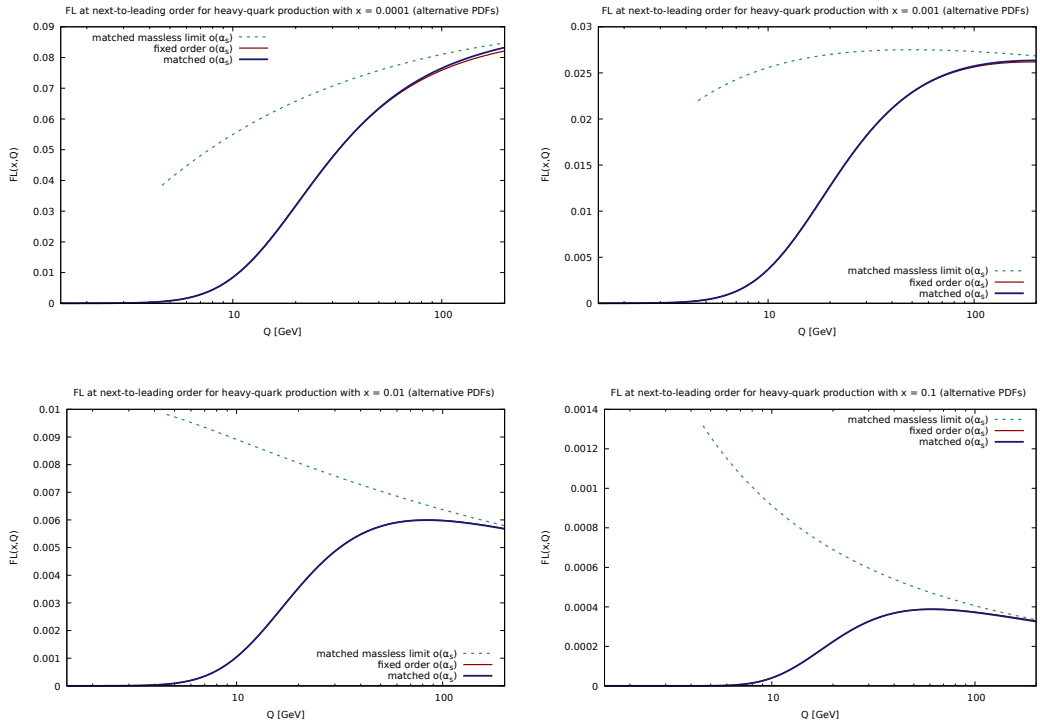

Figure 5.2. Same as fig. 5.1 but for $F_L^{\text{I.E.}}$.

this discontinuity problem has been addressed in detail and what emerged is that it becomes much less pronounced if LO PDFs are used instead of NLO ones. The reason of this behaviour is explained and commented in detail in appendix C.

5.1.1 μ_b variation

In this section, the dependence of the NLO results on the scale μ_b is studied in detail. This dependence, as mentioned in chapter 4, arises from the truncation to a certain finite order of an all-order expression and thus it can be exploited to estimate the uncertainties linked to the missing orders. For this reason, being less dependent on μ_b is, for a certain truncated result, an indicator of the perturbative counting correctness. This feature will be exploited in this section to compare the results obtained adopting the standard (eq. (4.9)) and the alternative (eq. (4.12)) 5FS PDFs while, in the rest of this chapter, it will be also exploited to compare the intermediate energy results proposed in this thesis with the FONLL ones.

However, it is important to underline that, although the μ_b dependence is, in most of the cases, a rather reliable uncertainty estimator, there are no theoretical reasons ensuring that this method provides a reasonable uncertainty band in every case. For instance, it is not granted that the results are either increasing or decreasing functions of μ_b and so the result obtained for $\mu_b = m_b$, which is considered the actual prediction, is not always included between the results obtained by increasing and decreasing μ_b. For this reason, in order to adopt a method which provides in every case a coherent uncertainty band, it has been chosen to construct the results for $\mu_b = 2m_b$ and $\mu_b = 0.5m_b$ and to symmetrize with respect to the one which most differ from the $\mu_b = m_b$ central result. In the following, the plots will contain an extra graph showing the ratios of the matched results obtained with $\mu_b = 2m_b$ and

$\mu_b = 0.5m_b$ over the $\mu_b = m_b$ one and the resulting symmetrized uncertainty band.

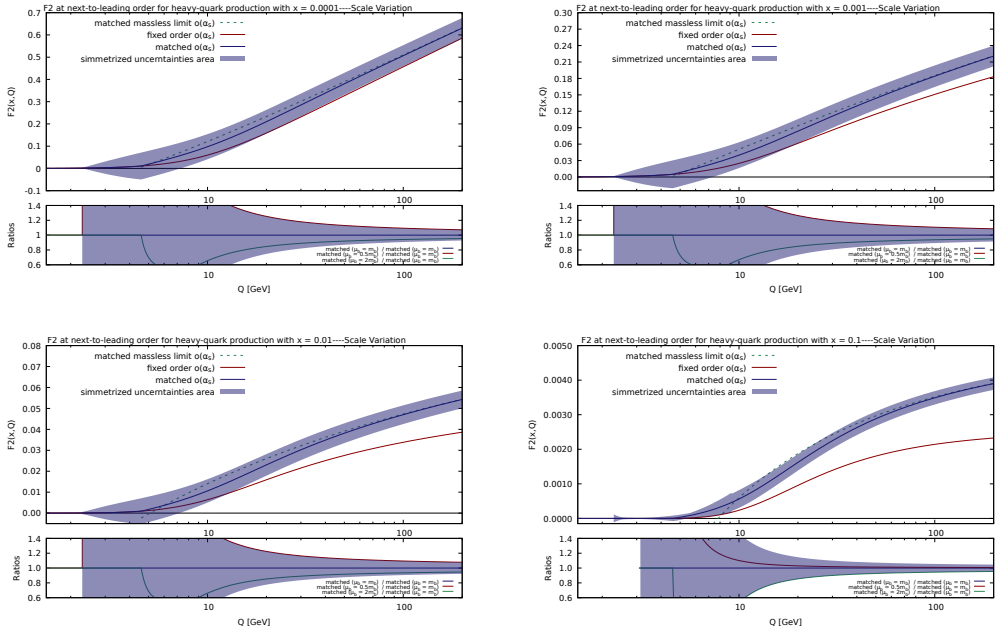

Figure 5.3. $F_2^{\text{I.E.}}$ at NLO as a function of Q for different values of the Bjorken's x. The ratio of the results obtained choosing $\mu_b = 0.5m_b$ and $\mu_b = 2m_b$ over the standard $\mu_b = m_b$ one are shown in the graph below, together with the obtained uncertainty area. The latter is also reported on the graph above. In this case the results have been constructed using the standard version of the 5FS PDFs.

In figs. 5.3 and 5.5, respectively the $F_2^{\text{I.E.}}$ and $F_L^{\text{I.E.}}$ results obtained with the standard 5FS PDFs are shown, while, in figs. 5.4 and 5.6 the analogous results obtained with the alternative PDFs are shown.

Comparing the standard and alternative PDF result versions, it is possible to note that, in particular for F_2, the μ_b dependence is slightly smaller in the alternative PDFs case. This is confirmed by the plots of fig. 5.7 in which the ratios over the FO of the matched results obtained for the three μ_b values and with both the standard and alternative PDFs are shown. The F_L case of fig. 5.8 seems to follow the opposite trend but, the extremely small size of the uncertainties makes difficult any speculation.

5.1.2 Comparison with FONLL-A

In this section, the comparison between FONLL-A and the intermediate energy NLO results proposed in this thesis, in both their standard and alternative PDF versions, will be carried out. In both cases, the main parameters of comparison will be the μ_b dependence and the smoothness of the results, in particular near the threshold region.

In figs. 5.9 and 5.10 the comparison between FONLL-A and the NLO result proposed in this thesis for $F_2^{\text{I.E.}}$, respectively obtained with the standard and the alternative PDFs, is shown. It is possible to see that, especially for the alternative PDF version, the μ_b dependence is slightly higher in FONLL-A case. In $F_L^{\text{I.E.}}$ case, figs. 5.11 and 5.12, this behaviour is much more pronounced, especially in the threshold region, for both the standard and the alternative PDF versions. Moreover,

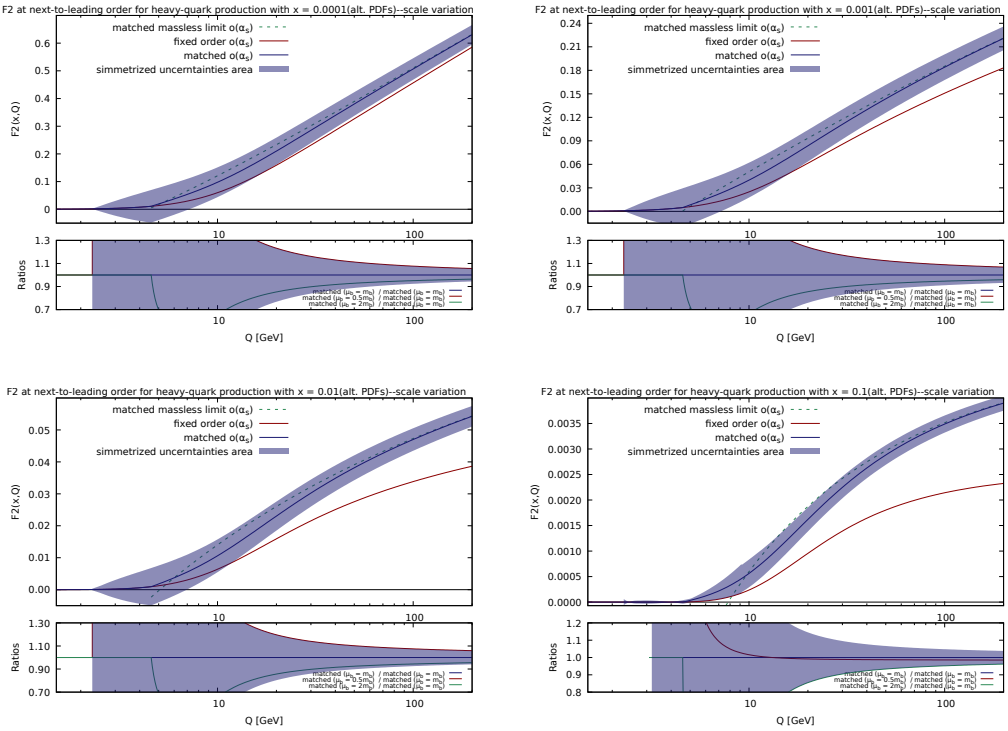

Figure 5.4. Same as fig. 5.3 but constructed adopting the alternative version of the 5FS PDFs.

the slope discontinuity in the threshold region appears, especially in $F_L^{\text{I.E.}}$ case, much more pronounced for the FONLL-A results. It is then possible to conclude that, at least at this order, the adoption of the counting proposed in this thesis leads to better results in the $Q \gtrsim \mu_b$ region than the adoption of the standard one, especially if one correctly adopts the alternative PDFs.

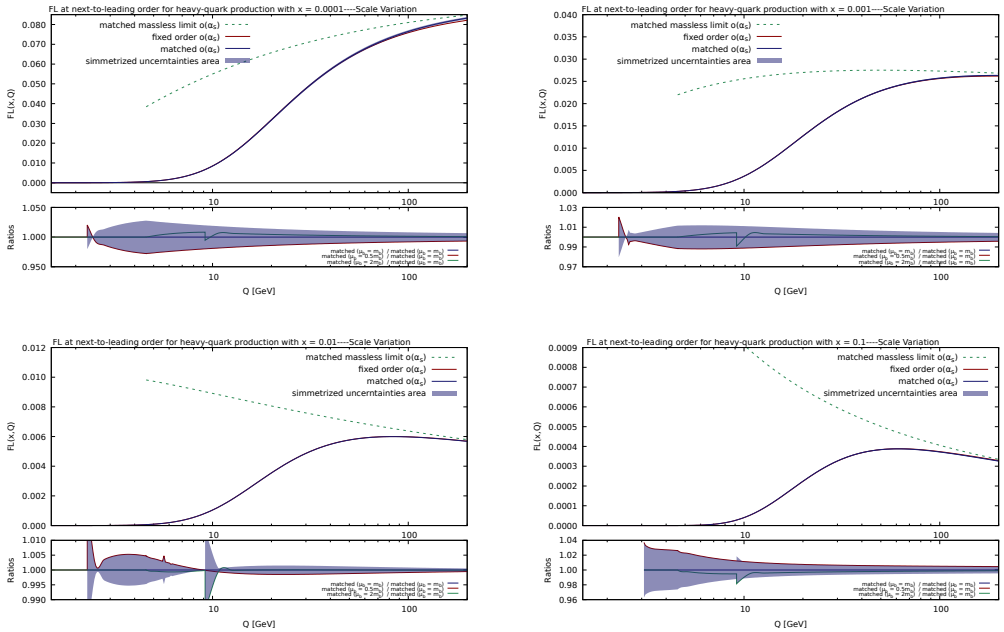

Figure 5.5. Same as fig. 5.3 but for $F_L^{\text{I.E.}}$.

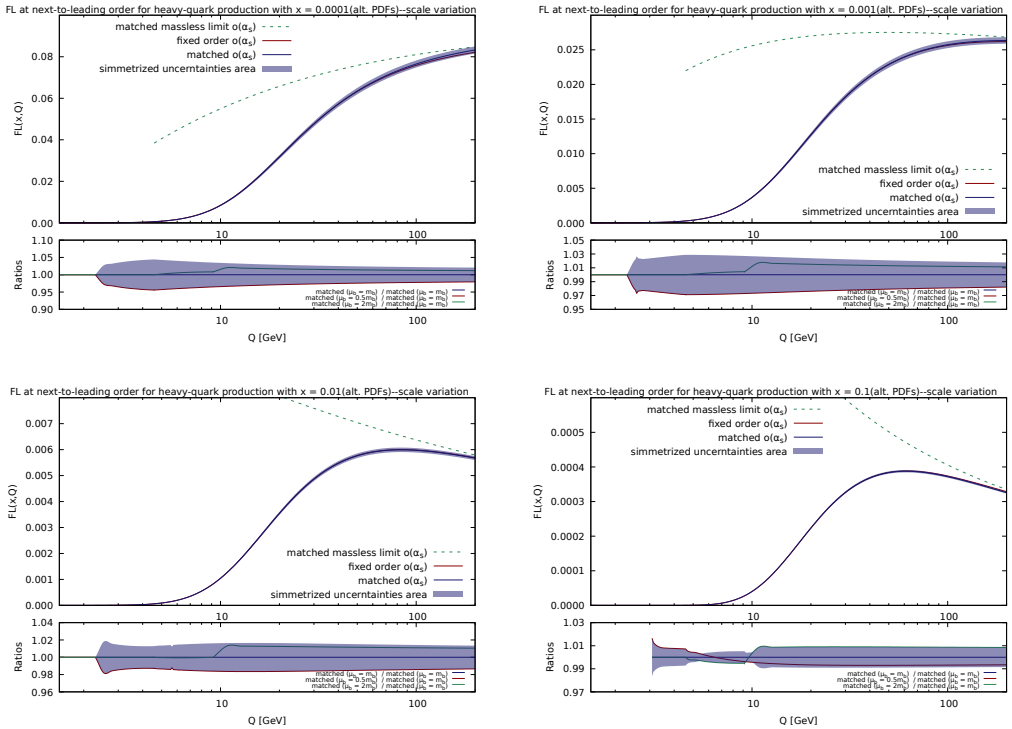

Figure 5.6. Same as fig. 5.4 but for $F_L^{\text{I.E.}}$.

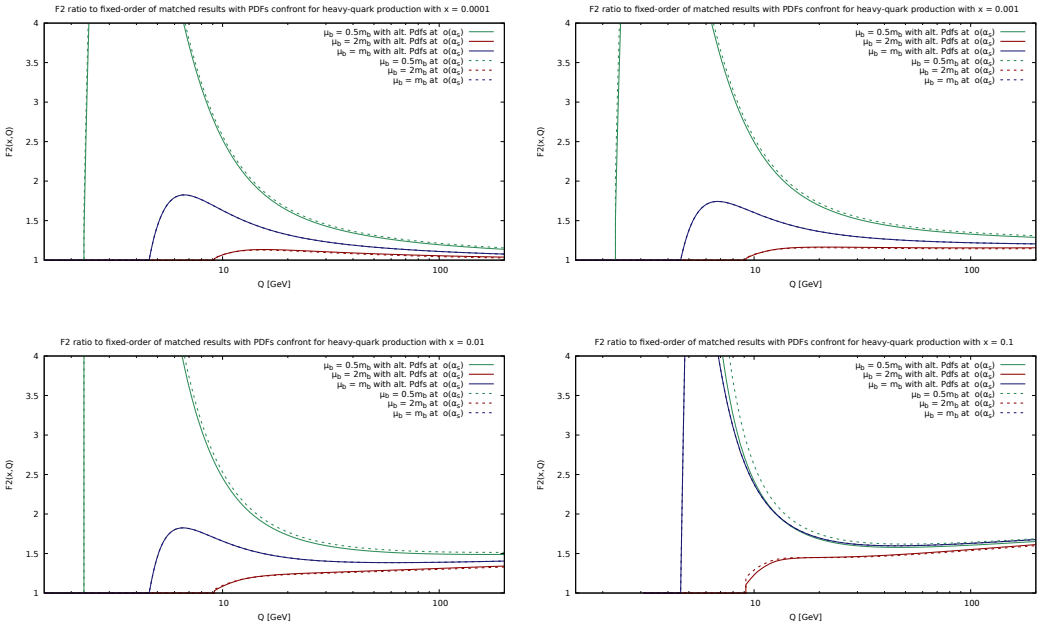

Figure 5.7. Ratio of $F_2^{\text{I.E.}}$ matched result over its fixed-order at NLO as a function of Q for different values of the Bjorken's x and μ_b. The ratios are obtained trough both the standard and the alternative PDFs in order to analyze the different μ_b dependence in the two cases.

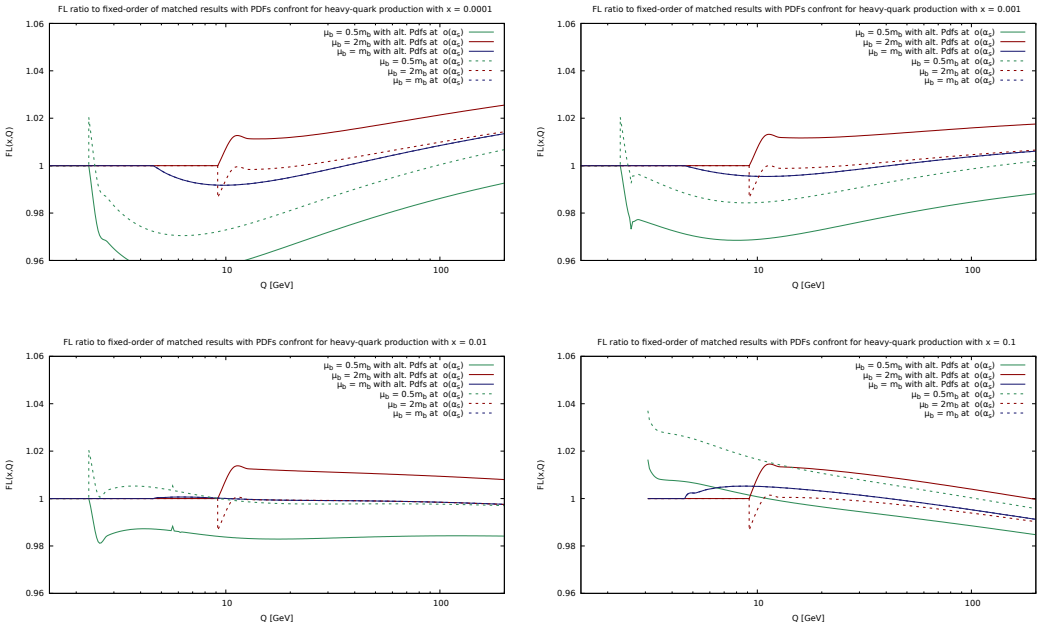

Figure 5.8. Same as fig. 5.7 but for $F_L^{\text{I.E.}}$.

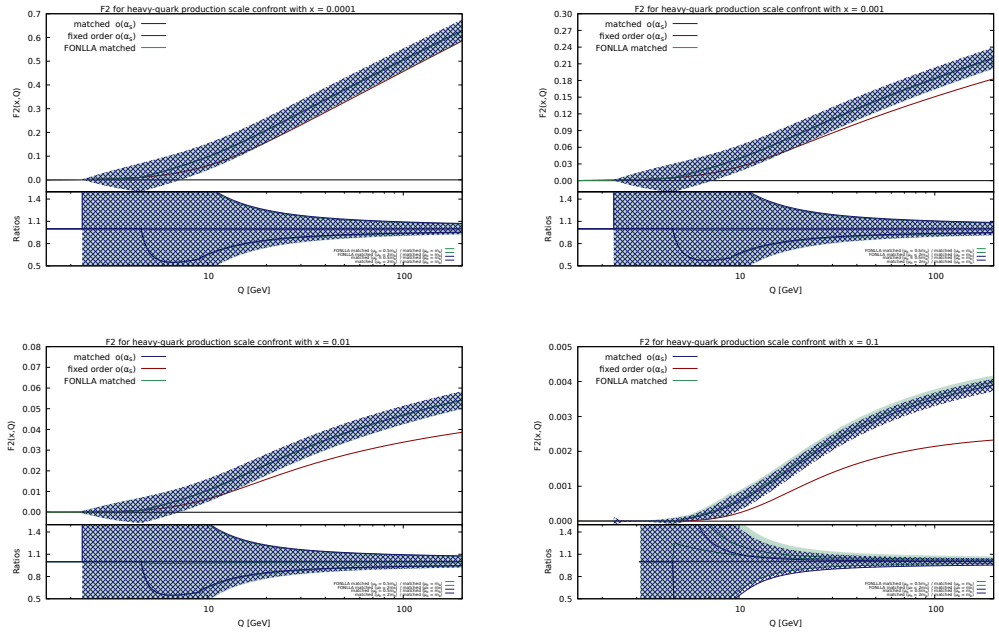

Figure 5.9. F_2 in the FONLL-A scheme and in the intermediate energy NLO scheme proposed in this thesis as a function of Q for different values of the Bjorken's x. The ratio of the results obtained choosing $\mu_b = 0.5m_b$ and $\mu_b = 2m_b$ over the standard $\mu_b = m_b$ one are shown in the graph below, together with the obtained uncertainty area. The latter is also reported on the graph above. In this case the results have been constructed using the standard version of the 5FS PDFs.

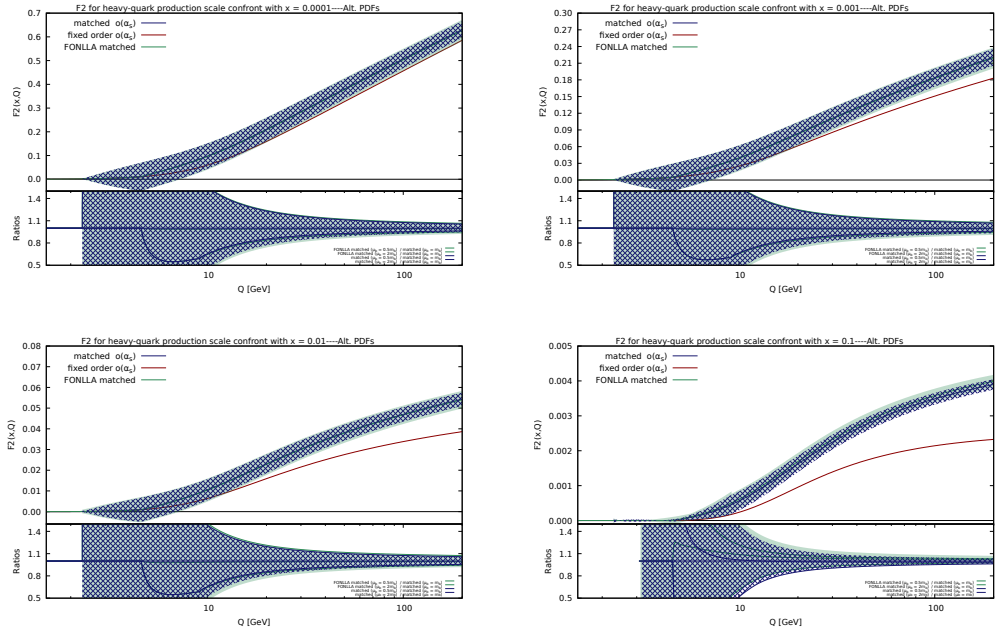

Figure 5.10. Same as fig. 5.9 but constructed with the alternative version of the 5FS PDFs.

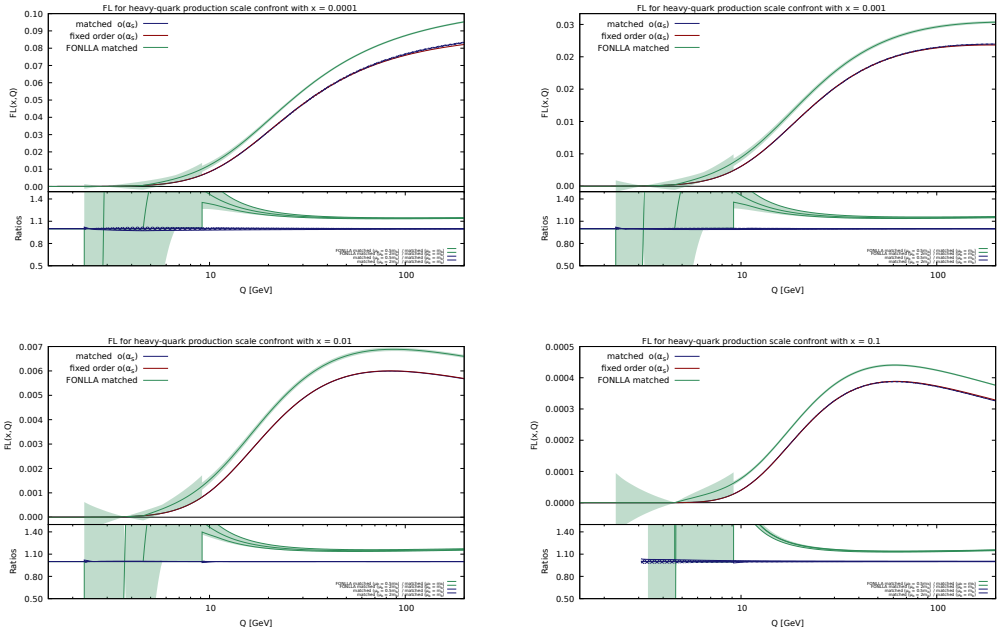

Figure 5.11. Same as fig. 5.9 but for F_L.

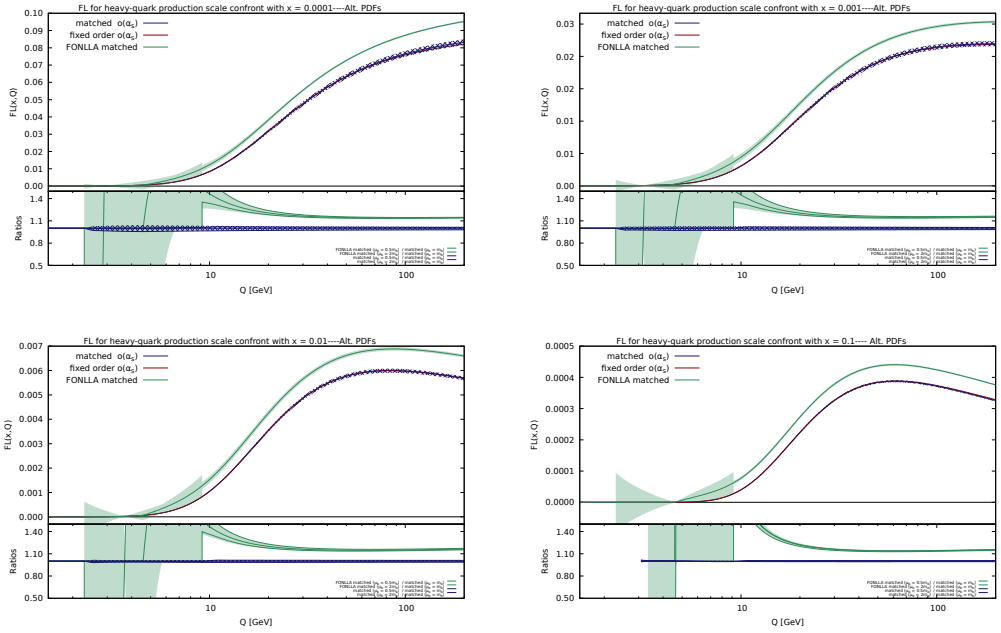

Figure 5.12. Same as fig. 5.10 but for F_L.

5.2 NNLO results

This section will follow the same structure of the previous one but for the NNLO results. In addition, the comparison between standard and cross-expansion procedures will be shown and, in sec. 5.2.3, the NLO and the NNLO results will be shown together in order to analyze the improvement given by an additional perturbative order.

In figs. 5.13 and 5.14, the NNLO $F_2^{\text{I.E.}}$ results obtained with the alternative PDFs and respectively with the standard and the cross-expansion procedures are shown. The analogous plots for $F_L^{\text{I.E.}}$ are shown in figs. 5.15 and 5.16. In both cases, the cross-expansion procedure, although it is in principle the correct way of constructing the results, does not seem to make any tangible improvements, except for an apparent small improvement in the slope discontinuity in the threshold region for some x values. Given the complication in adopting such a procedure, which needs two sets of PDFs, it can be concluded that it is not worth adopting it.

5.2.1 μ_b variation

In this section, the μ_b dependence comparison between the standard and the alternative PDFs NNLO results of both $F_2^{\text{I.E.}}$ and $F_L^{\text{I.E.}}$ will be analyzed. In figs. 5.17 and 5.18 the plots showing the $F_2^{\text{I.E.}}$ dependence on μ_b respectively for the standard and alternative PDFs cases are shown, while the analogous ones for $F_L^{\text{I.E.}}$ are shown in figs. 5.19 and 5.20.

The first thing to note is that, as expected, all uncertainties have decreased in this case compared to the analogous NLO plots. However, although the slope discontinuity in the threshold region is still less pronounced in the alternative PDFs results, their better quality from an uncertainty point of view, which was clearly visible in the NLO case, is not as much clear in this case. In fact, as it is also possible to note from figs. 5.21 and 5.22, the uncertainties do not always respect a clear hierarchy and they have, in general, a rather irregular behaviour. This could mean that the adoption of the alternative PDFs proposed in this thesis does not actually improve the results, but could also be just the consequence of the non-optimal method used to estimate the uncertainties.

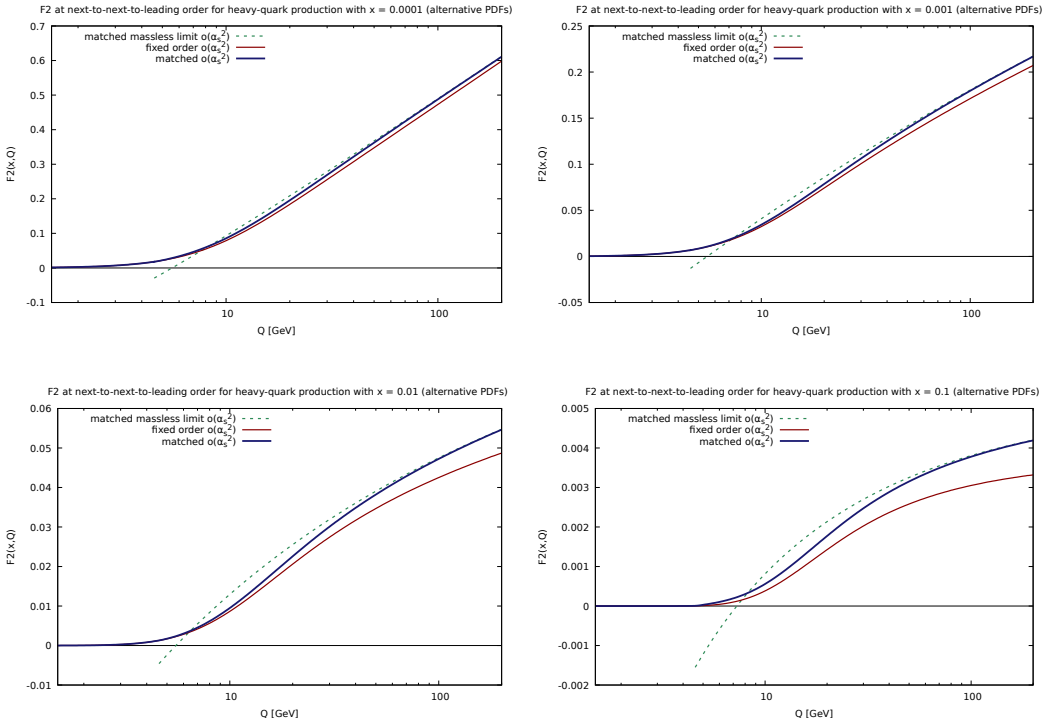

Figure 5.13. $F_2^{\text{I.E.}}$ at NNLO as a function of Q for different values of the Bjorken's x. In this case the results have been constructed using the alternative version of the 5FS PDFs.

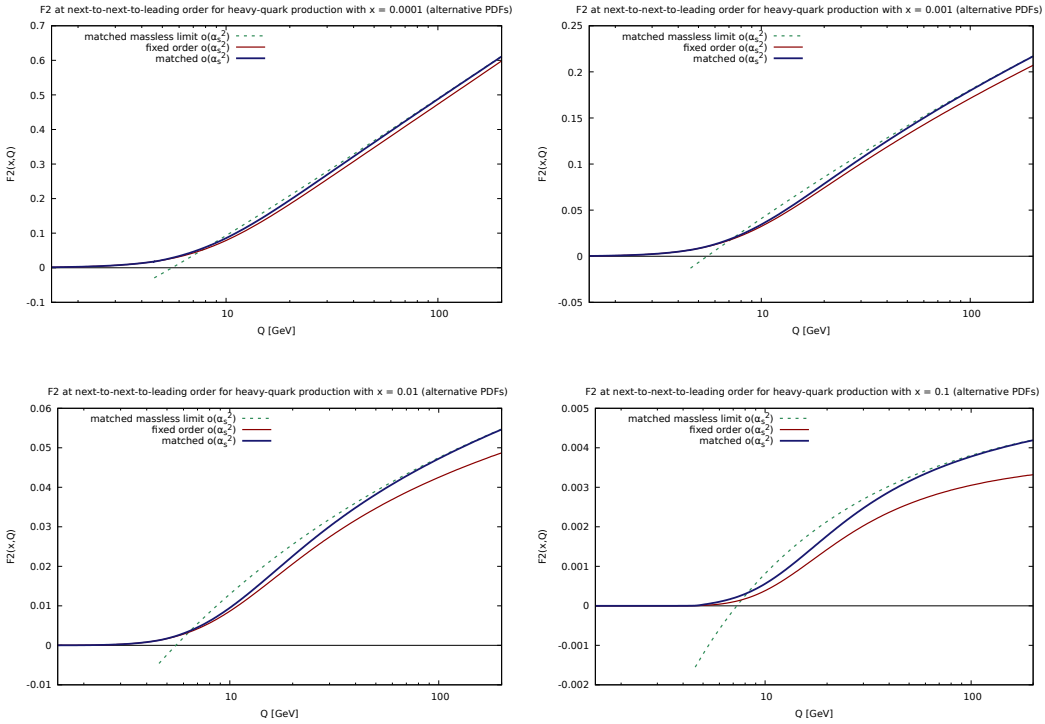

Figure 5.14. Same as fig. 5.13 but constructed adopting the cross-expansion procedure for the PDFs.

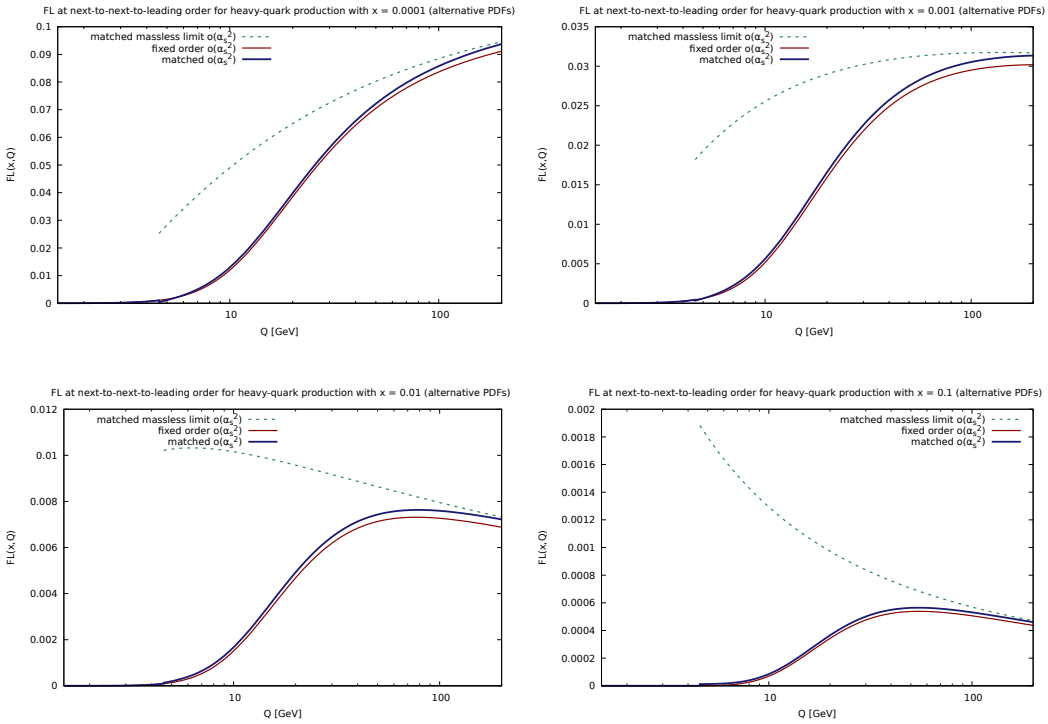

Figure 5.15. Same as fig. 5.13 but for $F_L^{\text{I.E.}}$.

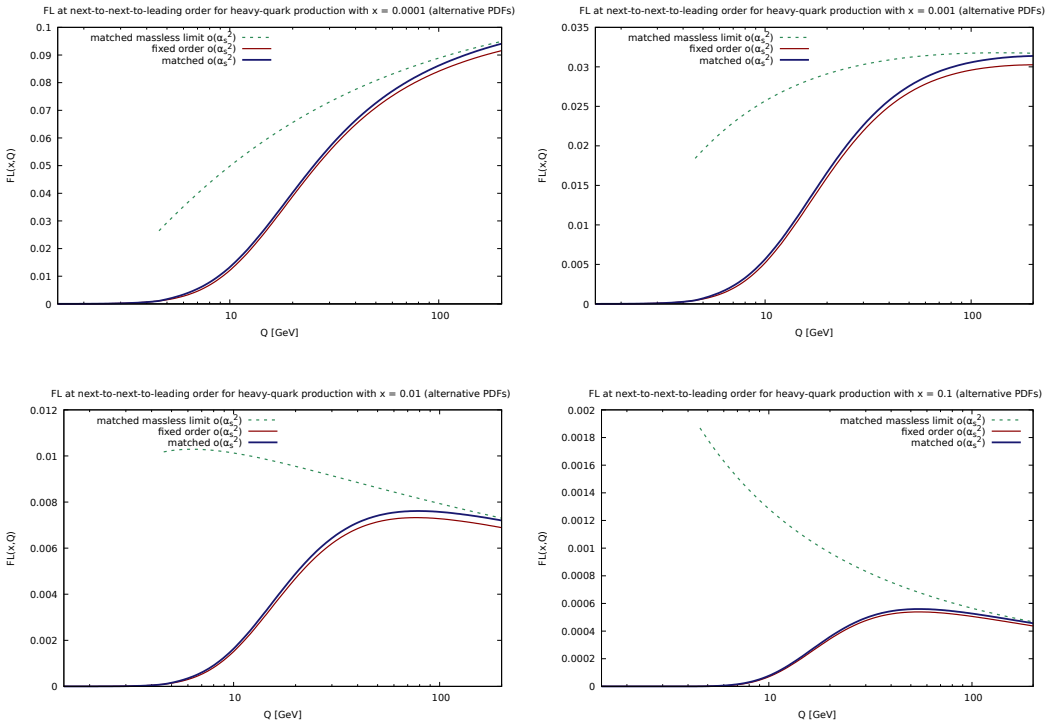

Figure 5.16. Same as fig. 5.14 but for $F_L^{\text{I.E.}}$.

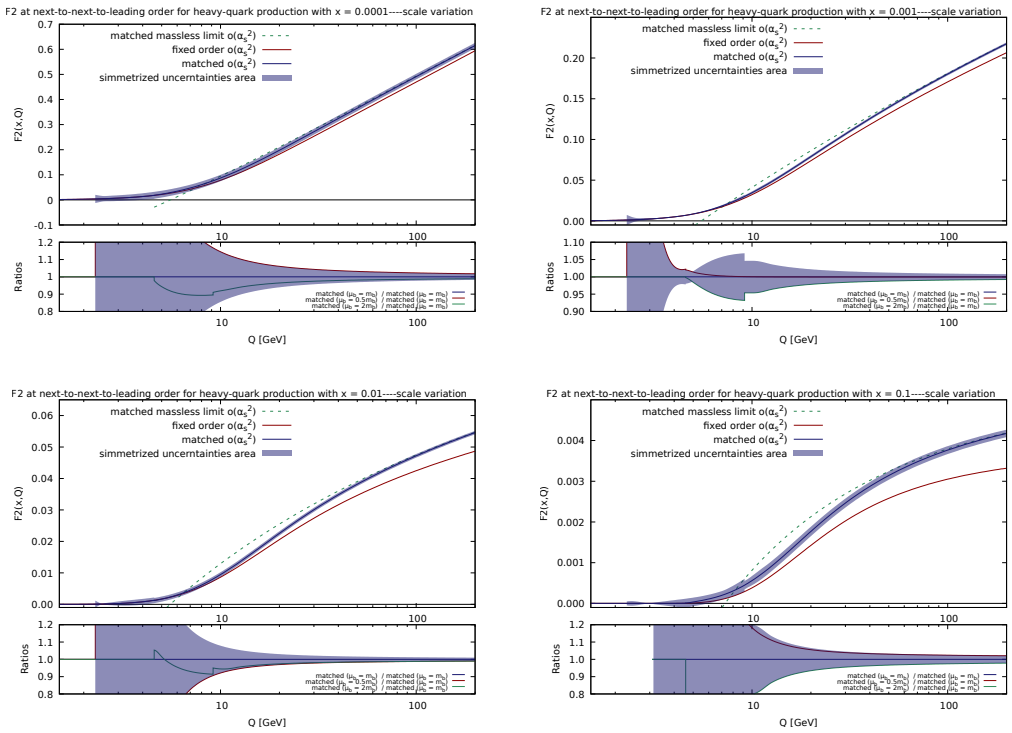

Figure 5.17. $F_2^{\text{I.E.}}$ at NNLO as a function of Q for different values of the Bjorken's x. The ratio of the results obtained choosing $\mu_b = 0.5m_b$ and $\mu_b = 2m_b$ over the standard $\mu_b = m_b$ one are shown in the graph below, together with the obtained uncertainty area. The latter is also reported on the graph above. In this case the results have been constructed using the standard version of the 5FS PDFs.

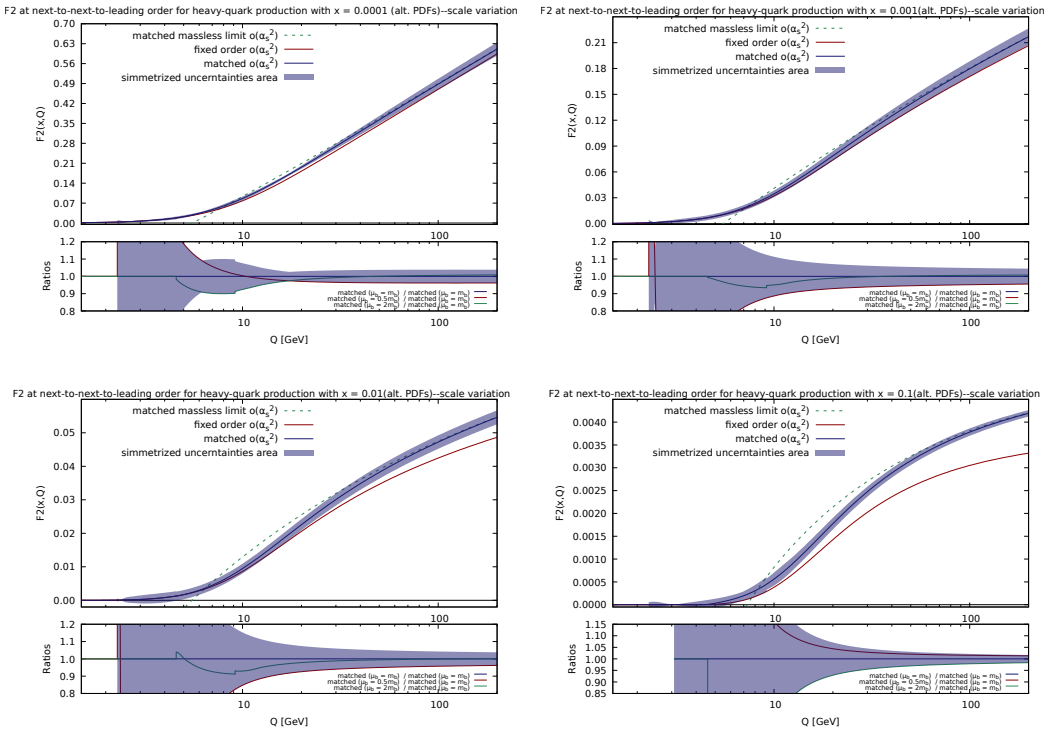

Figure 5.18. Same as fig. 5.17 but constructed using the alternative version of the 5FS PDFs.

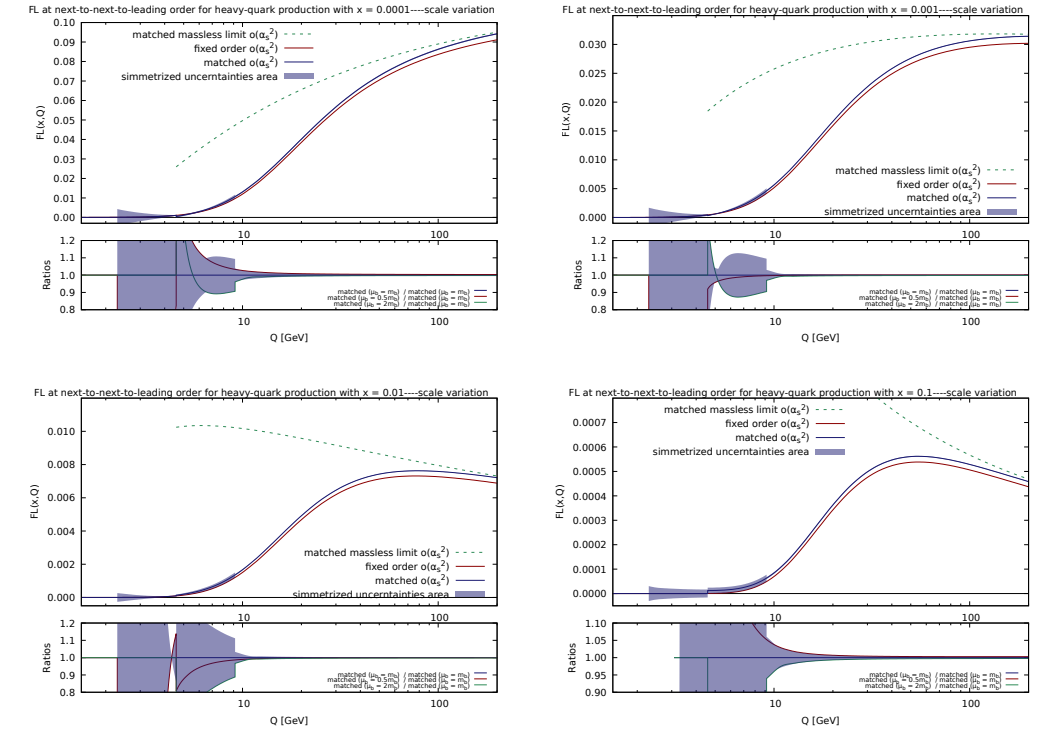

Figure 5.19. Same as fig. 5.17 but for $F_L^{\text{I.E.}}$.

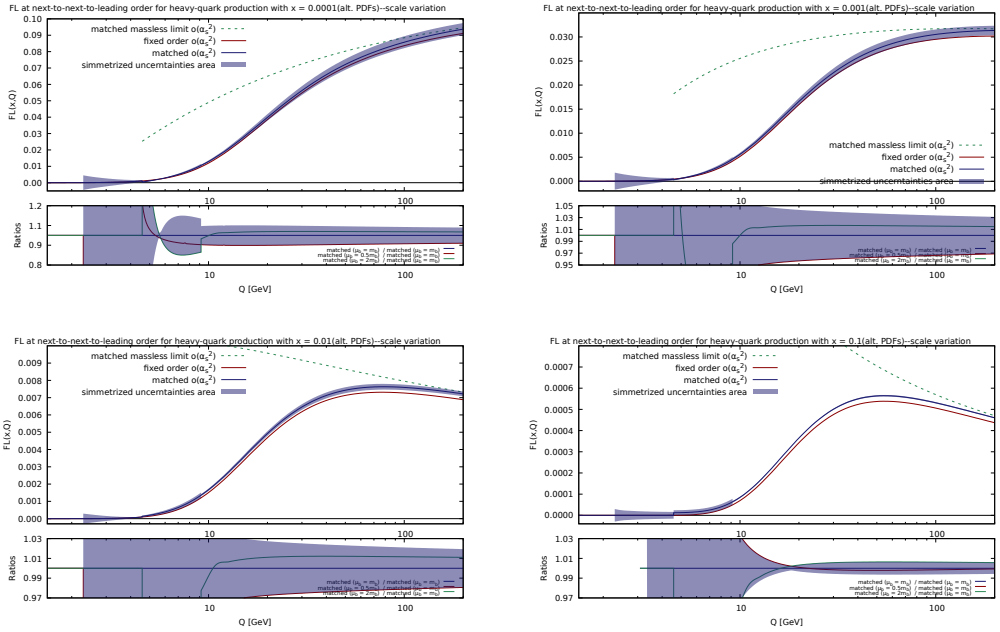

Figure 5.20. Same as fig. 5.18 but for $F_L^{\text{I.E.}}$.

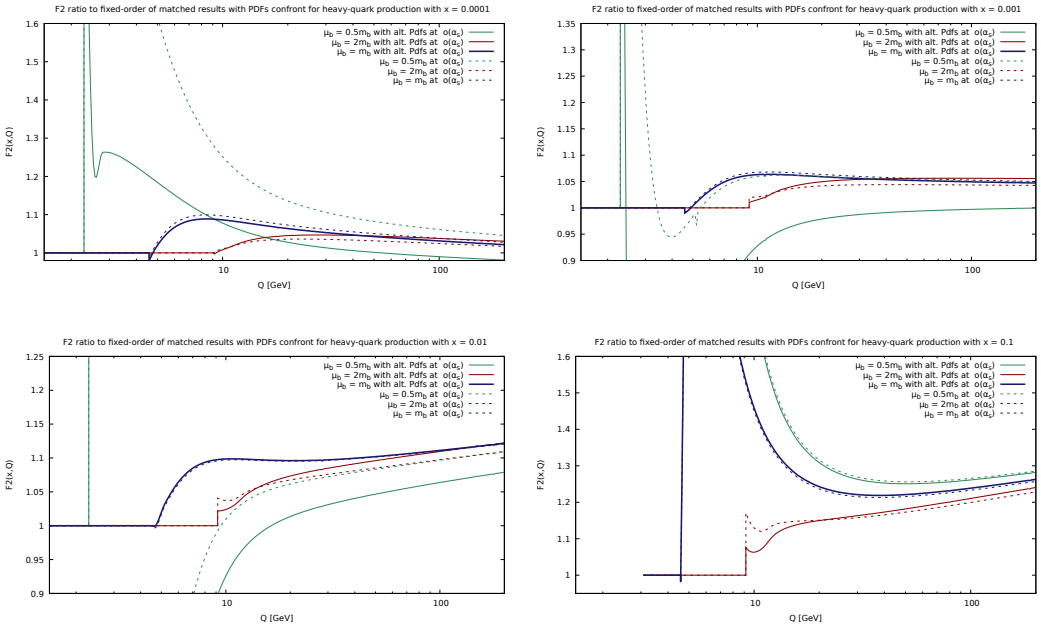

Figure 5.21. Ratio of $F_2^{\text{I.E.}}$ matched result over its fixed-order at NNLO as a function of Q for different values of the Bjorken's x and μ_b. The ratios are obtained trough both the standard and the alternative PDFs in order to analyze the different μ_b dependence in the two cases.

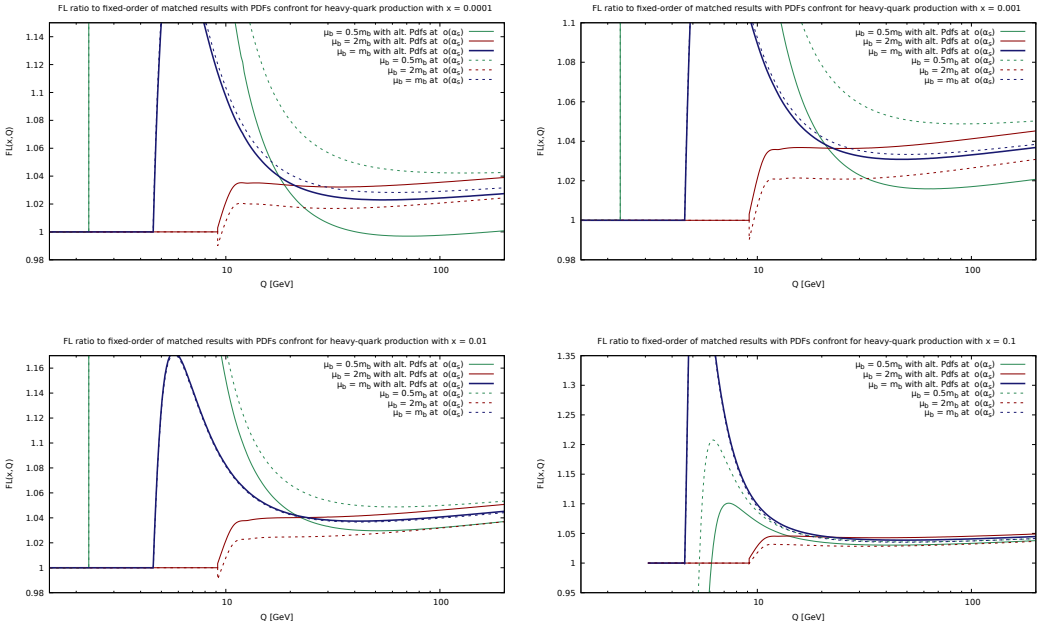

Figure 5.22. Same as fig. 5.21 but for $F_L^{\text{I.E.}}$.

5.2.2 Comparison with FONLL-C

In this section, the NNLO intermediate energy results proposed in this thesis will be compared to FONLL-C scheme, for both the structure functions F_2 and F_L and for both their standard and alternative PDFs versions. In figs. 5.23 and 5.24 the μ_b dependence of the NNLO result for $F_2^{\text{I.E.}}$ is compared to the FONLL-C one, respectively in the standard and alternative PDFs cases. The same plots for F_L are reported in figs. 5.25 and 5.26.

Also in this case, the μ_b dependence of the results do not seem to decrease with the alternative PDFs adoption. However, as in NLO case, the scale dependence of the NNLO intermediate energy results proposed in this thesis have a better behaviour with respect to the FONLL-C one, especially in the threshold region where the FONLL-C curves have more pronounced discontinuities. This means that, since, as mentioned in sec. 4.3, FONLL-B is equivalent to the NNLO intermediate energy result proposed in this thesis, FONLL-B actually provides better results than FONLL-C, even if, in FONLL's prescription, FONLL-C accounts for an higher perturbative order than FONLL-B. This is another proof of what has been discussed in sec. 4.3.

5.2.3 Perturbative order comparison

In this section, the NLO and the NNLO results, for both $F_2^{\text{I.E.}}$ and $F_L^{\text{I.E.}}$ and in the alternative PDFs case, will be shown together in such a way to underline the impact of an additional perturbative order. In both the $F_2^{\text{I.E.}}$ (fig. 5.27) and the $F_L^{\text{I.E.}}$ (fig. 5.28) cases, it is possible to note that the fixed order and the massless resummed results are much more similar to the matched result in the NNLO case than in the NLO one. This is exactly what was expected because the resummation corrections which have to be summed to the fixed order result in order to obtain the matched one are, in the NNLO case, $\mathcal{O}(\alpha_s^2)$ and thus they are smaller than the $\mathcal{O}(\alpha_s)$ ones of the NLO case.

Moreover, it is important to notice that, in both the F_2 and F_L cases, the difference between NLO and NNLO is much larger in the FO result than in the matched result. This means that the resummation also improves the perturbative series stability.

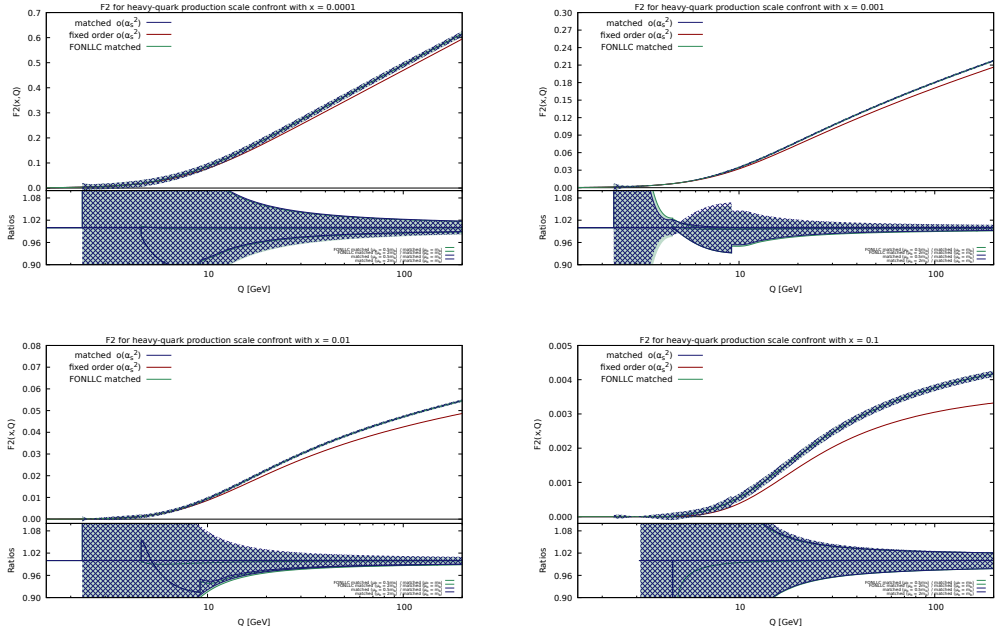

Figure 5.23. F_2 in the FONLL-C scheme and in the NNLO intermediate energy scheme proposed in this thesis as a function of Q for different values of the Bjorken's x. The ratio of the results obtained choosing $\mu_b = 0.5m_b$ and $\mu_b = 2m_b$ over the standard $\mu_b = m_b$ one are shown in the graph below, together with the obtained uncertainty area. The latter is also reported on the graph above. In this case the results have been constructed using the standard version of the 5FS PDFs.

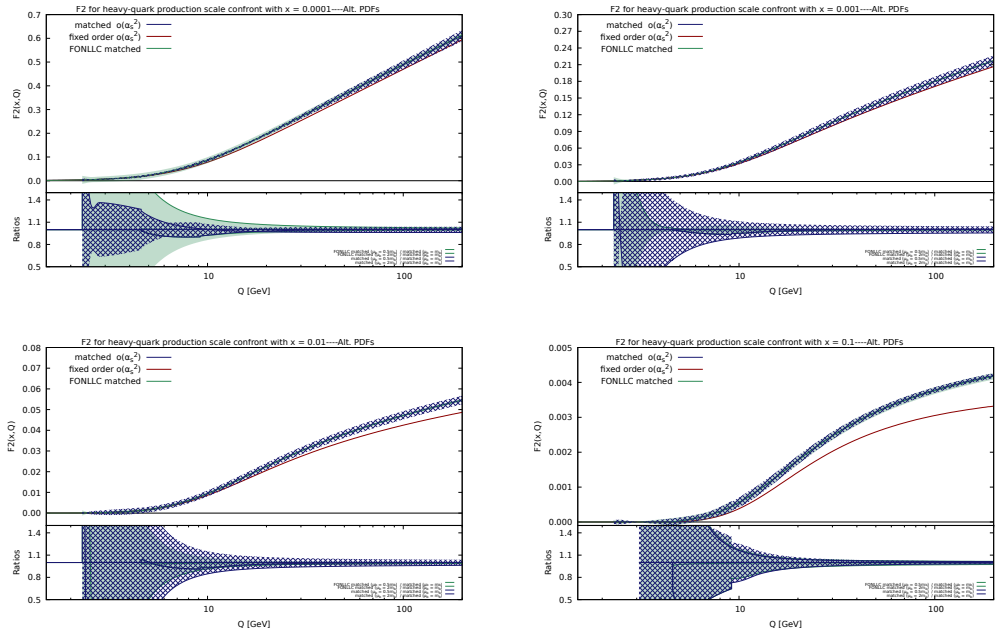

Figure 5.24. Same as fig. 5.23 but constructed using the alternative version of the 5FS PDFs.

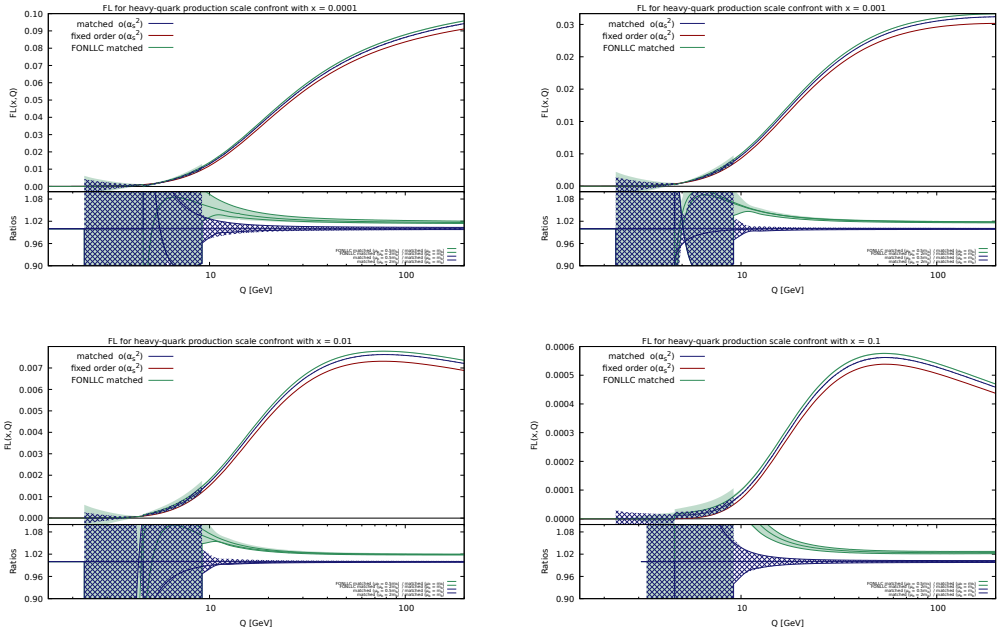

Figure 5.25. Same as fig. 5.23 but for F_L.

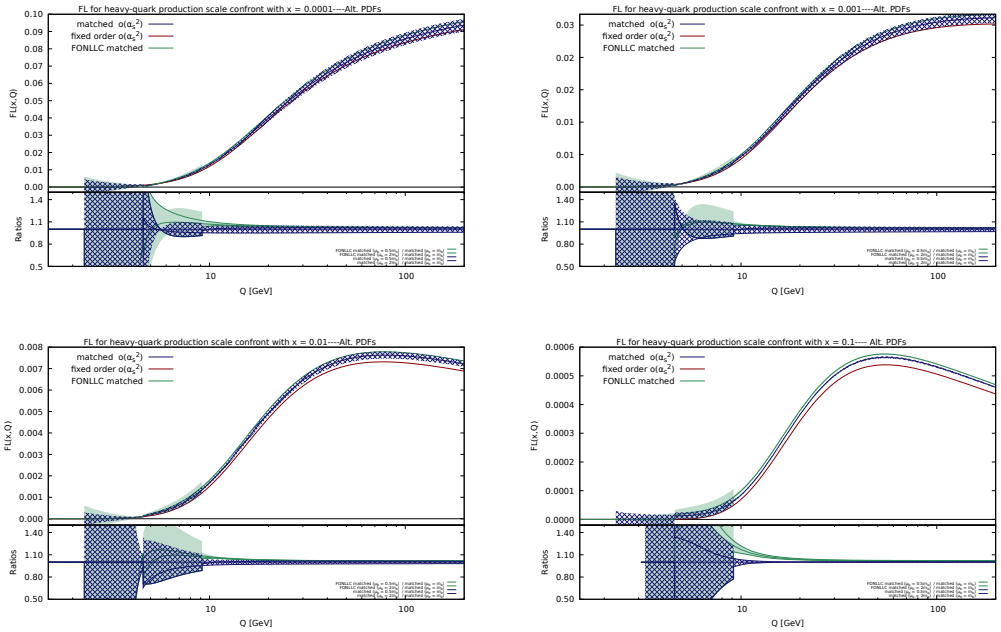

Figure 5.26. Same as fig. 5.24 but for F_L.

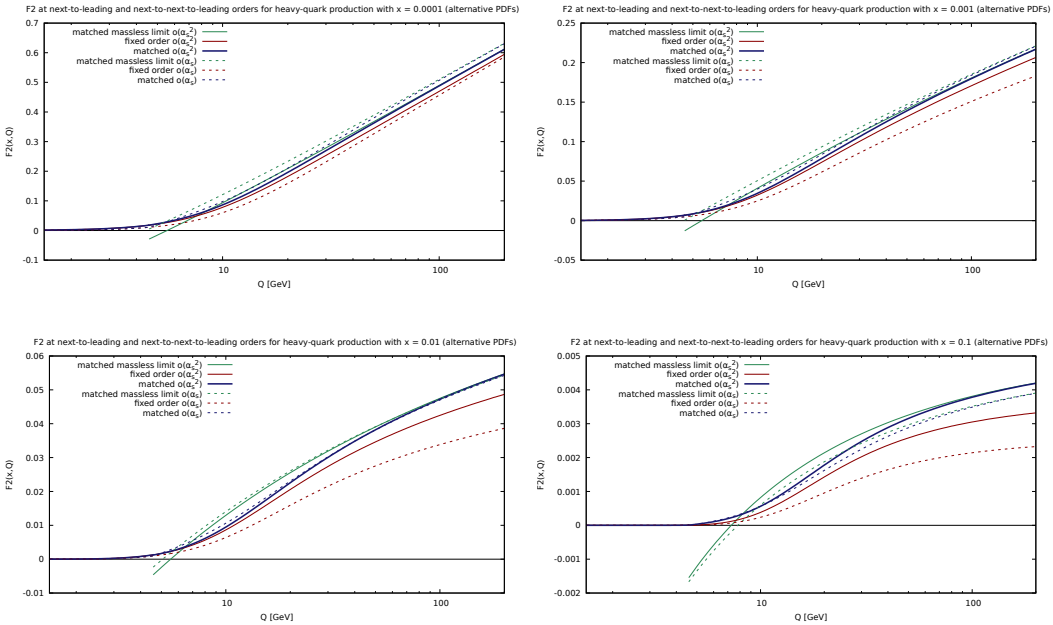

Figure 5.27. $F_2^{\text{I.E.}}$ matched result, together with FO and R results, at NLO and NNLO as a function of Q for different values of the Bjorken's x. In this case the results have been constructed using the alternative version of the 5FS PDFs.

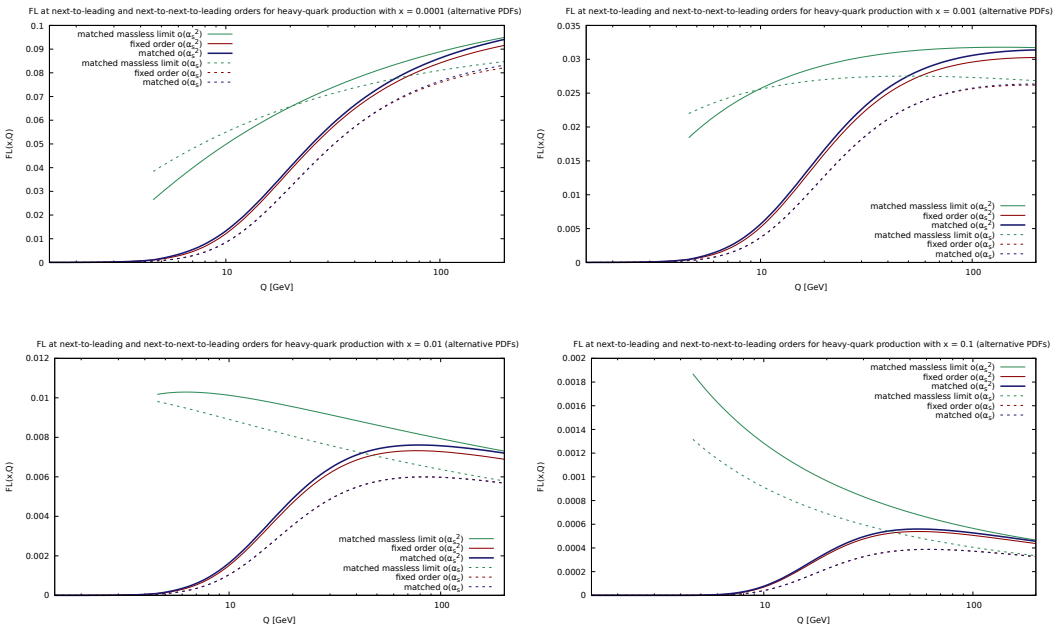

Figure 5.28. Same as fig. 5.27 but for $F_L^{\text{I.E.}}$.

5.3 Extension of the result to higher energies

The results shown in the previous sections, in their different versions, were either obtained adopting the standard counting of eq. (4.10), in FONLL case, or the one proposed in this thesis (eq. (4.11)). However, as mentioned in sec. 4.2, one is more appropriate than the other depending on the considered energy scale. In particular, if $Q \gtrsim \mu_b$, it is better to adopt the counting proposed in this thesis, but, for much higher energies, it is better to adopt the standard one. Since the goal of this thesis is to provide a method to construct a reliable prediction in a wide kinematic region, it is worth combining the two countings in such a way to extend the results to higher energies.

In particular, the FONLL-A result will be combined with the NLO intermediate energy result proposed in this thesis, constructing the $\mathcal{O}(\alpha_s)$ final extended result, while the FONLL-C result will be combined with the NNLO intermediate energy result proposed in this thesis, constructing the $\mathcal{O}(\alpha_s^2)$ final extended result (table 4.1). Such combinations will be carried out trough the energy damping function

$$\chi(Q) = (1 - (m_b/Q)^a)^b, \tag{5.1}$$

which implements the transition between the two energy regions.

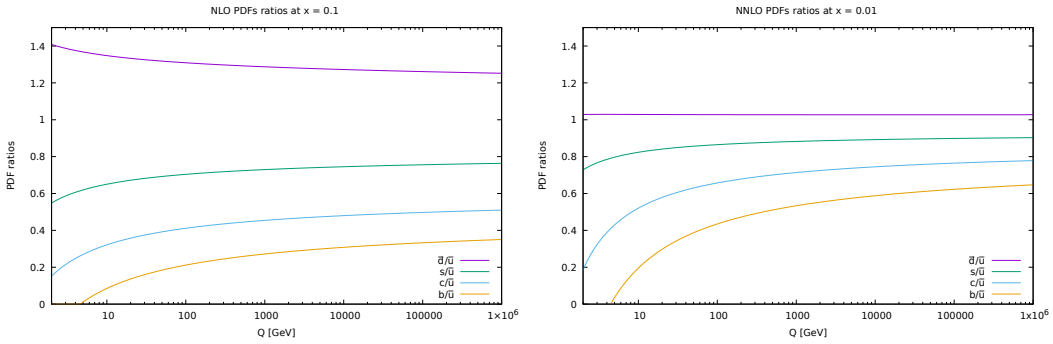

Figure 5.29. Ratios of the $\overline{d}$, s, c and b PDFs over the $\overline{u}$ one in the NLO and NNLO cases.

In order to choose the a and b values, the behaviour of the ratios of the $\overline{d}$, s, c and b PDFs over the $\overline{u}$ one, in both the NLO and NNLO cases, has been analyzed (fig. 5.29). In this way it is possible to estimate the value of the energy scale in which the heavy-quark PDFs start to be of $\mathcal{O}(1)$ (sec. 4.2). As it is possible to see in the plots, the s, c and b PDF ratios start to stabilize around Q = 100 GeV and essentially stop to grow around Q = 1000 GeV. This feature is exactly respected by the damping function

$$\chi(Q) = (1 - \sqrt{m_b/Q})^4, \tag{5.2}$$

obtained for $a = 0.5$ and $b = 4$. In fact, with these values of the parameters, it starts to grow around Q = 10 GeV in such a way to reach the $\chi(Q) \sim 0.5$ value at Q $\sim$ 100 GeV and $\chi(Q) \sim 1$, at Q $\sim$ 1000 GeV.

The final expressions for the extended (EX) results for a generic structure function are then

$$F_{\text{NLO}}^{\text{EX}} = F_{\text{NLO}}^{\text{I.E.}} + \chi(Q)\left[F^{\text{FONLL-A}} - F_{\text{NLO}}^{\text{I.E.}}\right], \tag{5.3}$$

for the NLO, and

$$F_{\rm NNLO}^{\rm EX} = F_{\rm NNLO}^{\rm I.E.} + \chi(Q)[F^{\rm FONLL\text{-}C} - F_{\rm NNLO}^{\rm I.E.}], \tag{5.4}$$

for the NNLO. In figs. 5.30 and 5.31 are shown the F_2^{EX} results respectively in the NLO and NNLO case. The analogous ones for F_L^{EX} are shown in figs. 5.32 and 5.33. As it is possible to note, in F_2 case the extended result does not depart much from the matched result in the visible kinematic region. In F_L case, instead, especially in the NLO case, the transition between $F_L^{\rm I.E.}$ and the FONLL results is much more pronounced. This behaviour is due to the fact that, as it is also possible to note from secs. 5.1.2 and 5.1.2, the difference between FONLL results and the intermediate energy results proposed in this thesis are much larger in F_L case than in F_2 case.

As mentioned in sec 4.3, the necessary ingredients to construct the $\mathcal{O}(\alpha_s^3)$ prediction following the prescription proposed in this thesis will be probably available soon, either in an exact or approximate form. It is then worth reporting also the N^{3}LO expression of this high-energy expansion of the results

$$F_{\rm N^3LO}^{\rm EX} = F_{\rm N^3LO}^{\rm I.E.} + \chi(Q)[F^{\rm FONLL\text{-}E} - F_{\rm N^3LO}^{\rm I.E.}]. \tag{5.5}$$

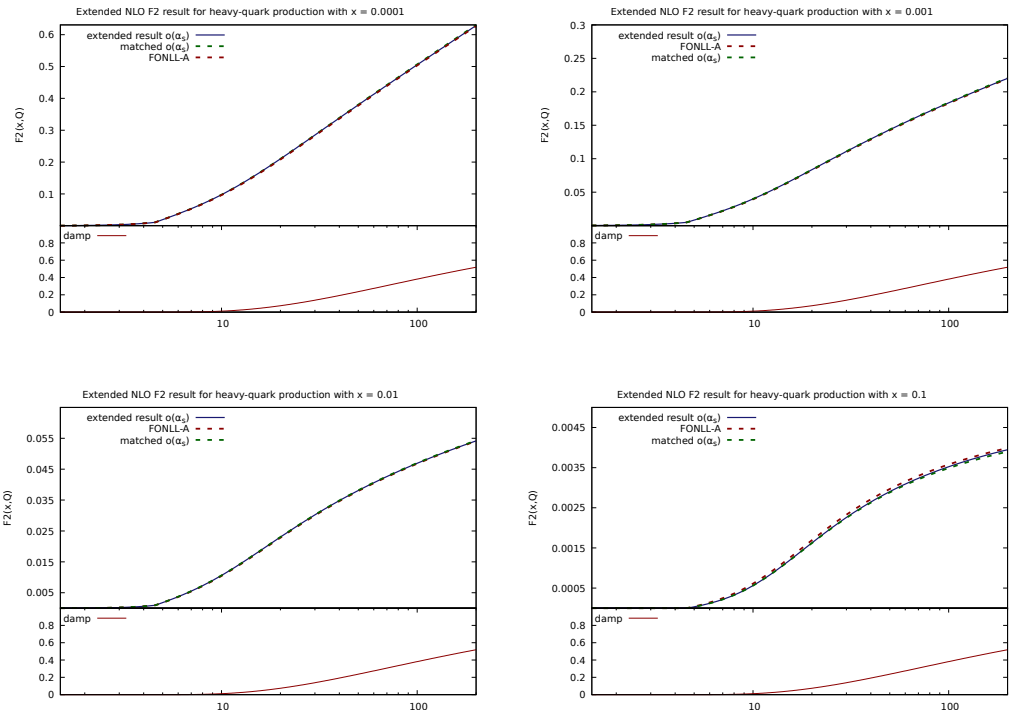

Figure 5.30. $F_2^{\rm I.E.}$ matched result, fixed-order and obtained trough the combination of the two countings at NLO as a function of Q for different values of the Bjorken's x. In the plot below, the shape of the energy dumping function $\chi = (1 - \sqrt{m_b/Q})^4$ used to combine the two countings is shown.

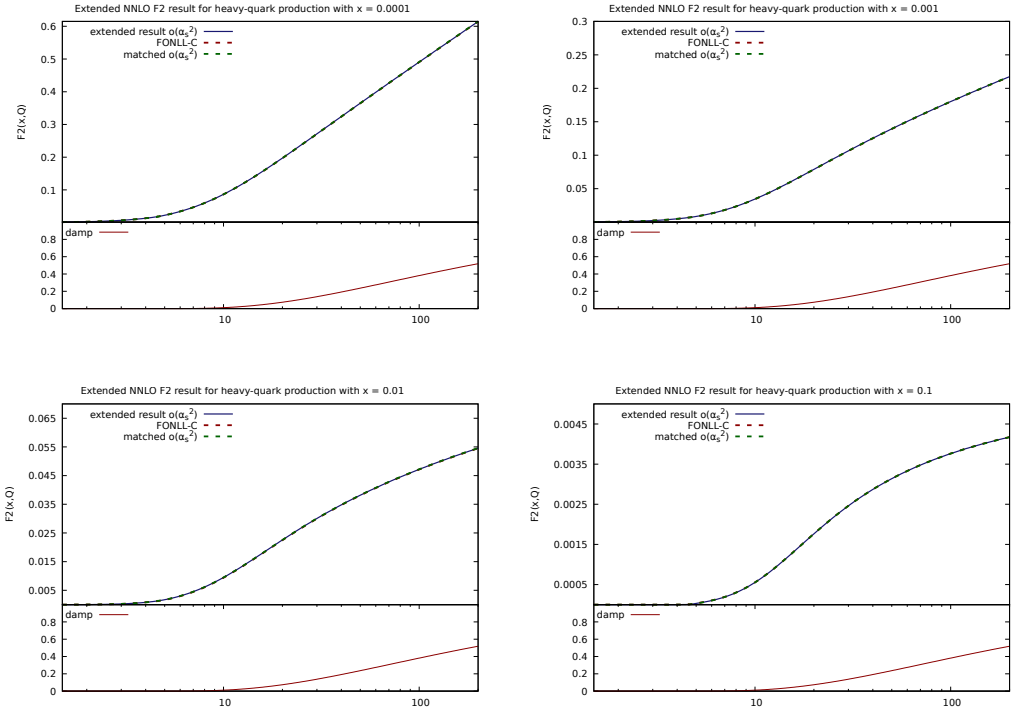

Figure 5.31. $F_2^{\text{I.E.}}$ matched result, fixed-order and obtained trough the combination of the two countings at NNLO as a function of Q for different values of the Bjorken's x. In the plot below, the shape of the energy dumping function $\chi = (1 - \sqrt{m_b/Q})^4$ used to combine the two countings is shown.

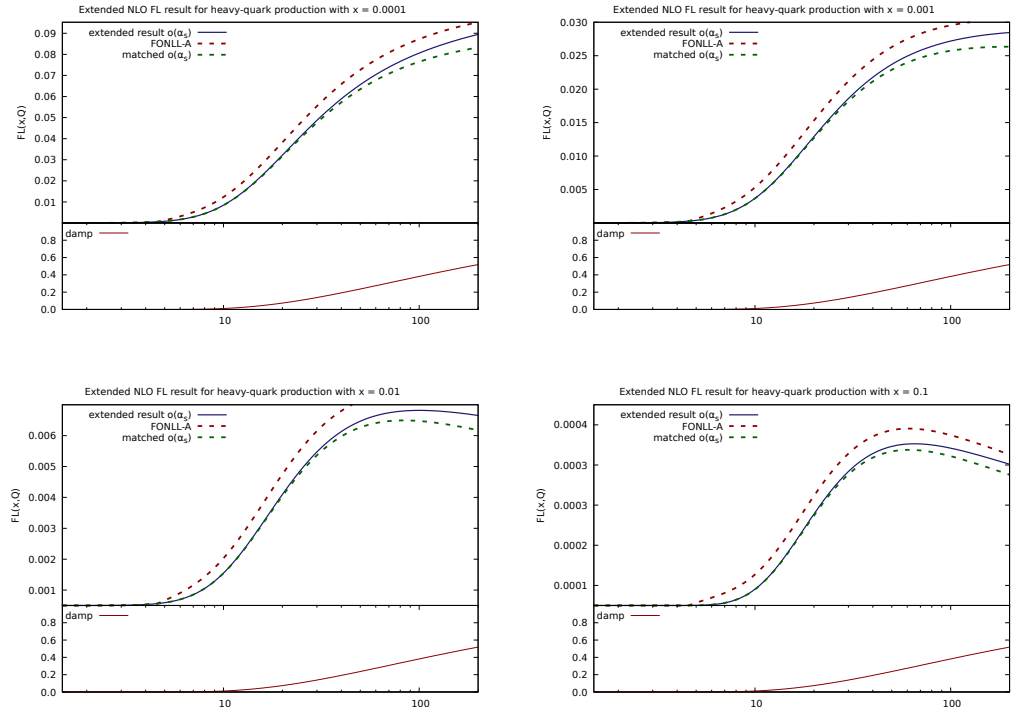

Figure 5.32. Same as fig. 5.30 but for F_L.

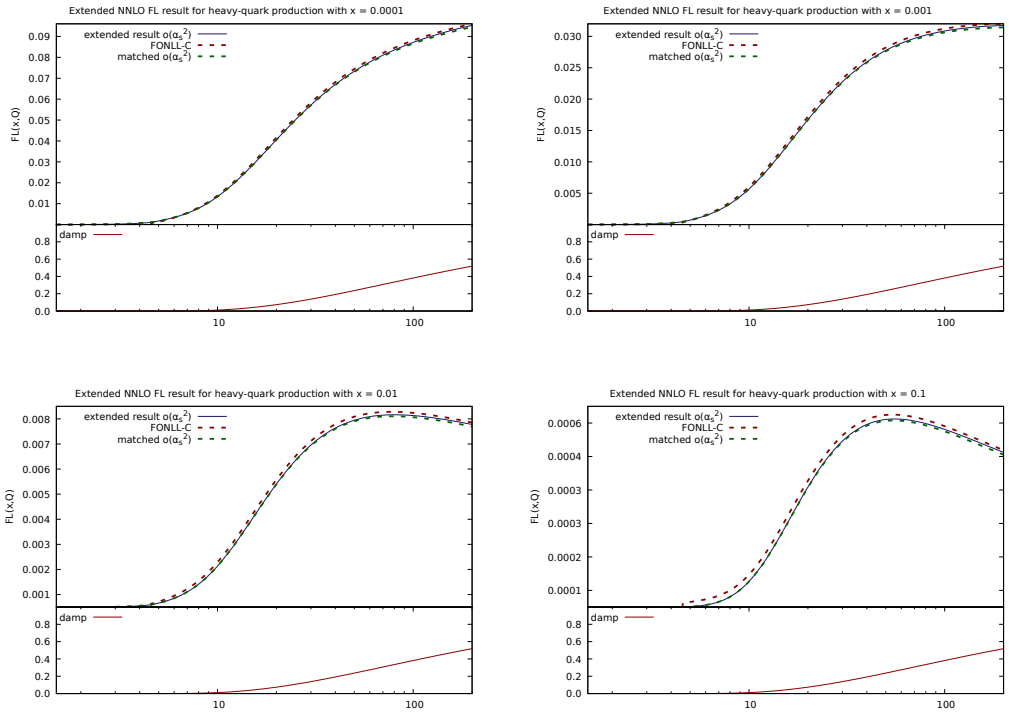

Figure 5.33. Same as fig. 5.31 but for F_L.

Conclusions

In this thesis, a method to construct predictions which are reliable in a wide range of the kinematic region has been proposed and explicitly applied to the heavy quark production sector of DIS. In particular, this has been done trough a matched result which combines the power-mass corrections with the benefits given by the resummation to all orders of the collinear logarithms appearing in the perturbative series. In this context, some changes, with respect to the usually adopted procedures, have been proposed and justified, including a different perturbative counting, which takes into account the perturbative nature of the heavy PDF, and an alternative version of the perturbative terms that contribute to the PDF evolution. The consequences related to these proposals have been extensively analyzed in the numerical results and what emerged partially confirmed their correctness.

In particular, it turned out that the alternative PDF version leads to better numerical results than the standard version from both an uncertainty and a smoothness points of view. This proved to be true for most the NLO and NNLO structure function predictions. Regarding the other cases, it is reasonable to think that they are caused by the non-optimal way in which uncertainties are estimated and thus they do not necessarily indicate that the adoption of the alternative PDFs is not convenient.

Likewise, the results obtained by adopting the proposed counting turned out to be better than the standard results. In particular, the NLO and NNLO results appeared to be smoother and less dependent on the threshold scale respectively than the FONLL-A and FONLL-C schemes. However, a more thorough investigation is recommended in this case as well.

Finally, an high-energy extension of the results have been proposed, obtained combining the two countings trough an energy damping function. This version can be considered the ultimate result proposed in this thesis.

The general conclusion is that the impact on the high-energy predictions of the collinear logarithms resummation is fundamental, especially with the coming high-precision era of hadron colliders. The method in which it has been implemented in this thesis, which can be easily generalized to two hadron-initiated processes, allows the construction of reliable predictions in a wide kinematic range and it has shown several improvements with respect to the others available in literature. Moreover, in future it should be applied also to the N^3LO DIS, which will open the doors to N^3LO PDF fits, and to other processes, as, for instance, single-top production.

Appendix A

Phase-space expressions

In this appendix, the phase-space expressions exploited in chapter 2, will be obtained. In the first section the massless case will be treated, so the computation will be carried out in dimensional regularization, i.e. with d space-time dimensions. In the second section, the massive case will be addressed and thus the computation will be carried out in the 4 standard space-time dimensions.

A.1 Massless case

The phase-space measure in d-dimensions for two final particles can be written as

$$d\phi_2(P;k_1,k_2) = \frac{d^{d-1}k_1}{(2\pi)^{d-1}2k_1^0}\frac{d^{d-1}k_2}{(2\pi)^{d-1}2k_2^0}(2\pi)^d\delta^{(d)}(P-q-k), \tag{A.1}$$

where k_1 and k_2 are the four-momentum of the final particles, $P=\sum_{ini}p_i$ is the total initial four-momentum and $\delta^{(d)}$ denotes the d delta functions acting on each dimension. Exploiting the spatial $(d-1)$ delta functions to integrate on k_2, results in

$$d\phi_2(P;k_1,k_2) = \frac{d^{d-1}k_1}{(2\pi)^{d-2}4k_1^0k_2^0}\delta(P^0-q^0-k^0), \tag{A.2}$$

where a single delta function which acts on the temporal component is left.

Switching to spherical coordinates in d-dimensions

$$d^{d-1}k_1 = \left|\vec{k_1}\right|^{d-2}d|k_1|d\Omega_{d-1}, \tag{A.3}$$

where $d\Omega_{d-1}$ is the d-dimensional solid angle, and exploiting the fact that $k_1^2=k_2^2=0$, it is possible to get

$$d\phi_2(P;k_1,k_2) = \frac{1}{(2\pi)^{d-2}}\frac{\left|\vec{k_1}\right|^{d-2}d|k_1|d\Omega_{d-1}}{4\left|\vec{k_1}\right|P^0}\delta\left(\left|\vec{k_1}\right|-\frac{\sqrt{\lambda}}{2P^0}\right), \tag{A.4}$$

with

$$\lambda(P^2;k_1^2,k_2^2) = (P^2)^2+(k_1^2)^2+(k_2^2)^2-2P^2k_1^2-2P^2k_2^2-2k_1^2k_2^2 = s^2 \tag{A.5}$$

the standard lambda function.

Exploiting the delta function to integrate on $\left|\vec{k_1}\right|$ results in

$$d\phi_2(P;k_1,k_2) = \frac{1}{(2\pi)^{d-2}4P^0}\left(\frac{\sqrt{\lambda}}{2P^0}\right)^{d-3} d\Omega_{d-1}. \tag{A.6}$$

The solid angle $d\Omega_{d-1}$ can be expressed recursively as

$$d\Omega_{d-1} = (d\theta \sin^{d-3}(\theta))d\Omega_{d-2}, \tag{A.7}$$

where θ is the radial angle, which becomes

$$d\Omega_{d-1} = dy 2^{d-3}[y(1-y)]^{\frac{d-4}{2}} d\Omega_{d-2} \tag{A.8}$$

if one express it in terms of $y = (1+\cos\theta)/2$. Notice that the invariance of the process for azimuth rotations makes it possible to integrate on $d\Omega_{d-2}$, which results in

$$\int d\Omega_{d-2} = \frac{2\pi^{\frac{d-2}{2}}}{\Gamma(\frac{d-2}{2})} = \frac{2\pi^{1-\epsilon}}{\Gamma(1-\epsilon)}, \tag{A.9}$$

obtained exploiting the general integral

$$\int d\Omega_n = \frac{2\pi^{n/2}}{\Gamma(n/2)}. \tag{A.10}$$

Putting everything together, it is possible to get the final result

$$d\phi_2(P;k_1,k_2) = \frac{1}{8\pi}\frac{(4\pi)^\epsilon}{\Gamma(1-\epsilon)}\left(\frac{1-x}{x}\right)^{-\epsilon} Q^{-2\epsilon} y^{-\epsilon}(1-y)^{-\epsilon} dy, \tag{A.11}$$

where $s = Q^2(1-x)/x$ has been used.

A.2 Massive case

In the massive case the computation is carried out in the standard 4 space-time dimensions, so the phase-space measure takes the form

$$d\phi_2(P;k_1,k_2) = \frac{d^3k_1}{(2\pi)^3 2k_1^0}\frac{d^3k_2}{(2\pi)^3 2k_2^0}(2\pi)^4\delta^4(P-k_1-k_2). \tag{A.12}$$

Exploiting the property

$$\frac{d^3k_i}{2k_i^0} = d^4k_i\delta(k_i^2-m^2)\theta(k_i^0) \tag{A.13}$$

and integrating on d^4k_2 using the 4-dimensional delta, it is possible to get

$$\begin{aligned} d\phi_2(P;k_1,k_2) &= \frac{1}{(2\pi)^2} d^4k_1\delta(k_1^2-m^2)\delta(k_2^2-m^2)\theta(k_1^0)\theta(k_2^0) \\ &= \frac{1}{(2\pi)^2} d^4k_1\delta(k_1^2-m^2)\delta((P-k_1)^2-m^2)\theta(k_1^0)\theta(P^0-k_1^0), \end{aligned} \tag{A.14}$$

where now $k_1^2 = k_2^2 = m^2$. The integral over the three-momentum $\vec{k_1}$ can be cast into spherical coordinates obtaining

$$= \frac{\left|\vec{k_1}\right|^2 d\left|\vec{k_1}\right| dE_1 d\Omega_2}{(2\pi)^2} \delta(E_1^2 - \left|\vec{k_1}\right|^2 - m^2)\delta((\sqrt{s} - E_1)^2 - \left|\vec{k_1}\right|^2 - m^2)\theta(E_1)\theta(\sqrt{s} - E_1), \tag{A.15}$$

where $E_1 \equiv k_1^0$ and it has been used the fact that $P = (\sqrt{s}, \vec{0})$ in the rest frame of the initial particles system.

Finally, both the integrals on the energy E_1 and on the three-momentum size $\left|\vec{k_1}\right|$ can be carried out trough the two delta functions obtaining the final result

$$d\phi_2(P; k_1, k_2) = \frac{\lambda^{1/2}(s, m^2, m^2)}{8(2\pi)^2 s} d\Omega_2, \tag{A.16}$$

where the lambda function definition has been also used.

Appendix B

PDF sets evolution with APFEL++

In this appendix, the way in which the PDF sets used to obtain the numerical results presented in chapter 5 have been constructed, is discussed. Other than a 4FS PDF set, used to implement the fixed order approximation, two different 5FS PDF sets, called standard and alternative, were necessary. These are respectively related to the expressions of eqs. (4.9) and (4.12) and they respectively represent the standard way in which the results are usually obtained and one of the original proposal of this thesis.

All of them have been obtained starting from the PDF4LHC15 PDF set at 2 GeV and evolving it with DGLAP equations in a different way depending on the final wanted set. The DGLAP evolution has been implemented trough the APFEL++ environment [27] interfaced with the LHAPDF database [30] from which the starting PDF set has been taken. Therefore, the different required PDF sets have been obtained only changing the way in which APFEL++ performed the evolution.

In particular, in order to switch from a 4FS set to a 5FS one it has been enough to change the value of the bottom threshold scale μ_b, fixing it to be at least one order of magnitude bigger than the bottom mass m_b. In practice, this has been implemented forcing μ_b to be always proportional to m_b as $\mu_b = n m_b$, in such a way $n \approx 30$ led to the 4FS PDFs, while $n = 0.5$, $n = 1$ and $n = 2$ led respectively to the $\mu_b = 0.5 m_b$, $\mu_b = m_b$ and $\mu_b = 2 m_b$ standard 5FS PDF versions.

The implementation of the alternative 5FS PDF sets has required more care. The reason is that, in order to obtain them, it is necessary to postpone the apparition of the gluon and light-quarks matching functions of one perturbative order. Although this procedure seems counterintuitive, because in eq. (4.12) the heavy quark matching functions are postponed instead, it is the most convenient way to proceed from an implementation point of view. For instance, this procedure ensures that $\tilde{f}_g^{\{1\}}$, $\tilde{f}_q^{\{1\}}$ and $\tilde{f}_b^{\{2\}}$, necessary for the NNLO result, are correctly evolved at NNLO and thus belong to the same set. In the same way, $\tilde{f}_g^{\{0\}}$, $\tilde{f}_q^{\{0\}}$ and $\tilde{f}_b^{\{1\}}$ belong to an NLO set.

In particular, the matching functions $K_{gg}^{(1)}$, which appear at NLO in the standard PDFs, have been postponed to NNLO. Consequently, the $K_{gg}^{(2)}$ has been removed from the NNLO PDFs, together with the $K_{gq}^{(2)}$ and the $K_{qq}^{(2)}$, which have been simply substituted by the identity.

Appendix C

Slope discontinuity and leading-order PDFs

In this appendix, the problem of the slope discontinuity in the threshold region, which is possible to note, for instance, in fig. 5.1, will be addressed and analyzed. From several tests that have been carried out on the NLO $F_2^{\text{I.E.}}$ matched result, it has been observed that, as it is possible to see in fig. C.1, the discontinuity appears much less pronounced if one adopts the LO 5FS PDFs instead of their NLO version. Moreover, it has been also observed that if one neglects the $C_b^{(0)}$ term, the discontinuity disappears completely.

The goal of this appendix is then to give a theoretical reason to this behaviour. Let's define

$$\begin{aligned}\sigma &= \alpha_s^{[5]}[C_g^{[4](1)}(m_b) - C_b^{(0)}K_{bg}^{(1)}(m_b)]f_g^{[5]} + C_b^{(0)}f_b^{[5]} \\ \tilde{\sigma} &= \alpha_s^{[5]}C_g^{[4](1)}(m_b)f_g^{[5]},\end{aligned} \tag{C.1}$$

where the products must be understood as Mellin space convolutions. Then, it is clear that the origin of the discontinuity must be given by

$$\Delta\sigma = \sigma - \tilde{\sigma} = C_b^{(0)}[f_b^{[5]} - \alpha_s^{[5]}K_{bg}^{(1)}(m_b)f_g^{[5]}] = C_b^{(0)}\Delta(Q,\mu_b)f_g^{[4]}(\mu_b), \tag{C.2}$$

where

$$\Delta(Q,\mu_b) = U_{bb}^{[5]}K_{bg}^{(1)}(\mu_b)\alpha_s(\mu_b) + U_{bg}^{[5]} - \alpha_s(Q)K_{bg}^{(1)}(Q)U_{gg}^{[5]}. \tag{C.3}$$

Since the region of interest is the $Q \sim \mu_b$ region, where, in this context, μ_b is chosen to be equal to the bottom mass, in the following every expression will be expanded for $Q/m_b = 1 + \epsilon \simeq 1$. So one obtains

$$\Delta(Q,\mu_b) = U_{bg}^{[5]}(m_b(1+\epsilon), m_b) - \alpha_s(m_b(1+\epsilon))P_{qg}^{(0)}2\epsilon U_{gg}^{[5]}(m_b(1+\epsilon), m_b), \tag{C.4}$$

where the expression of $K_{bg}^{(1)}$, including the Taylor expansion of its logarithm, in terms of the splitting function P_{qg} has been used.

At this point, the LL expressions of the U_{gg} and U_{bg} evolution kernels are needed. The LL evolution can be diagonalized in the form [24]

$$U_{LL} = \mathcal{M}_+\left(\frac{\alpha_s(m_b(1+\epsilon))}{\alpha_s(m_b)}\right)^{-\frac{P_+}{\beta_0}} + \mathcal{M}_-\left(\frac{\alpha_s(m_b(1+\epsilon))}{\alpha_s(m_b)}\right)^{-\frac{P_-}{\beta_0}}, \tag{C.5}$$

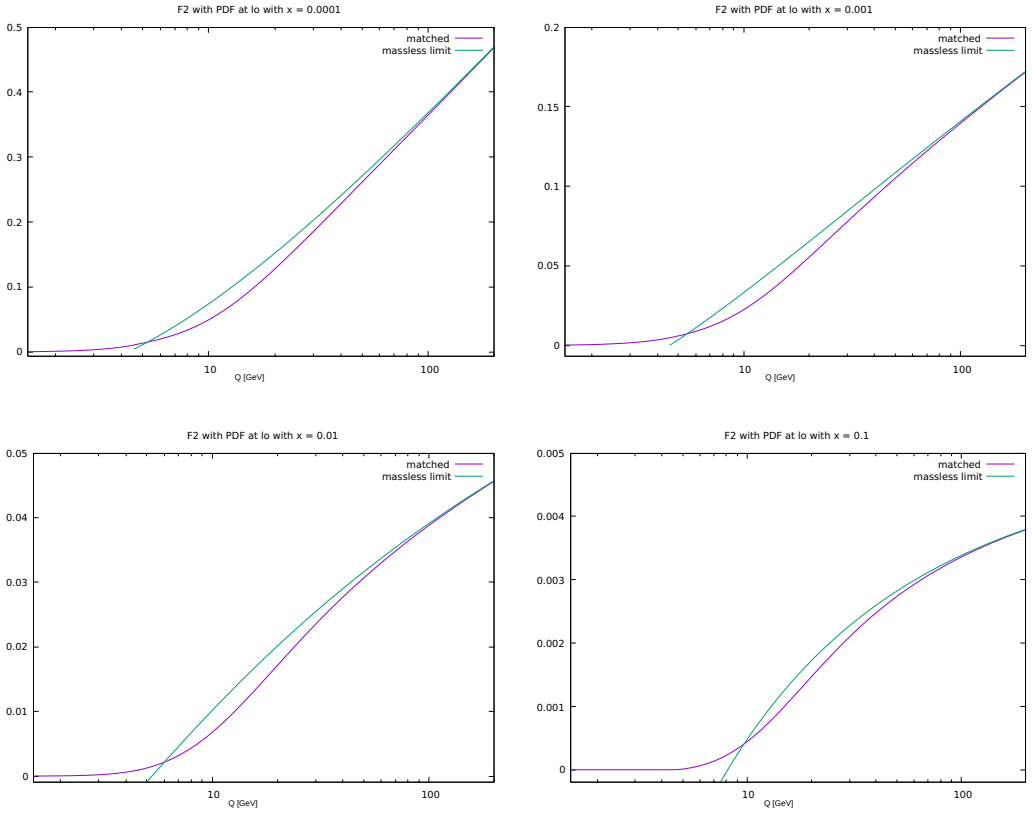

Figure C.1. $F_2^{\text{I.E.}}$ at NLO as a function of Q for different values of the Bjorken's x. In this case the results have been constructed using the LO of the standard version of the 5FS PDFs. As it is possible to see, the consequence of the LO PDFs adoption is the improvement of the result in the threshold region.

where

$$P_{\pm} = \frac{1}{2}(P_{gg} + P_{qq} \pm \sqrt{P_{gg}^2 + P_{qq}^2 - 2P_{gg}P_{qq} + 4P_{qg}P_{gq}}), \tag{C.6}$$

$$\mathcal{M}_{\pm} = \pm\frac{1}{P_+ - P_-}\begin{pmatrix} P_{\pm} - P_{qg} & \frac{(P_+ - P_{qg})(P_{qg} - P_-)}{P_{qg}} \\ P_{qg} & P_{gq} - P_{\pm} \end{pmatrix}. \tag{C.7}$$

From the last equation, it is possible to compute the needed LL evolution kernels expanding for $\epsilon \to 0$. This results in

$$\begin{aligned} U_{qg}^{LL} &\approx \frac{P_{qg}}{P_+ - P_-}[(1 + 2\alpha_s(m_b)\beta_0 \log\frac{m_b(1+\epsilon)}{m_b})^{\frac{P_+}{\beta_0}} - (1 + 2\alpha_s(m_b)\beta_0 \log\frac{m_b(1+\epsilon)}{m_b})^{\frac{P_-}{\beta_0}}] \\ &\approx \frac{\alpha_s 2\epsilon P_{qg}}{P_+ - P_-}[P_+ - P_-] \qquad \text{(C.8)} \\ &\approx \alpha_s 2\epsilon P_{qg} \qquad \text{(C.9)} \end{aligned}$$

and

$$U_{gg}^{LL} \approx \alpha_s 2\epsilon P_{qg} + \frac{1}{P_+ - P_-}[P_+(1+\alpha_s 2\epsilon P_+) - P_-(1+\alpha_s 2\epsilon P_-)] \tag{C.10}$$
$$\approx \alpha_s 2\epsilon P_{qg} + 1 + \alpha_s 2\epsilon \frac{P_+^2 - P_-^2}{P_+ - P_-}$$
$$\approx 1 + \alpha_s 2\epsilon P_{gg},$$

which give

$$\Delta = P_{qg}^{(0)} \alpha_s 2\epsilon - \alpha_s 2\epsilon P_{qg}^{(0)}(1 + \alpha_s 2\epsilon P_{gg}^{(0)}) = \mathcal{O}(\epsilon^2). \tag{C.11}$$

The last equation explains why the slope discontinuity disappears when the PDFs are evolved at LL. In the following, the reason why it appears in the first place when one adopts NLO PDFs is investigated.

At NLL the evolution cannot be diagonalized, hence it is necessary to find another way to compute the evolution kernels. A possible way is to follow the procedure in [24] to write them as

$$U_{ij} \simeq \delta_{ij} + \int_{m_b^2}^{m_b^2(1+\epsilon)} [P_{ij}^{(0)} \alpha_s(\mu^2) + P_{ij}^{(1)} \alpha_s(\mu^2)] \frac{d\mu^2}{\mu^2} \tag{C.12}$$
$$= \delta_{ij} + \int_{\alpha_s(m_b^2)}^{\alpha_s(m_b^2(1+\epsilon))} [\alpha_s P_{ij}^{(0)} + \alpha_s^2 P_{ij}^{(1)}] \frac{d\alpha_s}{-\beta_0 \alpha_s^2 - \beta_1 \alpha_s^3},$$

which, after the evaluation of the integrals and the expansion in ϵ, results in

$$U_{ij} \simeq \delta_{ij} + \alpha_s 2\epsilon P_{ij}^{(0)} - (\frac{P_{ij}^{(0)}}{\beta_0} - \frac{P_{ij}^{(1)}}{\beta_1}) \frac{\alpha_s^2 \beta_1 2\epsilon}{1 + \frac{\beta_1}{\beta_0}\alpha_s}. \tag{C.13}$$

Using the last equation to evaluate U_{bg}^{NLL} and U_{gg}^{NLL} and inserting them in eq. (C.4), leads to

$$\Delta = \alpha_s 2\epsilon P_{qg}^{(0)} - (\frac{P_{ij}^{(0)}}{\beta_0} - \frac{P_{ij}^{(1)}}{\beta_1}) \frac{\alpha_s^2 \beta_1 2\epsilon}{1 + \frac{\beta_1}{\beta_0}\alpha_s} - \alpha_s(1 - \alpha_s \beta_0 2\epsilon) P_{qg}^{(0)} 2\epsilon = \mathcal{O}(\epsilon). \tag{C.14}$$

What it has been shown is that, while at NLL the contribution which gives the slope discontinuity is of the same order of $\epsilon = Q/m_b - 1$, at LL the same piece is at the following order and so the discontinuity is less pronounced. This means that, the behaviour of fig. C.1 is given by an algebraic coincidence rather than by a profound theoretical reason. Therefore, it does not invalidate the choice of adopting NLO PDFs for the NLO result and, analogously NNLO PDFs for the NNLO result.

Ringraziamenti

Alla fine di questo percorso durato cinque anni, ci tengo a ringraziare tutte le persone (e non) che ne hanno reso possibile la sua riuscita e che l'hanno reso, consapevolmente o meno, un po' più piacevole.

Per primo è doveroso ringraziare il mio relatore, dr. Marco Bonvini, per il suo aiuto e per aver reso bella e interessante l'esperienza della scrittura di questa tesi. I suoi impagabili consigli hanno contribuito a chiarire il mio percorso futuro oltre che avermi reso un fisico migliore.

Ringrazio tutti i professori del Dipartimento di Fisica che ho conosciuto che, in un modo o nell'altro, mi hanno spinto ad andare avanti e a fare meglio.

Ringrazio tutti i colleghi che ho incontrato durante gli anni e con cui ho condiviso esperienze indimenticabili. Tra di loro ho trovato qualcuno che ho avuto il piacere di chiamare amico. A voi va un ringraziamento speciale perchè condividere con voi questa corsa a ostacoli che chiamano laurea è stato un privilegio e, probabilmente, una delle cose che l'ha resa affrontabile.

Ringrazio i miei amici (non fisici) di sempre: Riccardo, Melissa, Lorenzo (no, non sei fisico) e Vincenzo (tu sei fisico ma sei di sempre). Sapere che ci siete e ci sarete sempre è stato più importante di quanto non crediate.

Ringrazio tutti i componenti della mia famiglia. In particolare i miei genitori che mi hanno supportato e sopportato sempre, anche nelle tante giornate in cui non lo meritavo. Ringrazio anche mio fratello Federico perchè forse crederà che gli voglio bene se lo leggerà sulla mia tesi. Non può esserci scritto niente di sbagliato su una tesi di fisica, no?

Ringrazio anche Lucky, il mio cane, perchè, anche se tutto dovesse andare male, lui mi accoglierà sempre scodinzolando.

Infine voglio ringraziare una persona speciale. Una persona che è insieme collega, amica (fisica) e parte della mia famiglia. Una persona che è stata il più grande regalo che questi cinque anni mi hanno fatto. Francesca, grazie per aver reso speciale ogni giorno di questo lungo viaggio.

Bibliography

[1] "A new schedule for the lhc and its successor." https://home.cern/news/news/accelerators/new-schedule-lhc-and-its-successor, 2019.

[2] M. D'Onofrio, "Prospects for lhc run 3 and hl-lhc:experimental overview." https://indico.cern.ch/event/855882/contributions/3601848/attachments/1930307/3196895/Prospects_Run3_HLLHC_Fermilab.pdf, 2019.

[3] R. K. Ellis, W. J. Stirling, and B. R. Webber, *QCD and collider physics*, vol. 8. Cambridge University Press, 2, 2011.

[4] G. P. Salam, *Elements of qcd for hadron colliders*, 2011.

[5] S. Forte, E. Laenen, P. Nason, and J. Rojo, *Heavy quarks in deep-inelastic scattering*, *Nuclear Physics B* **834** (Jul, 2010) 116–162.

[6] M. A. G. Aivazis, F. I. Olness, and W.-K. Tung, *Leptoproduction of heavy quarks. i. general formalism and kinematics of charged current and neutral current production processes*, *Physical Review D* **50** (Sep, 1994) 3085–3101.

[7] M. A. G. Aivazis, J. C. Collins, F. I. Olness, and W.-K. Tung, *Leptoproduction of heavy quarks. ii. a unified qcd formulation of charged and neutral current processes from fixed-target to collider energies*, *Physical Review D* **50** (Sep, 1994) 3102–3118.

[8] R. S. Thorne, *Variable-flavor number scheme for next-to-next-to-leading order*, *Physical Review D* **73** (Mar, 2006).

[9] R. D. Ball, M. Bonvini, and L. Rottoli, *Charm in deep-inelastic scattering*, *Journal of High Energy Physics* **2015** (Nov, 2015).

[10] S. Weinberg, *The Quantum Theory of Fields*, vol. 2. Cambridge University Press, 1996.

[11] M. Srednicki, *Quantum field theory*. Cambridge University Press, 1, 2007.

[12] **Particle Data Group** Collaboration, P. Zyla et al., *Review of Particle Physics*, *PTEP* **2020** (2020), no. 8 083C01.

[13] T. Appelquist and J. Carazzone, *Infrared singularities and massive fields*, *Physical review D* **11** (May, 1975) 2856–2861.

[14] G. Altarelli, *Collider Physics within the Standard Model: a Primer*, 2013.

[15] P. Nason, *Introduction to QCD*, *Conf. Proc. C* **9705251** (1997) 94–149.

[16] G. Curci, W. Furmanski, and R. Petronzio, *Evolution of parton densities beyond leading order*, *Nuclear Physics B* **175** (1980).

[17] R. K. Ellis, H. Georgi, M. Machacek, H. Politzer, and G. G. ROSS, *Perturbation theory and the parton model in qcd*, *Nuclear Physics B* **152** (1978).

[18] R. K. Ellis, H. Georgi, M. Machacek, H. Politzer, and G. G. ROSS, *Factorization and the parton model in qcd*, *Physics letters* **78B** (1978).

[19] J. Stirling, "Parton distribution functions." https://indico.cern.ch/event/94815/contributions/1282690/attachments/1106827/1579062/LBLMIT_Stirling_v2.pdf.

[20] S. Alekhin, J. Blümlein, and S. Moch, *Heavy-quark production in deep-inelastic scattering*, 2013.

[21] F. Sefkow, *Heavy-quark production in Deep-Inelastic Scattering*, 2001.

[22] J. C. Collins, *Hard-scattering factorization with heavy quarks: A general treatment*, *Physical Review D* **58** (Sep, 1998).

[23] J. C. Collins, E. S. Davison, and G. Sterman, *Factorization for one-loop corrections in the drell-yan process*, *Nuclear Physics B* **223** (Nov, 1983).

[24] M. Bonvini, *Resummation of soft and hard gluon radiation in perturbative QCD*, 2012.

[25] M. Bonvini, A. S. Papanastasiou, and F. J. Tackmann, *Matched predictions for the $b\bar{b}h$ cross section at the 13 tev lhc*, *Journal of High Energy Physics* **2016** (Oct, 2016).

[26] V. Bertone, S. Carrazza, and J. Rojo, *Apfel: A pdf evolution library with qed corrections*, *Computer Physics Communications* **185** (Jun, 2014) 1647–1668.

[27] V. Bertone, *APFEL++: A new PDF evolution library in C++*, 2017.

[28] H. Kawamura, N. Lo Presti, S. Moch, and A. Vogt, *On the next-to-next-to-leading order qcd corrections to heavy-quark production in deep-inelastic scattering*, *Nuclear Physics B* **864** (Nov, 2012) 399–468.

[29] J. Vermaseren, A. Vogt, and S. Moch, *The third-order qcd corrections to deep-inelastic scattering by photon exchange*, *Nuclear Physics B* **724** (Sep, 2005) 3–182.

[30] A. Buckley, J. Ferrando, S. Lloyd, K. Nordström, B. Page, M. Rüfenacht, M. Schönherr, and G. Watt, *LHAPDF6: parton density access in the LHC precision era*, *The European Physical Journal C* **75** (Mar, 2015).